MODELING OPTICALLY ACTIVATED HIGH POWER SEMICONDUCTOR SWITCHES

BY

PHILLIP J. STOUT

B.S., University of Illinois, 1989
M.S., University of Illinois, 1991

THESIS

Submitted in partial fulfillment of the requirements
for the degree of Doctor of Philosophy in Electrical Engineering
in the Graduate College of the
University of Illinois at Urbana-Champaign, 1995

Urbana, Illinois

UNIVERSITY OF ILLINOIS AT URBANA-CHAMPAIGN

THE GRADUATE COLLEGE

NOVEMBER 1994

WE HEREBY RECOMMEND THAT THE THESIS BY

PHILLIP J. STOUT

ENTITLED MODELING OPTICALLY ACTIVATED HIGH POWER SEMICONDUCTOR SWITCHES

BE ACCEPTED IN PARTIAL FULFILLMENT OF THE REQUIREMENTS FOR

THE DEGREE OF DOCTOR OF PHILOSOPHY

Mark J. Kushner
Director of Thesis Research

N. Narayana Rao
Head of Department

Committee on Final Examination†

Mark J. Kushner
Chairperson

Umberto Ravaioli

K. W. Kim

James Coleman

Joseph J. Verdeyen

† Required for doctor's degree but not for master's.

O-517

MODELING OPTICALLY ACTIVATED HIGH POWER SEMICONDUCTOR SWITCHES

Phillip J. Stout, Ph.D.
Department of Electrical and Computer Engineering
University of Illinois at Urbana-Champaign, 1995
Mark J. Kushner, Advisor

A photoconductive semiconductor switch (PCSS) has high voltage hold-off and fast rise times. However, lock-on, nonuniformities in the electric field, and filamentation of current flow across the device when switching at high fields (~ 10 kV/cm) have been reported. These observations have raised concerns about the scaling of the PCSS to higher currents. To investigate these issues, a two-dimensional time dependent computer model of a GaAs PCSS has been developed. The model solves the continuity equations for electrons, holes, and traps, the energy equation for the lattice, Poisson's equation, and a circuit equation. Physical effects in the model include band-to-band impact ionization, trap impact ionization, photoionization, recombination radiation transport, and negative differential resistance. The model has the ability to address different switch geometries and the consequences of nonuniformities in carrier injection, permittivity, and illumination of the sample on switch operation.

Results from modeling bulk and coplanar geometry GaAs (Si:Cu) high power photoconductive switches show that the switching cycle is sensitive to the type of laser spatial distribution, the trap doping levels, the circuit parameters, and the geometry of the device. For a coplanar switch with an ungrounded base, field enhancement occurs near the anode and cathode as the switch begins to close. This enhancement shifts to the cathode during the on state of the switch. When the switch is opened, an electric field enhancement front begins to migrate back toward the anode. The mobile enhancement front is a consequence of negative differential resistance. The spatial shape of laser penetration affects the shape of this field enhancement. For the ungrounded base, field enhancement occurs only near the anode as the switch is closing. During the on state of the switch, the electric field collapses to the cathode. In the opening stage of the switch a high field region forms near the anode inhibiting the opening of the switch. As a result, switch opening is less sensitive to the opening laser pulse when a grounded base coplanar switch geometry is used.

Grading near the contacts causes the electric field peaks before triggering to occur in the bulk of the switch rather than at the contacts, which results in more uniform injection of the carriers at the contacts. Alternatively, a reduction in the electric field at the contact corners can be achieved by embedding the contacts, which enables the switch to hold off more voltage. Roughness at the contacts creates local charge excess which generates local peaks in the electric field which are probable precursors to filamentation. Delivering light directly under the contacts decreases the voltage closing level. A mechanism essential to closing the GaAs(Si:Cu) switch is intrinsic impact ionization.

The model has also been used to examine the important processes involved in trigger gain for an intrinsic GaAs coplanar switch operated in the nonlinear mode and activated with a laser spot. Results from the model show that band-to-band recombination radiation transport plays an important role in carrier transport when the switch is closed with a nonuniform laser pulse. Reabsorption of the radiation ultimately reduces the electric field at the contacts, which allows the switch to close. The model also predicts that the switch is sensitive to the location of the activating laser pulse. Less laser fluence is required to close the switch near the cathode than near the anode.

ACKNOWLEDGMENTS

The author imagines a spinning roulette wheel and a circling ball falling into a slot on the pot-marked wheel. One of those slots is marked "completion of Ph.D." It is a chance occurrence, and certainly unexpected, yet it has occurred. Why has such a decidedly unprobable event come to pass? The essential ingredients were an opportunity, an idea, and guidance.

There would never have been an opportunity to complete this thesis if it had not been for the funding and support of BMDO/IST, managed by the Office of Naval Research (Contract N00014-90-J-1967). The idea that motivates this work comes from Professor Karl Schoenbach and his BOSS concept. The author thanks Karl Schoenbach for his ideas, helpful advice, and the device concept from which the model in this work was originally formulated. Concerning guidance, the path up the exponential curve to greater knowledge is not an easy one to negotiate. A nightmare version of chutes and ladders would not do justice to the quagmire of failures and successes encountered when pursuing one's graduate studies. Without the guidance of the author's thesis advisor, Professor Mark J. Kushner, his attempts to complete graduate studies would resemble one long piece of chute.

Finally, in transitions of life such as these, the author's thoughts return to words spoken by his parents concerning his conception. In short, the author's conception was incidental to a more immediate goal that day. Well Ma and Dad, I hope you enjoyed yourselves, now look what you have done.

TABLE OF CONTENTS

I. INTRODUCTION

The traditional role of gas discharges, such as thyratrons and spark gaps as pulse power switches,[1] is being challenged by the high power photoconductive semiconductor switch (PCSS). Like a gas discharge switch, the PCSS is capable of high voltage hold-off scalable to hundreds of kilovolts and high current handling capabilities scalable to tens of kiloamps. However, a PCSS has very fast turn-on and turn-off (with switching in the subnanosecond range and limited primarily by the optical trigger speed),[2] higher thermal conductivity, faster recovery that allows higher repetition rates of kilohertz for continuous operation and gigahertz for bursts, optical isolation of the trigger, low trigger jitter in the 100 ps range, and more efficiency. Since the PCSS is made of semiconductor material, it is easier to manufacture, has a flexible geometry that allows fabrication of low inductance structures, is less bulky, is inexpensive, and has solid-state dependability.

The PCSS has found potential applications,[3] such as in the generation of ultrawide band pulses in radar,[4] where the rise time, reliability and jitter are important; rapid plasma generation for inertial confinement fusion;[5] high current particle accelerators;[6] and inductive energy storage.[7]

The PCSS operates by varying the conductivity of a semiconductor through photon absorption. Shining bandgap radiation from a laser on the sample generates electron-hole pairs (EHPs) via photon absorption, which increases the conductivity of the sample closing the switch. The photon absorption is extremely fast, being roughly proportional to the optical absorption depth divided by the speed of light, which results in subnanosecond rise times. When the laser pulse is terminated, the conductivity rapidly decreases due to electron-hole recombination, opening the switch. Auston[8] was the first to use photoconductivity to produce picosecond switching, albeit in a low power setting, for voltage pulse sampling in silicon photoconductors. The PCSS concept was later developed for higher powers.[9-12]

A fast opening switch has short EHP lifetimes,[13] since the EHPs introduced by the triggering laser recombine at a fast rate. For instance, in direct-gap semiconductors the radiative lifetimes are a few nanoseconds, and in specially prepared semi-insulating GaAs the EHP lifetime can be less than a nanosecond.[2] Although a short EHP lifetime is beneficial if fast opening times are required, it is undesirable if long conduction times (hundreds of nanoseconds to microseconds) are required. Maintaining photoconductivity during the closed phase of a switch cycle requires a large photon flux to

replace EHPs which have been lost by rapid recombination. If the lifetime is too short, the laser power required to maintain the carrier density may be prohibitively large. To address this issue, a GaAs(Si:Cu) bistable optically controlled semiconductor switch (BOSS) was developed by Schoenbach et al.[14] In the BOSS, the closing and the opening times of the switch are controlled by short laser pulses of different wavelengths, and the conductive phase is sustained without the continuous application of a laser to the switch to keep the free carrier level high.

Experimental observations of the GaAs PCSS have shown the presence of nonuniformities in the electric field,[15-20] lock-on of the opening voltage at critical electric fields,[21] and filamentation of current flow across the device during operation of the switch at high electric fields ($\approx$ 10 kV/cm).[22-24] These observations have caused concern about the scaling of the PCSS to larger currents. Filamentation can result in higher carrier densities by constricting currents to smaller cross-sectional areas. Local heating by filaments and point attachment to contacts can result in damage to the device. To investigate these issues, a two-dimensional time dependent computer model of a GaAs PCSS has been developed. The model solves the continuity equations for electrons, holes and traps, Poisson's equation, an energy equation, and a circuit equation.

After a basic understanding of the high power PCSS is established, a detailed explanation of the developed model will be given. The model has been applied to analysis of a PCSS with BOSS material as well as intrinsic GaAs. The model will be used to gain insight into the basic processes involved in a typical switching cycle of the PCSS, the consequences of switch geometries, material preparation, and laser light distributions on switch operation. Also, the importance of recombination radiation will be explored when a switch is triggered with a spot of light.

II. BACKGROUND

A. Si vs. GaAs as Switch Material

The semiconductor material of a PCSS is characterized by its absorption length vs wavelength, its dark hold-off voltage and thus its resistivity, the maximum hold-off electric field, its peak current handling capability, and its free carrier lifetime. The absorption length of the material determines the thickness of the switch and the options for laser trigger sources. If the switch is thinner then the absorption length, the optimal use of laser energy will be compromised as most of the light will be transmitted through the switch. Also, if a switch material requires a specific wavelength of light to switch properly, the laser source s availability may be an issue.

In the opened or off state, the switch is required to hold off large voltages. The larger the dark hold-off voltage or equivalently the larger its dark resistivity, the fewer is the number of switches required to scale to very high voltages. The dark hold-off voltage is the voltage a non-illuminated photoconductive switch can withstand before breaking down. A large dark resistivity is required for large hold-off voltages, since off-state or dark switch resistance is determined by the switch s dark resistivity. If current flowing through the switch is dissipating energy in the switch at high enough levels, there is an increase in the carrier density which decreases the off-state switch resistance lowering the dark hold-off voltage. The higher the dark resistance is, the lower the level of current flowing through the switch and the lower the level of thermal generation of carriers in the switch, and thus the more stable the hold-off voltage.

Contact separation is also an important consideration in the attempt to achieve large hold-off voltages. The larger the gap is between the contacts, the lower the average electric field between the contacts, and thus the larger the hold-off voltage one can apply across it before achieving the breakdown electric field of the material. However, the optical energy required to change the switch resistance scales as the square of the length of the switch. Therefore, minimizing the contact separation is desirable.[25] To minimize the contact separation, the maximum electric field the switch can handle has to be known. The larger the maximum electric field value is, the closer the contacts can be, which translates to less optical energy requirements to switch the device.

When the switch is closed and in a conductive or on state, it should conduct large currents. The current density limit of the material is important in defining its role in high power applications and is a factor in determining the width of the device. The lower the current density maximum, the larger the width of the device must be to handle the large currents. Other factors, such as the desired system inductance and the desired thermal resistance from the switch to the surrounding medium, also have to be considered when determining the width of the switch. It should be noted that the desired switches must have dimensions of several millimeters on each side in order to handle the high currents in the on state and the large hold-off voltages desired in the off state.

The carrier lifetime is also an important characteristic of the switch material. Lifetime is a measure of how quickly the switch will open when the laser trigger ends. The carriers could recombine faster than the EHPs being supplied by the laser trigger. If so, the optical power required to maintain a given carrier density scales approximately as the reciprocal of the carrier lifetime.[26] The faster the switch opens, the more trigger energy is required to sustain a closed state in the switch. Two natural semiconductors to choose for a PCSS are Si and GaAs, due to the large body of research associated with them and their availability in pure samples. Other materials being considered include diamond,[27] quartz,[28] 6H-SiC,[29] CdS:Cu, ZnS:Cu, Zn:O:Cu, ZnSe:Cu,[30,31] Fe:InP,[32] and ZnSe.[33] The following discussion will be limited to the characteristics of Si and GaAs, and how these characteristics make them viable choices as switch materials.

Silicon has an indirect bandgap at 1.12 eV, which makes it a strong absorber of Nd:YAG laser light at $\lambda = 1.06$ μm with an absorption depth of 1 mm.[34] The resistivity, ρ, of intrinsic Si is 10s of kΩ-cm which can hold off a few kV/cm (dc bias) before leakage current increases sharply due to thermal effects. Applying large voltages across Si increases its temperature due to joule heating by the dark current. The increase in temperature promotes the creation of thermal carriers which decrease silicon s resistance and eventually causes a thermal closing of the Si switch. Silicon must be pulse-charged to prevent thermal heating and eventual closure. Pulse biasing (1 μs) allows the semiconductor a chance for recovery and raises the maximum electric field held off to 40-60 kV/cm before the onset of thermal runaway.[35] This is analogous to gas switches which can hold off larger voltages when pulsed biased for times less than the time for avalanche to occur. The peak current

density for silicon before permanent damage is done to the crystal is ≈ 60 kA/cm^2.[36] Intrinsic silicon has a long carrier lifetime (μs to ms), which limits its use as a fast opening switch. However, introducing defects, which act as traps and recombination centers, can reduce the free carrier lifetime.[13] Defects can be introduced through radiation damage, impurities, or using polycrystalline or amorphous silicon. Silicon drawbacks are high leakage current and thermal runaway.

Gallium Arsenide comes in either an intrinsic or a semi-insulating form (GaAs:SI), achieved through Chrome doping or introducing a large number of crystal defects, such as EL2.[37] Gallium Arsenide has a direct bandgap at 1.424 eV which corresponds to an optical absorption wavelength of approximately 0.89 μm. The absorption length for $\lambda = 0.89$ μm light in GaAs is only a few μm. In general, optical absorption depths are short in intrinsic GaAs (micrometers) and are larger in doped or extrinsic GaAs when the optical wavelength is greater than the bandgap wavelength.[36] Large concentrations of defects in even the purest available GaAs result in deep energy states within the bandgap that contribute electrons and holes which are available for conduction. GaAs can be switched with 1.06 μm light by using a process called "extrinsic generation", which takes advantage of these deep states. The absorption depth of 1.06 μm light in commercially available GaAs is approximately 0.5 cm, which varies by a factor of five depending on the sample.[38] The large number of defects and impurities and the wide bandgap of semi-insulating GaAs lead to a large resistivity, $\rho = 10^7$ to 10^8 Ω-cm. The high resistivity value does lead to a lower leakage current but does not affect the electric field maximum.

The maximum electric field limit before breakdown for GaAs is 4-20 kV/cm (DC bias), which is only somewhat larger than for Si. However, at moderate electric fields most GaAs can support a voltage for a longer period of time and are not subject to thermal runaway or drastic resistance changes due to thermal carrier generation. Si must be pulse-charged to prevent thermal heating and self-closure. When pulse biasing GaAs, electric field limits of 100 to 140 kV/cm can be achieved with the limitation being surface flashover.[21] The direct bandgap means short carrier lifetimes in the range of a few picoseconds to a few nanoseconds. Typically, GaAs's carrier lifetime τ is 1 to 10 ns, with Chrome doped GaAs having a carrier lifetime $\tau < 1$ ns.[9] The short carrier lifetime allows extremely large repetition rates in linear operation. Although a neutron-irradiated or heavily Chrome-doped PCSS

achieves turn-on and turn-off times of less than 200 ps, when the neutron dose or doping concentration is high (>10^{15} cm^{-3}), the traps reduce mobility and, therefore, the optical sensitivity of the switch. At higher electric fields, nonlinear switching complicates the repetition rates.[39] The peak current densities for GaAs are larger than those for silicon, being around 500 kA/cm^2.[36]

B. Coplanar and Bulk Switch Geometries

Photoconductive switches fall into two basic categories of geometry: coplanar or bulk as shown in Figure II-1‡. Coplanar switches have contacts on the same plane, while in bulk switches contacts are on opposite sides of the device. Each switch geometry has associated with it advantages and disadvantages.

Since the contacts are on the same plane, coplanar switches are relatively easy to fabricate given current microelectronic technology. With the region between the contacts easily accessible by a laser trigger, coupling optical energy into the switch is straightforward. Depending on the laser wavelength used, the depth of the conductive region between the contacts can vary; however, the conductive channel formed lengthwise between the contacts will not vary, thus optimal use of the active region will always be achieved. Uniform coverage of the active region between the contacts is desired in order that no space charge enhancement of the electric field can affect the transit time of the carriers, and consequently, the rise and fall time of the switch. If carriers are created nonuniformly between the contacts, the closed stage of the switch will not occur until a conduction path has been established between the contacts. In a uniformly illuminated, coplanar, linear switch, the peak current and rise time depend only on the magnitude and shape of the optical pulse, the carrier recombination time, and the configuration of the switch in an external circuit.[40]

A drawback of the coplanar geometry is a semiconductor surface which is exposed to the full electric field. Because of this, careful preparation of the surface is necessary to reduce surface electric fields to less than ≈ 100 kV/cm to prevent surface flashover in order that the hold-off voltage is limited to the intrinsic breakdown level of the semiconductor between the electrodes and not the surface flashover level. However, localized electric field enhancement at the contact corners can still cause the semiconductor to experience bulk breakdown at average electric fields lower than intrinsic breakdown

‡ Figures and tables for each chapter will appear at the end of their respective chapters

level, since the electrical breakdown of a surface at the interface between two materials is usually less than that of either of the materials.[41] A way of reducing the electric field enhancement at the corners of the contacts is embedding the contacts into the switch. With embedded contacts reducing the electric field enhancement at the contact corners, coplanar switches have achieved in excess of 150 kV/cm for pulsed (~0.5 μs) bias voltages.[42]

In the bulk geometry, having the contacts on opposing sides results in a reduction of surface electric fields when compared with the coplanar geometry. A reduction in the surface electric fields minimizes the surface flashover and leads to larger hold-off voltages. Coupling optical energy into the switch, however, is more complicated. Illumination of the switch is typically done near a contact, which requires that at least one of the electrical contacts is transparent to the optical trigger or is perforated to allow the optical trigger access to the switch.[43] The transparent contact makes fabrication of the bulk switch more difficult than that of the coplanar switch. If carriers were created or injected only at the contacts and were required to separate and move across the insulating region, the electric fields produced by the non-neutral charge and time delays involved would limit the current rise time of the switch. Therefore, the use of long wavelength radiation is required for penetration into the interior of the device in the bulk geometry.[44]

C. Alternative Devices

The basic PCSS is a highly resistive semiconductor which is contacted with a metallic system in a bulk or coplanar geometry. There are, however, more traditional devices such as p-i-n junction devices,[45-47] optically activated thyristors (optothyristors),[48] and static induction transistors (SITs),[49-51] which are being developed into fast, optically triggered, high power semiconductor switches. However, the bulk or coplanar switches are the most ideally suited for high power (>30 MW) pulsed switching with sub-nanosecond rise-times.[52]

In the bulk device, high voltages can be used only on a pulsed basis, and formation of good ohmic contacts on high-resistivity material is difficult to achieve. With a p-i-n junction device, the reverse saturation current is significantly smaller than the leakage current of a bulk device. Therefore, the p-i-n diode can be reverse biased for long periods of time without thermal runaway. Also, in the p-i-n structure, ohmic contacts are applied to the p^+ and n^+ regions. Ohmic contacts are easier to make

with these highly doped regions than with the highly resistive regions typical of a PCSS. Limiting features of p-i-n structures are rise and fall times in the μs range, which limits their use as fast subnanosecond switches.[46]

Another alternative is the thyristor, which currently can hold off voltages of ~ 4 kV and conduct average currents of 4 kA. Although thyristors are usually triggered electrically, an optical trigger can be used which allows isolation from the switch, reduced jitter, and greater scalability. In designing optothyristors, the requirement on optical sensitivity results in a degradation in the dV/dt capability, and consequently, the noise immunity is reduced. Also, the dI/dt in these devices is reduced when an electrically triggered thyristor is converted to an optically triggered thyristor.[48]

The static induction transistor (SIT) is a unipolar, vertical channel field controlled semiconductor device.[53] In planar field-effect structures, such as the junction field effect transistor (JFET) and the metal-semiconductor field-effect transistor (MESFET), surface breakdown limits the voltage blocking capability of the device. In comparison, SIT's vertical channel geometry allows for higher blocking voltages as well as for parallel operation of interdigitated devices, which results in increased power handling capability. As with thyristors, SITs may be triggered by electrical or optical sources, with the optical trigger allowing isolation from the high-voltage switch assembly, consequently reducing jitter. As with the other devices mentioned, the SIT rise time is not subnanosecond in the power range of interest.[51]

D. Bistable Optically Controlled Semiconductor Switch

One specific device that is modeled in this document is the bistable optically controlled semiconductor switch (BOSS). The main difference between the BOSS and a generic PCSS is, in addition to the control of the closing phase of the switching cycle by a laser pulse, the opening phase is also controlled by a laser pulse. The opening phases of most PCSSs are determined by material properties such as doping level and carrier lifetime, and not by the time an opening laser pulse is applied.

The BOSS was developed by Schoenbach et al.[14] and has a deep acceptor that is compensated by a shallow donor. To close the switch, a photon energy is selected that is large enough to cause emission of electrons from the acceptor level and the valence band via the acceptor level (Figure II-2).

This on light increases the number of free electrons and holes, increasing the conductivity. When the on irradiation of the sample is terminated, the switch can remain conductive by selecting an acceptor species that is an inefficient electron trap and an efficient hole trap. At the termination of the on laser pulse, holes are quickly trapped by ionized acceptors. Excess free electrons can recombine only with the few remaining free holes or can be inefficiently trapped. The switch can remain closed for 100s ns to μs. The switch is opened by photoquenching the free electrons by selective photoexcitation of holes from the deep acceptor level. This is possible by selecting an off photon energy that is large enough to stimulate valence to acceptor trap transitions but small enough to prevent acceptor to conduction band transitions. Thus, holes are generated that quickly recombine with free electrons, which opens the switch.

A current versus time plot of a BOSS taken from Stoudt et al.[54] is shown in Figure II-3. The BOSS material is GaAs doped with Si and Cu, the switch dimensions are roughly 12 x 10 x 0.44 mm thick, and the geometry is planar with the contacts 1 cm wide and separated by 5 mm. The 1.06 μm on laser with a pulse energy of 2.1 mJ closes the switch, and later a 2.13 μm off laser (wavelength doubled) with a pulse energy of 5.0 mJ opens the switch. The laser produces a Gaussian pulse with a FWHM of about 140 ps.

E. Linear and Nonlinear Switching Modes

The PCSS can operate in a linear or nonlinear switching mode. In the linear mode, a one-to-one ratio exists between each photon absorbed in the switch and the number of EHPs created. In the nonlinear mode, which is experimentally observed only in direct bandgap semiconductors, the carrier density increases not only through the absorption of the laser light but also by gain mechanisms. Avalanche of carriers is possible in Si, but the gain mode has yet to be observed.

In the linear mode, the only source of excess carriers comes from the optical radiation. Therefore, the rate of change in the electron or hole density is proportional to the intensity of the optical radiation. To attain significant switching ($\rho \leq 0.1$ Ω-cm), an optical energy density on the order of 10s of mJ/cm^2 is required.[55] The absence of nonlinear effects which complicate the switching process translates into more predictable closing and opening of the switch. Also the jitter between a series of switches is dominated by the jitter between their optical triggers, which increases the degree of

switching control. Nothing is perfect, however. Even though the linear switch is very quick and controllable, there are other effects which can extend the closing time. For example, electrons and holes do not necessarily have the same effective lifetime. Various traps in semiconductors, such as GaAs, also play a role in the recombination process. Therefore, the switch opening time can have multiple time constants.[39]

In the nonlinear mode, there are gain mechanisms associated with high electric fields which multiply the initial EHPs created by the absorbed photons. Therefore, the number of carriers necessary for closing the switch is only partially supplied by the laser trigger. The rest are created through gain mechanisms. The hypothesized sources of gain in the nonlinear switching mode are band-to-band impact ionization, trap impact ionization, or any process which multiplies carriers when a certain threshold electric field is reached. When the switch is operating in the nonlinear mode, less optical energy is required to trigger the switch than for a switch operating in the linear mode. The minimum optical energy required to activate nonlinear high gain switching decreases as the average electric field increases across the switch. For example, in GaAs as the average electric field varies from 5 to 100 kV/cm, the optical energy necessary for switching decreases from 800 to 1 μJ. However, there is a limit on lowering the optical energy requirement by increasing the voltage across the switch. For example, GaAs can be triggered with optical energy densities of only a few nJ/cm^2 for average electric fields on the order of 40 to 60 kV/cm. Further increases in the electric field, however, do not lower the optical trigger energy threshold. The exact functional dependence between the optical trigger energy and the bias electric field is not completely understood.[40]

The gain mechanisms in the nonlinear switch allow complete switching, even when the optical trigger energy only partially fills the switch area between the contacts, such as a spot of light. When the switch is triggered with spots of light, it has been found that triggering is most efficient near the contacts. With a 0.5 μJ spot of light near the cathode and a 2 to 3 μJ spot near the anode, a GaAs switch can be switched in the nonlinear mode. It is much more difficult to trigger in the center of the switch between the contacts if the spot diameter is small compared to the contact separation.[56] Triggering near a contact does not change the delay and rise times to high gain switching, which implies a mechanism for rapid generation of carriers across the insulating gap. The method of this

carrier transport is such that carriers travel at speeds greater than the saturation velocity. Some estimates show velocities ten times the saturation velocity to traverse a 1.5 cm long switch in 6 ns.[57]

Switching in the nonlinear mode allows a large reduction in the optical trigger energy requirements when compared to the levels required for linear operation.[58] The gain that results in this reduction of the trigger energy affects other factors, such as the delay time between trigger application and switch closure, switch jitter, and the rate at which the switch closes. These switch attributes are no longer controlled by the optical trigger as in linear operation but by the creation of carriers through gain mechanisms. Since all the carriers required for switch closure are not created by the triggering laser, there is a delay time associated with creating the extra carriers through gain mechanisms. This delay time may vary from pulse to pulse. Therefore, the jitter, a measure of the time difference between switch closure from pulse to pulse, is affected and is larger than those in linear switching. This switching delay is inversely related to the average electric field across the switch at the time of activation. The jitter can be affected by fluctuations in the switched voltage, but the jitter is less as the switched voltage is increased. The switching rate is also affected when operating in the nonlinear mode. In the linear mode the closure rate is the rise time of the laser pulse. When the electric field threshold for the nonlinear mode is reached, the closure rate is determined by the avalanche process independent of the laser rise time. This rise time can be significantly shorter than the laser pulse. However, if the laser rise time is faster than the avalanche rise time but the laser amplitude is high enough, the optically generated carriers can dominate and the switch turn-on can be faster than its characteristic avalanche time.

This phenomenon of linear and nonlinear modes is also observed in thyristors. Current rise times in GaAs thyristors (nonlinear mode) are five times smaller than in Si thyristors (linear mode).[59] Also, the turn-on time is shorter in GaAs thyristors than the calculated transit time of carriers traveling across the base layers at saturation velocity. It is believed that internal generation and absorption of photons within the base region are important mechanisms for the fast turn-on.[60]

F. Lock-on

A phenomenon referred to as lock-on is associated with the nonlinear switching mode.[21] Usually a switch opens completely to the applied voltage with a rate determined by the recombination of

carriers when the laser trigger is removed. With lock-on it opens to a characteristic voltage called the lock-on voltage. The switch remains in a conductive state for many recombination times after the optical trigger pulse has ended by "locking-on" to this characteristic voltage. This Zener-like fixed voltage drop across the device after triggering is independent of circuit parameters and the initial bias voltage.[61] The switch current varies with the initial charging voltage and is independent of the optical trigger energy. The current is determined by the lock-on voltage and the resistance of the photoconductive switch, and is limited by the circuit. An example of the voltage across a switch exhibiting lock-on is shown in Figure II-4.

Lock-on is essentially an unusual form of "controlled" breakdown at significantly lower electric fields (10-30 kV/cm) than avalanche breakdown. It is also less destructive.[62] These electric field levels cannot be reached in the closed state of the switch, since the load is dropping most of the applied voltage. As the switch begins to open and starts dropping more of the applied voltage, the electric field level will eventually exceed the characteristic lock-on field. Thus, when the switch begins to open, and the critical electric field is exceeded, the switch resistance stops rising or even begins to fall, eventually settling to a resistance $R = V_{lock\text{-}on}/I_{circuit}$ as does a Zener diode. The open switch resistance returns when the electric field drops below the lock-on field. Consistent recovery is observed after 1 ms. The fastest single pulse recovery observed is 30 ns. Slow recovery is always observed from nonlinear, high electric field switching, provided current pulse amplitudes and widths are below the point of catastrophic damage. Thermal memory may be a problem for fast recovery of nonlinear switches, although cooling of samples to 77 K achieved little change in the lock-on field, even when the optical triggering threshold changed by three orders of magnitude.[39]

The lock-on voltage is not the threshold voltage required to initiate nonlinear switching. The threshold voltage is indirectly related to the optical trigger energy and is always larger than the lock-on voltage. Although the lock-on electric field has been found to be relatively independent of the switch length (lengths of 1 to 33.8 mm produce lock-on fields of 3.6 to 4.5 kV/cm), the initial voltage across the switch (2.5 to 4.0 kV charging, 1.9 kV lock-on), and the optical trigger energy, it has been found to be material dependent. Lock-on has not been observed in Si but has been observed in several varieties of GaAs, InP, and ZnSe switches,[61,63,64] with observed lock-on electric fields ranging from

3.6 to 14.4 kV/cm. The lock-on electric field is also dependent on the type and density of defects in the switch material. For example, in GaAs compensated with EL2 traps the lock-on electric field is in the range of 3.6 to 4.5 kV/cm whereas, for Cr:GaAs the lock-on electric field is between 8 and 9.5 kV/cm. It has been observed that the larger the number of defects in the semiconductor, the higher is the lock-on field. Therefore, higher resistivity material which has more defects shows a higher lock-on electric field than does lower resistivity material. Observations indicate that materials with longer mean-free paths have lower lock-on electric fields, which is consistent with avalanche carrier generation.[12,61]

G. Filaments

When a switch made with direct bandgap semiconductors in the nonlinear or lock-on mode is operated, one or more current filaments are always observed.[65] The observations of the filaments are usually made using infrared radiation measurements. Filaments force large currents in a small cross-sectional area, which increases the current density (10^6 A/cm^2), the impedance of the switch, and damage to the switch especially at the contacts. The large number of carriers recombining in these filamentary regions emit the bandgap radiation. For GaAs the carrier recombination radiation is 1.4 eV photons, which corresponds to 875 nm or infrared radiation. The wavelength of light observed from these filamentary structures is around 880 nm, with the discrepancy attributed to the absorption of the shorter wavelengths as the light travels through the material. If these filamentary structures are caused by surface flashover, their emitted spectrum would have a strong component of blue to UV radiation. Except for occasional bright spots near the contacts, filamentary light is completely invisible to the naked eye and is totally blocked with an infrared absorbing filter. The carrier densities inside the filaments are estimated by the observed light intensity to be roughly at least 10^{17} cm^{-3}.[22]

Although the formation mechanism of filaments is not completely understood, many qualitative and behavioral observations have been made.[57] Filaments do not remain fixed in one area of the switch, but instead they move around in the switch from pulse to pulse, often showing more than one channel. Abruptly ending filaments have been observed and are considered evidence of filaments branching more deeply into the switch. Their upper size limit ranges from diameters of 50 to 300 μm. The speed of a filament tip as it moves across the switch when it is first being formed has been estimated at 1-3 x10^9 cm/s.[66] It has also been observed that there is significant current growth after the

filament has crossed the insulating region between the contacts. Increasing the bias voltage or optical intensity produces an increase in the number of filaments per shot. For large optical trigger intensities applied uniformly between the contacts, the device is uniformly filled with filaments. The spatial behavior of the filaments is affected by the spatial characteristics of the applied illumination.[23,56] If a narrow stripe instead of uniform light between the contacts is used to activate the high gain mode, the filament follows the striped light source even when it is more than 45 deg off axis of the average electric field. If a 1.0 mm diameter spot of light is applied near contacts separated by $\approx$ 1.5 cm, the filaments intersect the spot. Although, if the optical energy is high enough, the filaments do not intersect the region of optical illumination. Figure II-5 taken from[57] shows two filament locations being controlled by the location of two laser spots. To put all of these qualitative observations in the proper perspective, it should be noted that recombination radiation is strongly self-absorbed in the GaAs wafer. Therefore, only filaments within a few micrometers of the surface can be observed and characterized by viewing the infrared radiation.

Damage caused by the current filaments is concentrated near the contacts and accumulates as successive filaments move to new positions. Observations reveal more damage near the contacts, with the most damage occurring near the positive contact. Damage occurs to both the switch contact metallization and the insulating region of the semiconductor near the contact boundary. Normally there is very little damage observed in the center of the switch. Contact damage may be caused by poor adherence of the contact to the semiconductor, large electrical potential barriers at the contact interface, high current densities due to current pinching of filaments, and elevated instantaneous temperatures. Introducing a region of increased conductivity under the contacts reduces the current pinching effect near the boundary. However, a consequence of ion implanting conductive layers below the contacts of the switch is an increase in the amount of laser energy or electric field necessary to activate the switch.[57]

H. Electric Field Nonuniformities

There has been experimental work in the measurement of the electric field profile during the triggering of the switches. Donaldson and Kingsley[16] used an electro-optic crystal to make measurements of switch surface electric fields during switch operation. The measurements are made by

placing an electro-optic crystal in the vicinity of the switch. The birefringence of the electro-optic crystal is modified by the stray electric fields on the surface of the switch. The electric field is measured by probing the electro-optic crystal with a fast, polarized optical pulse and monitoring the change in polarization. It should be emphasized that this technique measures only the surface electric fields of the switch and not the electric fields in the bulk. Electric field measurements have been done on bulk switches which are made of blocks of intrinsic GaAs contacted at either end. The circular contacts were perforated to allow the laser trigger accessibility to the switch. The electric field collapses uniformly near the anode (ground) of the switch, but it has areas of significant enhancement near the cathode (high negative voltage). The enhancement can be alleviated somewhat at the perforated region of the contact by illuminating more light through the cathode, but the collapse is never as complete as at the anode. The electric field which is enhanced at the cathode is also seen to collapse most slowly there. In general, switching efficiency decreases as the electric field increases. If only a single side is illuminated, the electric field collapses from the illuminated contact to the nonilluminated contact as the region of conduction propagates from the region of photogeneration to the nonilluminated contact. For illumination on both-sides, the electric field collapses more quickly and to a lower final value than for single-sided illumination.[20]

The electric field enhancement at the contacts is sensitive to the boundary conditions. If neither contact is carrier injecting, the switches suffer from extreme enhancement of the electric fields at both contacts during switching. If an n-i-n structure is used, there is a forward biased junction at the cathode and the enhancement of the electric field at the cathode virtually disappears. If a p-i-n structure is used, the p-type contact provides a forward biased junction at the anode and the enhancement of the electric field at the anode is reduced, though not as significantly as at the cathode (4.0 kV/cm reduction in a 14.0 kV/cm peak).[15]

Electric field measurements have also been performed on a coplanar device by using the electro-optic crystal technique. The coplanar device has both contacts on the same side and the electric field is measured on the side opposite the contacts. Below the threshold for lock-on, the average electric field along a line parallel to the contacts and through the center of the switch shows a rapid collapse followed by a rapid recovery for a few hundred picoseconds followed by a slower final recovery to the bias

voltage in approximately 5 ns. Above lock-on, the temporal development of the average electric fields is much more complicated. The average electric field initially behaves as it did in the below lock-on threshold case with a rapid collapse and a rapid initial recovery. About 1 ns after the application of the peak illumination, the collapse begins again. This second collapse of the average electric field is much slower than the first optically induced collapse. It is also oscillatory in nature. The two-dimensional structure of the electric field (Figure II-6) shows an initial uniform collapse of the electric field to the contacts. After complete switching has occurred, the electric field enhancement increases at the cathode (negative high voltage contact) to levels above the initial bias electric field. As lock-on commences, the electric field enhancement at the cathode extends to the anode (ground) as a region of low electric field or high conductivity extends from the anode to the cathode.[67]

Schoenbach et al. have made measurements of the electric fields of a GaAs (Si:Cu) BOSS[18] and semi-insulating GaAs[19] by making optical absorption measurements near the band gap of GaAs. The BOSS is a specific type of semiconductor switch. High electric fields can reduce the band gap of GaAs (Franz-Keldysh effect), which increases the amount of absorption of near band-gap laser energy. Large areas of absorption can then be interpreted as regions of high electric field. It is noted that large temperatures and large carrier densities ($>10^{16}$ cm^{-3}) also decrease the band gap of GaAs. When only a voltage pulse is applied to the switch with no laser activation, electric field enhancement is observed near the cathode throughout the voltage pulse (Figure II-7a). There is also evidence of temperature effects in the absorption measurements, given the presence of a reduced absorption region near the cathode after the voltage pulse has ended. Increasing the magnitude of the applied voltage (with still no optical trigger) increases the electric field enhancement at the cathode. As the voltage level is increased, enhancement begins to appear near the anode as well (electric field average $\approx$ 24.5 kV/cm across switch). Eventually the two enhancement regions begin to merge. When the voltage pulse is applied and the switch is triggered with 2 mJ/cm^2 of light energy density, the electric field becomes uniform throughout the switch for the duration of the voltage pulse. If 0.16 mJ/cm^2 of light energy density is applied after the application of the voltage pulse, a temporary homogenization of the switch absorption occurs at the time of laser application. After the application of the laser pulse, an absorption pattern has reformed (Figure II-7b). The increased joule dissipation in the regions of higher electric fields and the

corresponding local increase in the temperature caused the patterns to stay long after the switch voltage was set to zero. Therefore, high laser intensities are necessary to eliminate electric field inhomogeneities in the switch and to allow the switch to return quickly to its undisturbed state. Laser activation at low intensities caused the switch to conduct, but it led to a strong distortion of the electric field and temperature distribution, an effect evident several hundred nanoseconds after the switch current ceased.

The electro-absorption measurements on semi-insulating GaAs switches[65] show that for low applied voltages operating in the linear mode, a 100 μm cathode layer with high electric field intensity occurs. At higher voltages, absorption bands at both the cathode and the anode are observed after laser activation. Typical measurements of the electric fields are shown in Figure II-8.[19] Calibration measurements indicate that the magnitudes of the electric fields in the absorption bands exceed 50 kV/cm. The reasons for enhancement at the two contacts differ. The cathode layer is considered voltage dependent, since it decays when the voltage is removed from the switch. The anode absorption structure is current related, since reducing the intensity of the light activation at constant applied voltage causes the structure in the anode region to fade away, and in the case of linear switch operation the anode pattern fades away with diminishing current.

When the current after laser activation is recorded, the lock-on current is always connected with the occurrence of at least one filament. This is possibly caused by collisional ionization in the high electric field domain. The filament shorts out the high electric field regions.

I. Previous Modeling

As the modeling work has progressed on the GaAs photoconductive switch, it has remained mostly one-dimensional.[68] Most models have been either analytic phenomenological formulations or standard drift-diffusion models differing by the extra effects added. There have also been other types of modeling done, such as an electromagnetic transmission line model. In the transmission line model, a coplanar switch is represented as a distributed circuit consisting of a collection of resistors, capacitors, and inductors whose values vary over the length of the switch.[69] The modeling efforts have recognized different processes as important in explaining the lock-on and filament formation phenomena observed. These mechanisms include avalanche injection,[70] electric field dependent trap filling,[71] metastable impact ionization,[72] localized impact ionization,[73] and double-injection and carrier trapping.[74-76]

A one-dimensional time-dependent drift-diffusion model of semi-insulating GaAs switches including negative differential resistance and impact ionization[77] was used to show the enhancement of the electric field near the cathode as the switch closed. The electric field enhancement at the cathode was shown to be a consequence of the negative differential resistance.

A steady state, one-dimensional model with no recombination, drift limited, regional approximation, and avalanche injection[70] also shows the negative differential resistance effect as a necessary condition for the transition of the device to the lock-on state. In the model, the switch has been assumed to be pulse triggered, either electrically or optically, in order that it is in the steady state conduction mode. The conduction mode is the result of double injection of holes at the anode and electrons at the cathode. With this assumption, the device is divided into three regions. The first region near the cathode has a linear velocity - electric field relationship up to the velocity saturation regime. The second region, which is the bulk, consists of constant densities of electrons and holes with a saturated electron velocity. The third is a high electric field avalanching region close to the anode boundary, whose existence is the result of a theorized formation of a localized static Gunn domain. With these assumptions, electric field lock-on threshold values were predicted and were shown to be dependent on the presence of Gunn domains.

Avalanche injection is a mechanism used to explain the injection of holes at the anode, even though the anode is biased to block the injection of holes. Avalanche injection is a form of virtual injection near a contact. It is a mechanism for injecting carriers from a nonohmic contact. If a high electric field region is close to a contact and is large enough to produce carriers through impact ionization, it becomes an alternative source of carriers near the contact. For example, in n-i-n structures the anode is not a hole injecting contact. If a high electric field near the anode creates holes through impact ionization, however, there is hole injection effectively from the virtual contact to the bulk of the device, even though the contact itself does not inject holes.

Electric field dependent trap filling is a mechanism that has been used to explain the voltage threshold observed for lock-on, the voltage dependent delay observed between the beginning of optical illumination and the onset of switching, and the avalanche-like increase of current observed as the optical illumination is applied.[71] The model which examined this effect is a drift-diffusion model with

spatially dependent optical intensity, impact ionization and dynamic trapping. In dynamic trapping, an increasing electric field is assumed to increase the trapping cross sections. The enhanced level of charge trapping suppresses the photocurrent until all the traps are filled. Once all of the traps are filled, the photocurrent rises sharply if the optical pulse is still on. The model also suggested that impact ionization of valence electrons caused by electric field enhancement through negative differential resistance may not be the dominant switching mechanism in fast, high-voltage GaAs switches. Their calculations show carrier trapping and recombination quenching intrinsic photoavalanching. Therefore, avalanching is effectively producing no new carriers to affect the current through the switch.

Many of the models explore mechanisms which enhance the electric field in order that intrinsic impact ionization becomes a viable process, even when biasing the switch at lower lock-on electric field levels. Other theories of lock-on are based on a process occurring at a lower electric field threshold nearer the lock-on electric field. One such process is metastable impact ionization of EL2 traps. This process has been suggested as an alternative to intrinsic impact ionization for the carrier generation deemed necessary for lock-on at lower electric fields.[72] The lower electric field threshold for trap impact ionization compared to intrinsic impact ionization is a consequence of only a single carrier being produced by ionization (instead of an EHP), of EL2 being in the center of the bandgap (thus half the band gap energy), and of thermally assisted tunneling and Poole-Frenkel barrier lowering at the high electric fields. Light applied to the material is theorized to provide optical "bleaching" of EL2 and related states into metastable states. The "bleaching" of EL2 causes an increase in the mean-free path for optical phonon emission and, consequently, a decrease in the electric field level for avalanche. This electric field impact ionization process occurs at lower electric field thresholds than does intrinsic impact ionization and, consequently, electric field thresholds where lock-on is observed.

One approach to a quasi-two-dimensional model which has been done by Capps et al.[73] is coupling a one-dimensional drift-diffusion filament model with a one-dimensional drift diffusion bulk model in the form of a cylinder. The center of the cylinder contains the filament model, and the region surrounding the inner cylinder is the bulk model. They are coupled only by the axial electric field and the boundary conditions. An electric field enhancement factor is also introduced at the cathode end of the filament model. As the optical pulse is applied, the increased enhancement at the cathode of the

filament portion of the model is sufficient to generate carriers through impact ionization. These extra carriers eventually form an ionization front that moves toward the anode trailing a large density of carriers behind the front. Therefore, filament formation is initiated by localized impact ionization near a electric field enhanced point in the switch which eventually forms an ionization front.

Other models theorize on qualitative aspects of the lock-on steady state portion of the switching cycle and the on state of the switch. Using a basic drift-diffusion equation system with Poisson's equation, coupled to radiation transport equations, and including impact ionization,[74] they come to the conclusion that double injection sustains the lock-on mode. Through electron injection at the cathode and hole injection at the anode, or double injection, the trap sights near the contacts become completely filled and charged.[75] Eventually, with the large injection of carriers, traps in the center of the switch are filled in addition to the traps near the contacts. With no traps to reduce the carrier level in the switch, the carrier level begins to increase. When there is a large enough density of mobile carriers, a solid-state plasma forms, increasing the current through the switch sharply. It is recognized that free carrier sources other than double injection are necessary to completely fill the traps.

In the modeling to date, the investigators recognized the inadequacy of their one-dimensional models to completely explain all the phenomena associated with the photoconductive semiconductor switch discussed in this chapter. Therefore, it is necessary to extend the modeling of photoconductive high power semiconductor switches into two dimensions to more completely understand switch behavior.

Modeling specific to the GaAs(Si:Cu) BOSS, which is emphasized in this work, has also covered only one spatial dimension. Early work has been done with a zero-dimensional model which emphasized the kinetics of a BOSS.[78] Later, a one-dimensional model was developed to explore current transport and the phenomena of lock-on.[79] This work extends the earlier efforts to two dimensions, which allows enhancement of the electric field through switch geometry and the study of the consequences of spatial nonuniformity of device parameters, such as carrier flow and electric field on device performance.

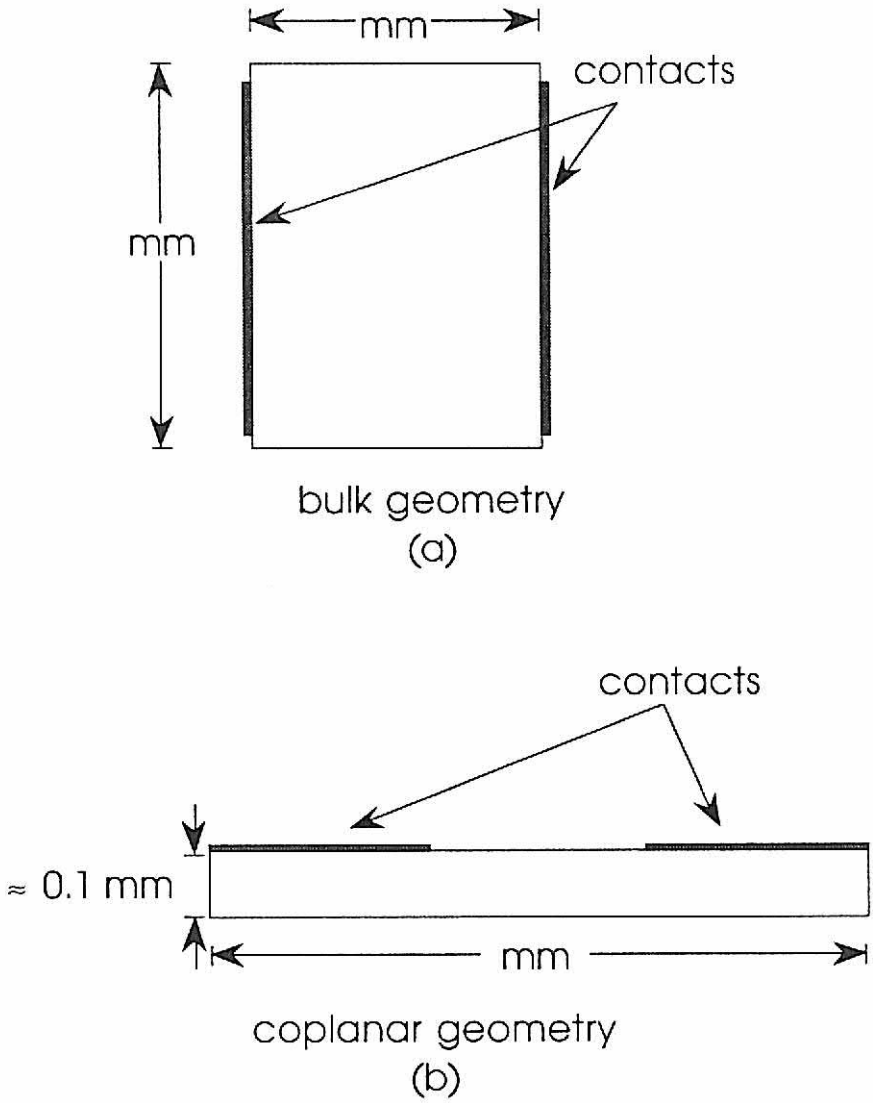

Figure II-1. Two types of PCSS geometries are the bulk and coplanar geometries. (a) The bulk geometry has contacts on either side of the semiconductor, while (b) for the coplanar geometry the contacts are on the same side or plane. The typical device dimensions are millimeters.

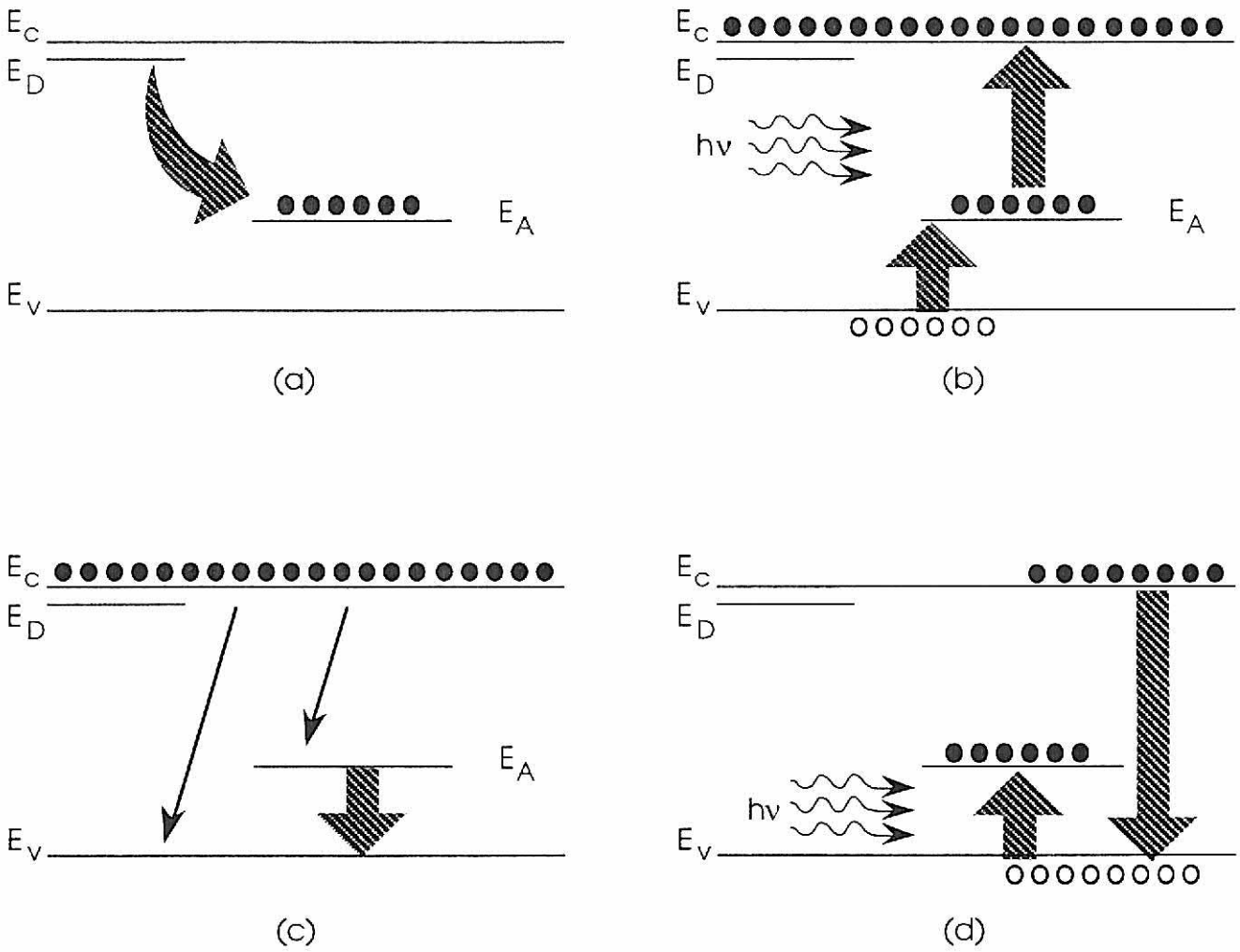

Figure II-2. Operation of the BOSS. (a) The deep acceptors are compensated by shallow donors, which gives the switch a high dark resistance and a large voltage hold-off. (b) A photon energy of $h\nu > E_C - E_A$ is applied to the switch, which prompts electron emission from compensated acceptors and hole emission from unionized acceptors. The large number of carriers reduce the resistivity and close the switch. (c) The switch stays closed after initial recombination of excess holes given the small electron capture cross section. (d) The switch is opened by applying a photon energy $h\nu$ such that $E_C - E_A > h\nu > E_A - E_V$. A photon in this energy range causes hole emission at the deep acceptor level, but not electron emission. So, the conduction band electrons now have a recombination path. The subsequent reduction of free carriers opens the switch.

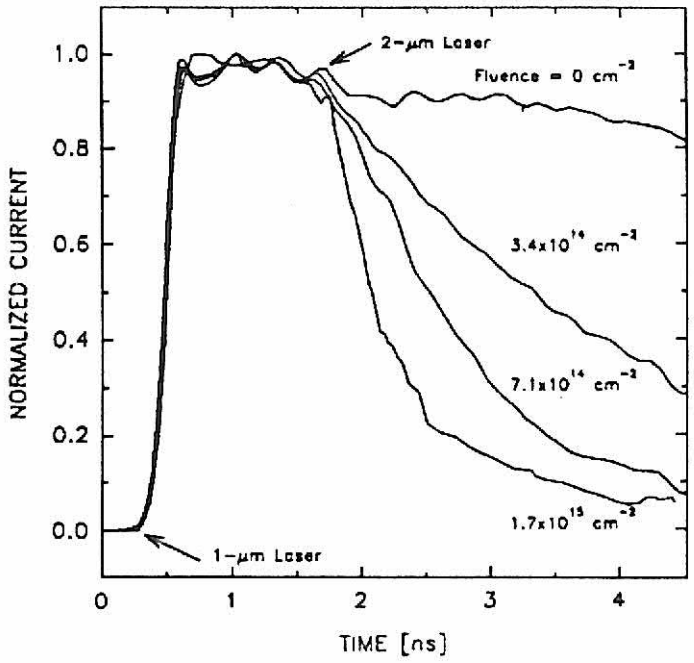

Figure II-3. From Stoudt et al.[54] A current vs. time plot showing the operation of a BOSS. The pulse width of the current waveform is controlled by a laser pulse instead of exclusively by electron-hole recombination. A 1.06 μm laser pulse closes the switch and a 2.13 μm laser pulse opens the switch. The opening time is shown to be dependent on the mid-gap recombination center density which is controlled by neutron irradiation of the sample.

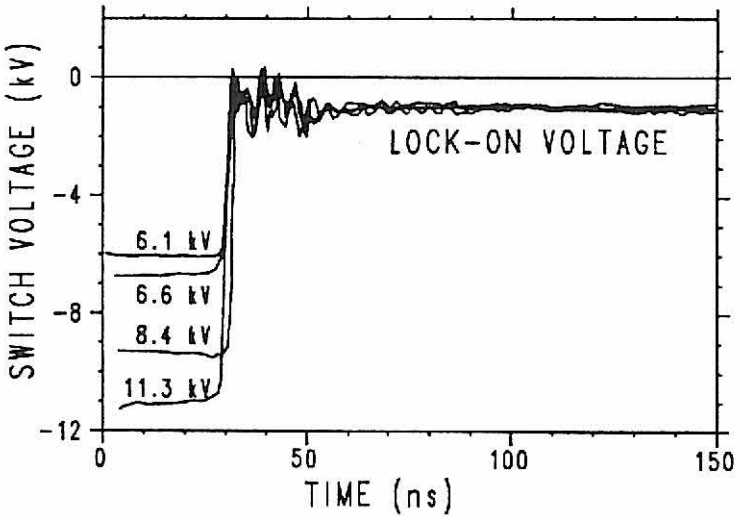

Figure II-4. From Loubriel et al.[61] A voltage vs. time plot showing a lock-on voltage of ≈ 1 kV. The switch should have returned to its original value in 10-20 ns (as determined by its linear operation) but instead is locking on to a voltage. This lock-on voltage is shown to be independent of the switch voltage.

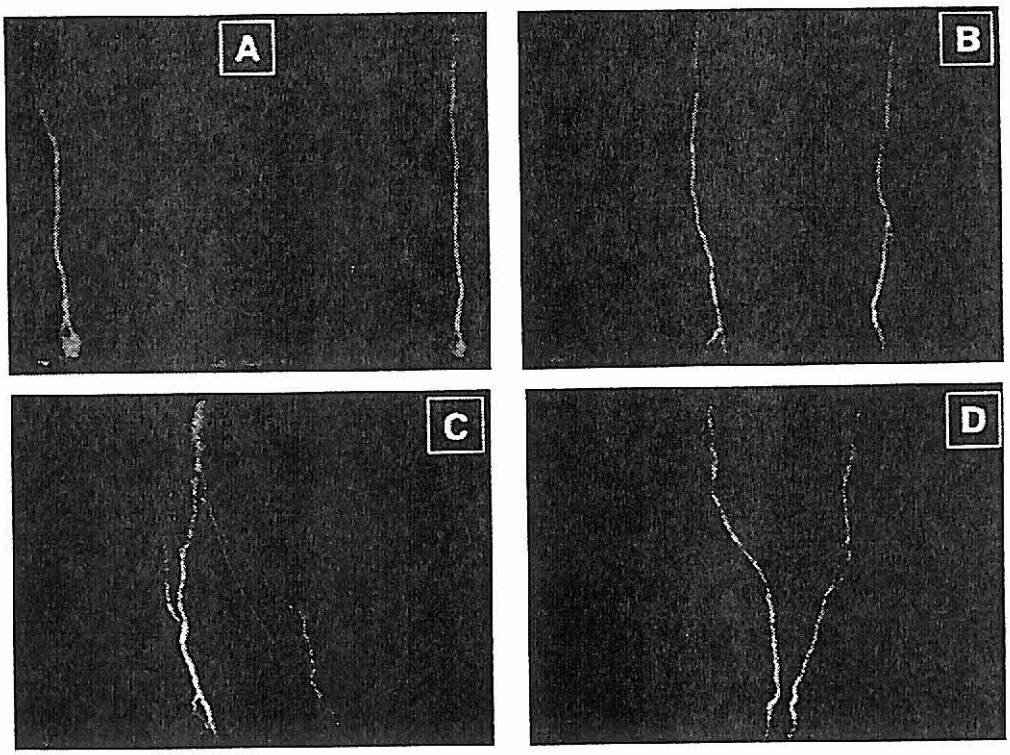

Figure II-5. From Zutavern et al.[57] The typical shape of filaments observed when infrared radiation measurements are used. The illustration demonstrates the control of filament formation location when a spot of laser light is used to trigger the switch. The filaments form near the laser spots, and the laser spots are being brought closer together from (a) to (d).

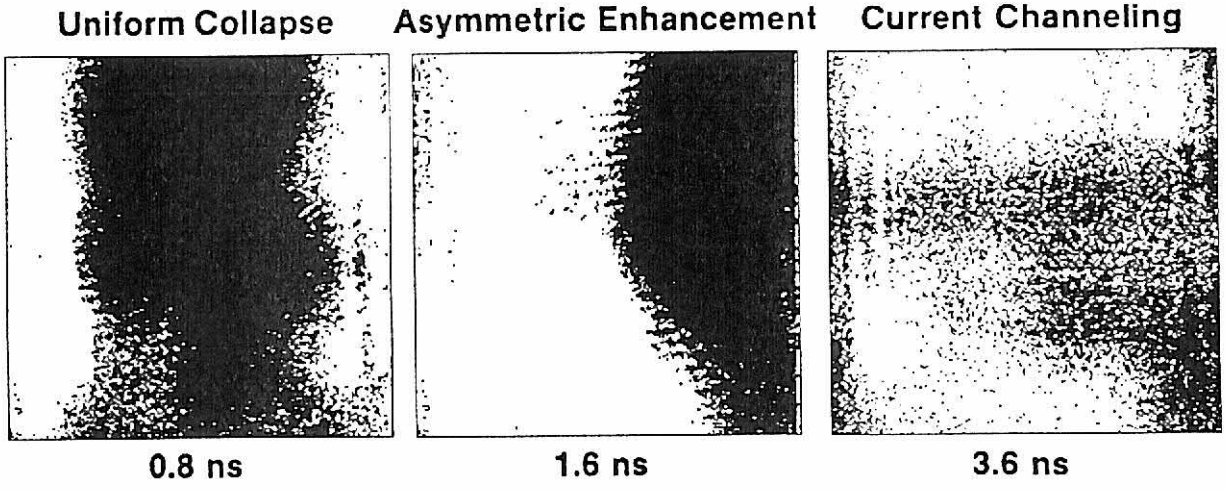

Figure II-6. From Donaldson et al.[67] Time evolution of the surface electric field of a coplanar geometry photoconductive switch. The right of each picture is the grounded anode and to the left is a high negative voltage cathode. The black regions are surface electric fields less than 16 kV/cm. The white regions are electric fields greater than 16 kV/cm.

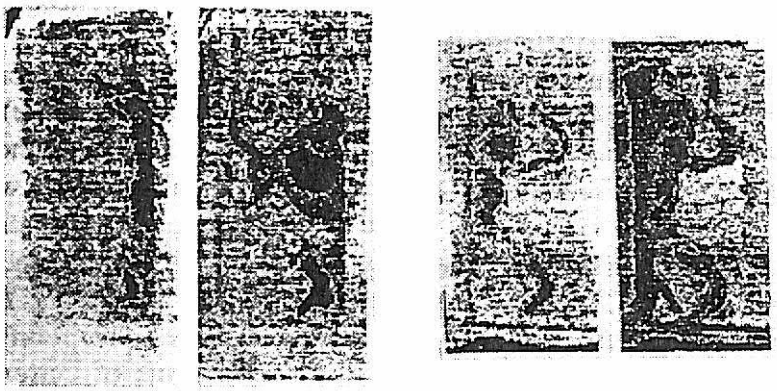

Figure II-7. From Schoenbach et al.[18] Time evolution of absorption measurements of a coplanar geometry BOSS switch. The right of each picture is the grounded cathode and the left is the anode. The black regions are regions of high absorption. (a) Electric field enhancement occurs without laser activation with 2.19 kV and 2.94 kV applied across a 1.2 mm coplanar gap between contacts. (b) Electric field enhancement also occurs with laser application (0.16 mJ/cm^2 with an applied voltage 3 kV).

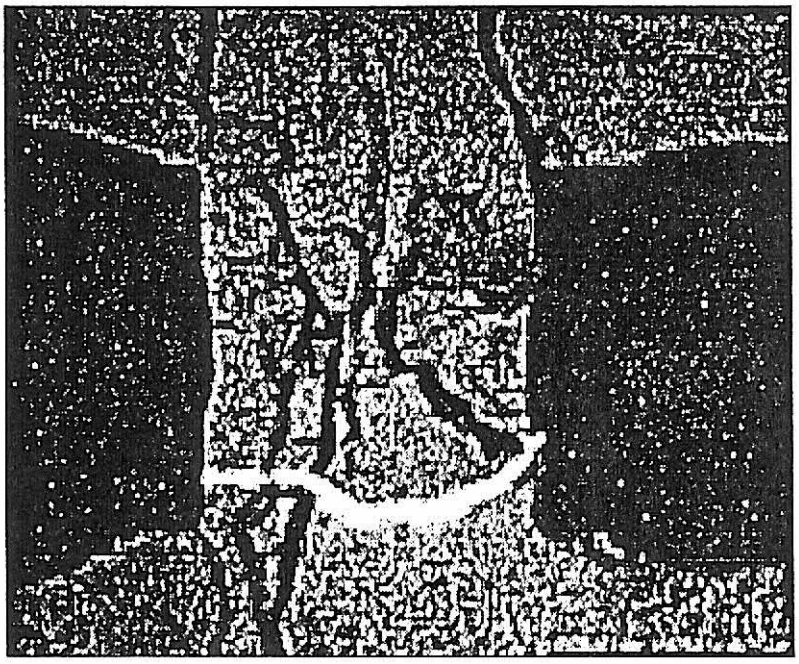

Figure II-8. From Kenney et al.[19] The results of an absorption measurement of a high power switch during activation. The dark bands are electric field enhancement, and the light band is a filament which is always present when the switch is triggered in the nonlinear mode. The filament shorts out the field bands that it crosses.

III. METHOD

A two-dimensional time-dependent computer model has been developed to investigate a variety of PCSSs. The two types of switches that will be explored in detail are GaAs doped with Si and Cu, which is a specific type of BOSS, and intrinsic GaAs. The model was initially formulated with a GaAs(Si:Cu) BOSS in mind and was later generalized to semi-insulating GaAs. The basic operation of a BOSS is detailed in Chapter II.

The general flow of the model is as follows. The continuity equations for electrons, holes and impurities (Eqs. (III.1) - (III.4)), the energy equation for the lattice (Eq. (III.5)), and the steady-state radiation density transport equation (Eq. (III.6)) are solved on a rectangular or cylindrical mesh having variable spacing. Derivatives are formulated using finite differencing. Flux conservative donor cell techniques are used to approximate the drift and diffusion terms. The electron and hole fluxes are integrated over the contacts to calculate the conduction current through the device. A circuit equation is included to provide the voltage across the device. Poisson's equation (Eq. (III.7)) is solved for the electric field by using an implicit successive-over-relaxation (SOR) technique.[80] These procedures are repeated for the next time step. Referring to Table I for the symbol definitions, the pertinent equations are

$$\frac{d}{dt}[n_e] = -\nabla\cdot\left[n_e\vec{v}_e - D_e\nabla n_e\right] - \sigma v_{th} n_e N_A - \sigma v_{th} n_e N_D^+ - k_r n_e n_p$$
$$+ \sigma_0\Phi_{on}N_D + \sigma_0\Phi_{off}N_D + \sigma_0\Phi_{on}N_A^-$$
$$+ \sigma_t\left|\vec{v}_e\right| n_e N_A^- + \sigma_t\left|\vec{v}_e\right| n_e N_D$$
$$+ \alpha_i\left|\vec{E}\right|\mu_e n_e + \alpha_i\left|\vec{E}\right|\mu_p n_p + n_i^2 k_r + \frac{n_\phi}{\tau_\phi} \qquad \text{(III.1)}$$

$$\frac{d}{dt}[n_p] = -\nabla\cdot\left[n_p\vec{v}_p - D_p\nabla n_p\right] - \sigma v_{th} n_p N_A^- - \sigma v_{th} n_p N_D - k_r n_e n_p$$
$$+ \sigma_0\Phi_{off}N_A$$
$$+ \sigma_t\left|\vec{v}_e\right| n_e N_A^- + \sigma_t\left|\vec{v}_e\right| n_e N_D$$
$$+ \alpha_i\left|\vec{E}\right|\mu_e n_e + \alpha_i\left|\vec{E}\right|\mu_p n_p + n_i^2 k_r + \frac{n_\phi}{\tau_\phi} \qquad \text{(III.2)}$$

$$\frac{d}{dt}[N_A] = \sigma v_{th} n_p N_A^- - \sigma v_{th} n_e N_A + \sigma_o \Phi_{on} N_A^- - \sigma_o \Phi_{off} N_A + \sigma_t \left| \vec{v}_e \right| n_e N_A^- \quad \text{(III.3)}$$

$$\frac{d}{dt}[N_D] = \sigma v_{th} n_e N_D^+ - \sigma v_{th} n_p N_D - \sigma_o \Phi_{on} N_D - \sigma_o \Phi_{off} N_D - \sigma_t \left| \vec{v}_e \right| n_e N_D \quad \text{(III.4)}$$

$$\frac{d}{dt}\left[\rho C_p T_{lat}\right] = -\nabla \cdot \left[\kappa \nabla T_{lat}\right] + \vec{j} \cdot \vec{E} \quad \text{(III.5)}$$

$$\frac{d}{dt}[n_\phi] = D_\phi \nabla^2 n_\phi + n_e n_p k_r - \frac{n_\phi}{\tau_\phi} = 0 \quad \text{(III.6)}$$

$$\left\{\frac{\nabla \varepsilon_r}{\varepsilon_r}\right\} V(t+\Delta t) + \nabla^2 V(t+\Delta t) = -\frac{1}{\varepsilon_o \varepsilon_r}\left\{\rho_o(t) + \Delta t \frac{d\rho_o(t+\Delta t)}{dt}\right\} \quad \text{(III.7)}$$

$$\rho_o = q\left\{ n_p - n_e + N_{Si}^+ + N_{EL2}^+ + N_{EL5}^+ - N_{Cu_B}^- - N_{Cu_A}^- - N_{RC}^- \right\} \quad \text{(III.8)}$$

The rate equations (Eqs. (III.1) - (III.4)) are written for generic donor and acceptor traps which makes the formalism applicable to a variety of PCSS material. Keeping the GaAs(Si:Cu) BOSS in mind, the acceptors in the model are Cu_A and Cu_B, the donors are Si, EL2, and EL5. The band diagram for the material is shown in Figure III-1(a). Given that Si is a shallow donor, it is assumed to be completely ionized at all times at room temperature. Therefore, the rate equations do not include silicon. All of the other impurities trap both electrons and holes as shown in Figure III-1(b). Also shown in the figure is band-to-band recombination which with the impurity trapping and Auger recombination are all the recombination mechanisms of the model.

As with other materials with satellite valleys in their conduction bands, GaAs exhibits negative differential resistance, which makes the carrier velocities a nonlinear function of the electric field. This negative differential resistance can lead to electric field instabilities due to the Gunn effect. In GaAs, the steady-state drift velocity reaches a maximum at an electric field of ≈ 3 kV/cm and then decreases, eventually saturating at high electric fields. Due to saturation of the drift velocity, substantially lower mobilities are obtained at high electric fields. The electron drift velocity v_e

(Eq. (III.9)) in the model is a functional fit of experimental data[81] having a saturation velocity of v_s = 7 x 10^6 cm/s. A comparison of the formalism and the data is shown in Figure III-2. The hole velocity (Eq. (III.10)) is a linear function of the electric field until the saturation velocity is reached ($v_p = 8.0 \times 10^6$ cm/s for $E \geq 2.0 \times 10^4$ V/cm).

$$v_e = v_s \left[\frac{1.0 + \frac{8500\left|\vec{E}\right|}{v_s} - 1.0}{1.0 + 0.051\left(\frac{8500\left|\vec{E}\right|}{v_s}\right)^{2.2}} \right] \quad \text{cm/s} \qquad \text{(III.9)}$$

$$v_p = \mathit{Min}\left\{ 8.0 \times 10^6, 400\left|\vec{E}\right| \right\} \quad \text{cm/s} \qquad \text{(III.10)}$$

Photoionization is the generation of excess carriers when a photon is absorbed by the material. It is incorporated in the model by specifying a laser photon flux Φ for the closing (Φ_{on}) and opening (Φ_{off}) of the switch. The magnitude of the photon flux together with the position of the band energies of the traps relative to the band edges (Figure III-1(a)) determine whether and to what level trap photoionization occurs. If the photon energy applied is less than the trap energy level to the band edges, no photoionization occurs. The magnitude of Φ is directly proportional to the concentration of excess carriers produced. With the BOSS material, two different photon energies are required for a switching cycle. Assuming an on photon flux of 1.1 eV and an off photon flux of 0.7 eV, the on laser flux induces electron and hole emission from all traps as depicted in Figure III-1(c). The off laser flux induces hole emission from CU_A and CU_B, electron and hole emission from EL2 and RC, and electron emission from EL5 as depicted in Figure III-1(d). These laser photon fluxes are varied in time and space in the model. The time dependence is Gaussian (i.e., a functional form of $\Phi = \Phi_o \exp -\{|t-t_o|/\Delta t\}^2)$ for $2\Delta t$ before and after a peak pulse time t_o. A plot of Φ_{on} and Φ_{off} with Δt = 2 ns and applied at 6 ns and 12 ns respectively is shown in Figure III-3.

The two other ionization processes considered are band-to-band impact ionization and trap impact ionization. If the electric field in the switch is of sufficient magnitude, an electron or hole can be accelerated to a sufficiently large kinetic energy that a collision with the an electron in the lattice

or in a trap generates extra carriers. Band-to-band impact ionization occurs when a high energy particle collides with the lattice, imparting enough energy to an electron to excite it from the conduction band to the valence band generating an EHP. The trap impact ionization considered here occurs when a high energy electron collides with either an ionized acceptor or an unionized donor, exciting the extra electron into the valence band. It should be noted that band-to-band impact ionization generates an EHP and, thus, two extra carriers, while trap impact ionization generates only one extra carrier as depicted in Figure III-1(e). Also, band-to-band impact ionization requires more energy than trap impact ionization since the excited particle has to traverse the band gap, and thus larger electric fields are necessary for it to be a significant process.

The band-to-band impact ionization coefficient α_i (Eq. (III.11)) is approximated as a function of the local electric field and is a functional fit of data from Sze.[81]

$$\alpha_i = e^{16} \exp\left[\frac{-2.16 \times 10^6}{\left|\vec{E}\right|}\right] \quad cm^{-1} \tag{III.11}$$

Using the expressions for v_e and α_i, a plot of $\alpha_i v_e$ as a function of electric field is shown in Figure III-4, where $\alpha_i v_e$ represents the change of the electron density per unit of time. When does band-to-band impact ionization become an important process? The plot shows that a percent change per nanosecond of the electron density requires an electric field of 1.38×10^5 V/cm.

The trap impact ionization cross section σ_t has an exponential dependence (Eq. (III.12)) on the electric field.[82]

$$\sigma_t = \sigma_{to} \exp\left[\frac{-E_t}{\left|\vec{E}\right|}\right] \quad cm^2 \tag{III.12}$$

The characteristic electric field E_t for each trap is determined by the relative position of the trap energy level to the band edges. The maximum cross section σ_{to} is chosen for effect with a typical value around 1.0×10^{-14} cm^2. The characteristic electric field values are orders of magnitudes lower

than the 1.38×10^5 V/cm electric field strengths required for band-to-band impact ionization to become a contributing process.

All of the electron and hole recombination and generation processes discussed are summarized in Table II as well as the trapping cross sections σ, photoionization cross sections σ_o, and proportionality constants. The work of Ko et al.[78] is the basis for many of the constants. The recombination coefficient cited is for intrinsic GaAs and differs from the value used in the simulations, which is $k_r = 7 \times 10^{-6}$ cm^3/s for most of the GaAs(Si:Cu) results as opposed to 7×10^{-10} cm^3/s for the intrinsic GaAs results. To open at subnanosecond time scales, the recombination rate coefficient has been chosen as an effective recombination rate rather than the intrinsic recombination rate cited. Stoudt et al.[54] have shown that neutron-irradiated material reduces the opening time of the switch and that the neutron irradiation increased the density of a recombination center. Thus the recombination rate coefficient used in this model reflects the recombination rates due to processes such as recombination centers in the material as well as the intrinsic recombination rate cited in Ko.[78]

The lattice energy conservation equation (Eq. (III.5)) includes thermal conduction and joule heating used to obtain the lattice temperature T_{lat}. Given the fast energy relaxation times of electrons and holes ($\tau_e \approx \tau_h \approx 10^{-12}$ s) compared to the simulation times of interest (10s ns), the electron and hole temperatures will differ little from the lattice temperature. The thermal conductivity $\mathcal{K}$ is assumed to be spatially uniform at 0.46 J/cm-s-K. The specific heat is 0.35 J/g-K, and the density ρ_{GaAs} is 5.32 g-cm^{-3}. The temperature of all boundaries was set to 300 K. The thermal velocity (Eq. (III.13)) and the intrinsic carrier density n_i (Eq. (III.14)) are functions of the lattice temperature. The intrinsic carrier concentration is used in the thermal recombination and generation terms, and the thermal velocity is used in the trapping terms of the continuity equations. The intrinsic carrier density n_i is a functional fit of data from Sze.[81]

$$v_{th} = \sqrt{\frac{8}{\pi}\frac{kT_{lat}}{m^*}} \quad \text{cm/s} \tag{III.13}$$

$$n_i = 10^{16} T_{lat}^{1.5} \exp\left[\frac{-9300}{T_{lat}}\right] \quad \text{cm}^{-3} \tag{III.14}$$

The voltage drop V_S across the switch is obtained by using the circuit shown in Figure III-5, where the photoconductive semiconductor switch is modeled as a resistor in parallel with a capacitor. A load resistor and an inductor are in series with the switch. The particle current through the switch is obtained by integrating the electron flux ϕ_e collected at the anode and the hole flux ϕ_p collected at the cathode. The total switch current I_S shown in (Eq. (III.15)) includes the particle current and the displacement current. Specifically at the anode only electron drift into the contact is allowed, and at the cathode only collection of holes through drift is allowed. The displacement current is calculated at both contacts. The displacement current derivative is calculated temporally by finite differencing of values separated by ten time steps . The current I_S is used to determine the resistance of the switch (Eq. (III.16)).

$$I_s = \int_{\text{anode}} \left[\phi_e + \varepsilon \frac{d\vec{E}}{dt} \right] dA + \int_{\text{cathode}} \left[\phi_p + \varepsilon \frac{d\vec{E}}{dt} \right] dA \qquad \text{(III.15)}$$

$$R_s = \frac{V_s(t)}{I_s} \qquad \text{(III.16)}$$

The temporal development of the voltage across the switch V_S and the current through the switch I are calculated from the integration of the circuit equations (Eqs. (III.17) - (III.19)). The updated values are given in Eqs. (III.20) - (III.22).

$$V_s = V - V_l - L\frac{dI}{dt} \qquad \text{(III.17)}$$

$$V_s = \left[I - C \frac{dV_s}{dt} \right] R_s \qquad \text{(III.18)}$$

$$V_l = IR_l \qquad \text{(III.19)}$$

$$I(t + \Delta t) = [I(t) + V - V_l(t) - V_s(t)] \frac{\Delta t}{L} \qquad \text{(III.20)}$$

$$V_s(t + \Delta t) = \frac{\Delta t}{C} I(t) + \left[1 - \frac{\Delta t}{R_s C} \right] V_s(t) \qquad \text{(III.21)}$$

$$V_l(t + \Delta t) = I(t + \Delta t)\, R_l \qquad \text{(III.22)}$$

Carrier injection is modeled at the anode and cathode. The process begins by calculating the total current (Eq. (III.15)) as determined by integrating the electron, hole, and displacement fluxes across the contacts. The level of electron flux injected through the cathode and the level of hole flux injected at the anode are determined by applying current continuity at the contacts. The total current minus the amount of current leaving is the amount of injected current necessary to keep current continuity at the anode and cathode boundaries. Taking the cathode as an example, the injected electron current is determined by subtracting the current due to holes drifting out of the device and the displacement current at the contact from the total current. This injected electron current is then converted into an electron flux with the option of nonuniform injection being proportional to the electric field.

The time step (Eq. (III.23)) is chosen to limit the fractional amount that E, ρ, n_e, or n_p can change during each time step, and also by the Courant condition which is usually less stringent than the previous limitations.

$$\Delta t = \underset{i\ j}{Min}\left[\mathcal{F}_E \frac{E(t)}{E(t) - E(t\text{-}t_o)}[t - t_o],\ \mathcal{F}_\rho \frac{\rho(t)}{\rho(t) - \rho(t - t_o)}[t - t_o],\ \mathcal{F}_n\, n\left\{\frac{dn}{dt}\right\}^{-1},\ \frac{\Delta r}{v_{er}},\ \frac{\Delta z}{v_{ez}} \right]_{i,j} \qquad \text{(III.23)}$$

For the electric field and charge density, past values at time t_o and present values at time t are used to obtain the Δt that is necessary so as not to exceed a maximum desired fractional change $\mathcal{F}$. For the n_e and n_p terms (denoted by n in Eq. (III.23)), the previous derivatives (Eqs. (III.1) and (III.2)) are used. For the Courant condition, Δr and Δz are the dimensions of a cell in the mesh, and v_{er} and v_{ez} are the r and z components of the electron velocity. The hole particle is not used in the Courant condition since its mobility is much lower than the electrons. Also, changes in separate trap densities are not considered, given that n_e or n_p are also changing by the same amount. The final Δt is the minimum of these conditions over all mesh points (i,j). Typical time step values are in the 10^{-12} to 10^{-13} s range.

The model switch geometry is either bulk or coplanar. A cylindrical coordinate system is used for the bulk geometry. A Cartesian coordinate system is used for the two different views of the coplanar geometry. Of the two different views, the side view is used when the BOSS is simulated, and the top view is used when the intrinsic GaAs PCSS is simulated.

Table I. List of Symbols

Symbol	Defined	Unit
C_p	Specific heat	J/K-mol
D_e	Electron diffusion coefficient	cm^2/s
D_p	Hole diffusion coefficient	cm^2/s
D_ϕ	Radiation density diffusion coefficient	cm^2/s
E	Electric field	V/cm
J	Particle current density	A/cm^2
k_r	Band-to-band recombination rate	cm^3/s
K	Thermal conductivity	J/cm-K-s
n_e	Density of free electron	cm^{-3}
n_p	Density of free holes	cm^{-3}
n_i	Intrinsic free electron and hole concentration	cm^{-3}
n_ϕ	Band-to-band recombination radiation density	cm^{-3}
N	Density of impurities or traps	cm^{-3}
N_A	Density of neutral acceptor traps	cm^{-3}
N_A^-	Density of ionized acceptor traps	cm^{-3}
N_D	Density of neutral donor traps	cm^{-3}
N_D^+	Density of ionized donor traps	cm^{-3}
T_{lat}	Absolute temperature of the lattice	K
v_e	Electron carrier velocity	cm/s
v_p	Hole carrier velocity	cm/s
v_s	Saturation velocity	cm/s
v_{th}	Thermal velocity	cm/s
V	Voltage	V
∇	Differential operator	cm^{-1}
α_i	Band-to-band impact ionization rate	cm^{-1}
ε_o	Permittivity of vacuum	F/cm
ε_r	Relative permittivity	-
ν	Frequency of light	s^{-1}
ρ	Density of lattice	cm^{-3}
ρ_o	Charge density	cm^{-3}
Φ	Photon particle flux	$cm^{-2}\text{-}s^{-1}$
σ	Electron or hole capture cross section	cm^2
σ_o	Electron or hole photoionization cross section	cm^2
σ_t	Trap impact ionization cross section	cm^2
τ_ϕ	Radiation density recombination time	s
μ_e	Electron mobility	$cm^2/V\text{-}s$
μ_p	Hole mobility	$cm^2/V\text{-}s$
Δt	Time step	s

Table II. Particle Recombination/Generation Processes and Parameters

Trapping Process	σ (cm^2)	Reference
$e^- + Cu_A \rightarrow Cu^-_A$	8.0×10^{-21}	℘
$p^+ + Cu^-_A \rightarrow Cu_A$	3.0×10^{-14}	℘
$e^- + Cu_B \rightarrow Cu^-_B$	8.0×10^{-21}	78
$p^+ + Cu^-_B \rightarrow Cu_B$	3.0×10^{-14}	78
$e^- + EL_2^+ \rightarrow EL_2$	5.0×10^{-15}	78
$p^+ + EL_2 \rightarrow EL_2^+$	2.0×10^{-18}	78
$e^- + EL_5^+ \rightarrow EL_5$	4.0×10^{-16}	℘
$p^+ + EL_5 \rightarrow EL_5^+$	2.0×10^{-18}	℘

Photoionization Process	σ_o (cm^2)	Reference
$\Phi_{on/off} + Cu_A \rightarrow p^+ + Cu^-_A$	1.0×10^{-16}	℘
$\Phi_{on} + Cu^-_A \rightarrow e^- + Cu_A$	1.0×10^{-17}	℘
$\Phi_{on/off} + Cu_B \rightarrow p^+ + Cu^-_B$	1.0×10^{-16}	78
$\Phi_{on} + Cu^-_B \rightarrow e^- + Cu_B$	1.0×10^{-17}	78
$\Phi_{on/off} + EL_2^+ \rightarrow p^+ + EL_2$	3.0×10^{-17}	78
$\Phi_{on/off} + EL_2 \rightarrow e^- + EL_2^+$	8.0×10^{-17}	78
$\Phi_{on} + EL_5^+ \rightarrow p^+ + EL_5$	1.0×10^{-17}	℘
$\Phi_{on/off} + EL_5 \rightarrow e^- + EL_5^+$	1.0×10^{-17}	℘

Trap Impact Ionization Process	E_{mt} (10^6 V/cm)	Reference
$e^- + Cu^-_A \rightarrow e^- + e^- + Cu_A$	1.933	82
$e^- + Cu^-_B \rightarrow e^- + e^- + Cu_B$	1.495	82
$e^- + EL_2 \rightarrow e^- + e^- + EL_2^+$	1.254	82
$e^- + EL_5 \rightarrow e^- + e^- + EL_5^+$	0.6193	82

Band-to-Band Impact Ionization Process	$\alpha_i v_{e/p}$ (1/ns) †	Reference
$e^- \rightarrow e^- + e^- + p^+$	0.01	81
$p^+ \rightarrow e^- + p^+ + p^+$	0.01	81

Thermal Process	k_r (cm^3/s) ‡	Reference
$e^- + p^+ \rightarrow h\nu$	7×10^{-10}	78
$- \rightarrow e^- + p^+$	7×10^{-10}	78

† evaluated for an electric field of 1.38 kV/cm

‡ 7×10^{-6} cm^3/s value also used

℘ estimated

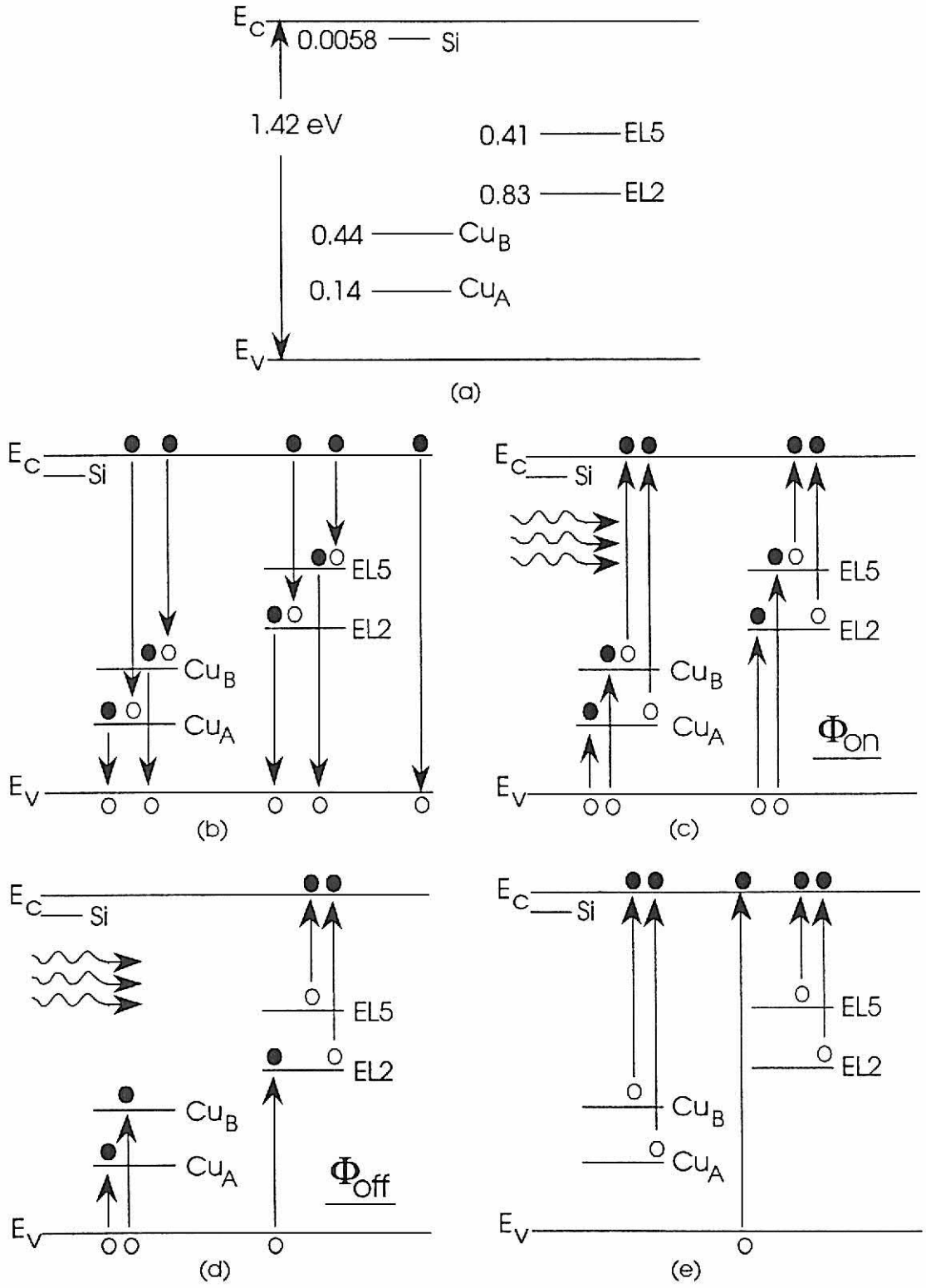

Figure III-1. (a) A band diagram of the GaAs(Si:Cu) material used for the BOSS. (b) All traps except silicon trap electron and holes. (c) Applying 1.1 eV on laser light causes electron and hole emission from all traps. (d) Applying 0.7 eV off laser light yields hole emission from the copper traps as well as EL2. The trap levels EL2 and EL5 also emit electrons, which would hinder the opening of the switch. (e) Impact ionization causes electron emission from the traps or from the valence band.

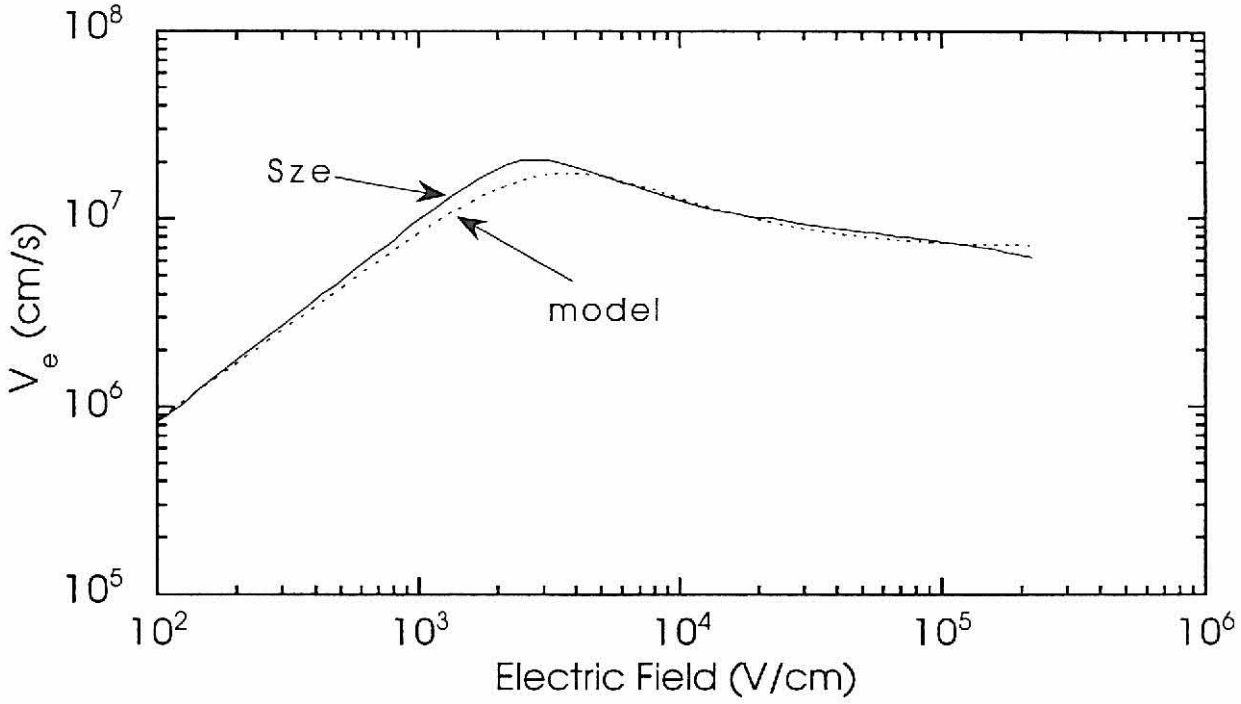

Figure III-2. The model takes into account negative differential resistance by having a functional dependence of the electron drift velocity v_e on the electric field. A comparison of the theoretical electron velocity used in the model (9) and the experimental electron velocities from Sze[81] shows good agreement.

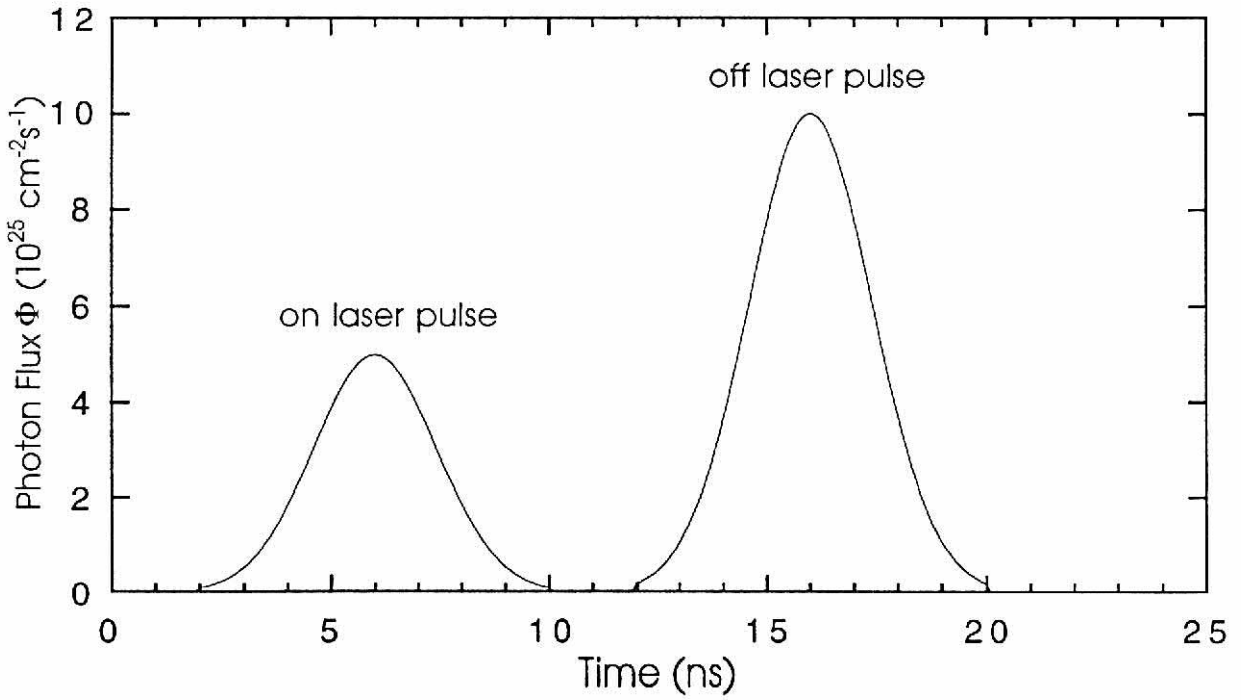

Figure III-3. A plot of the Gaussian laser pulses with respect to time. For this example, the peak on laser flux is 5 x10^{25} $cm^{-2}s^{-1}$ with Δt = 2 ns. The off laser flux peak is 1 x10^{26} $cm^{-2}s^{-1}$ with Δt = 2 ns.

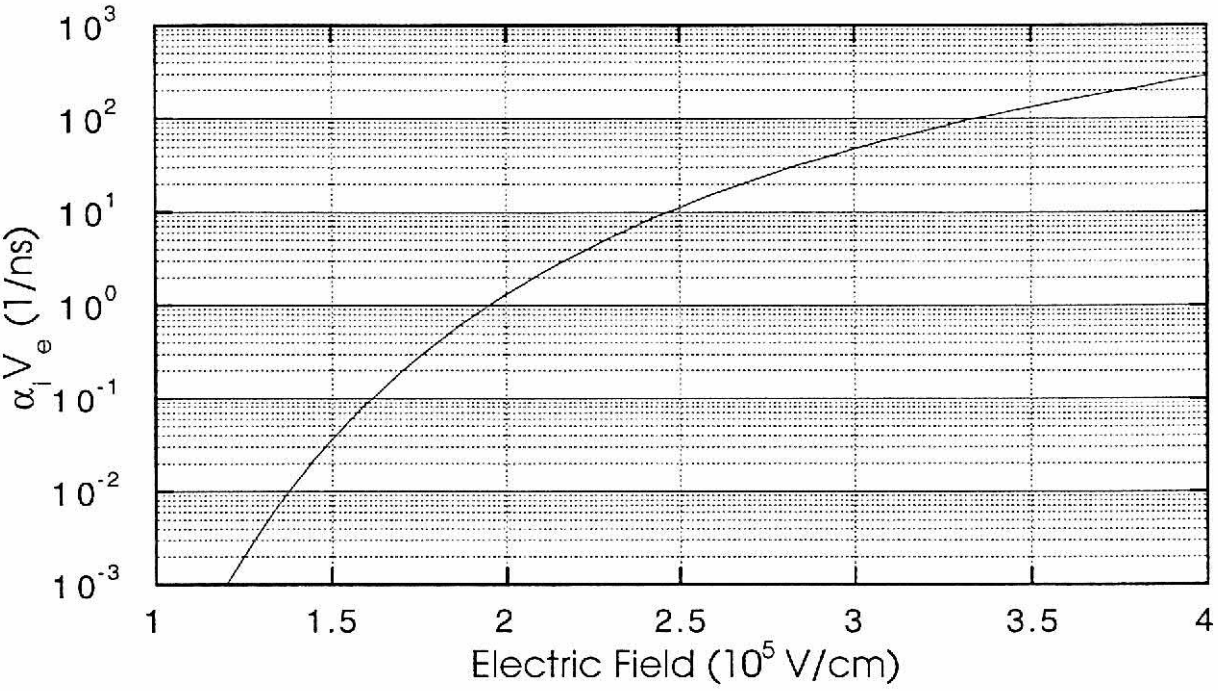

Figure III-4. Intrinsic impact ionization is included in the model and is a function of the electric field. To get an idea of when it becomes a significant process, a plot of $\alpha_i v_e$ vs. electric field (which is a plot of the percent change per nanosecond of the electron density vs. the electric field) shows a 1% change/ns in the density at an electric field of 1.38 x10^5 V/cm.

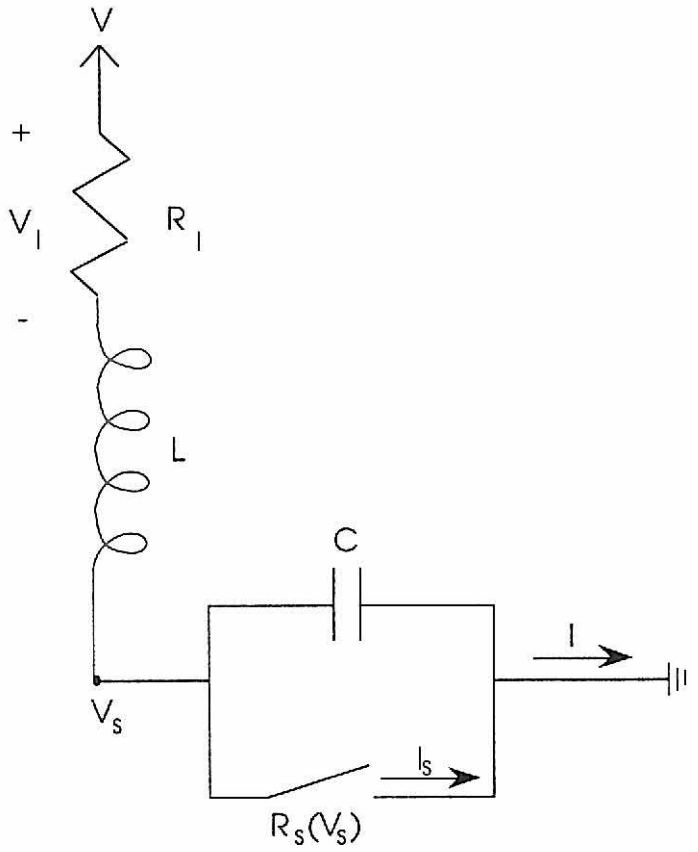

Figure III-5. A circuit model is included in order that switching characteristics can be explored. The switch is placed in parallel with a capacitance C in the pF range and in series with a 20 nH inductor L and a load resistance R_l, typically on the order of 100 Ω. The switch resistance R_s is a function of the voltage across it.

IV. BULK GaAs(Si:Cu) SWITCHES

A. Introduction

The model is first applied to a bulk BOSS device. The main motivation is to identify and gain a basic understanding in the important processes which determine a typical switch cycle. To this end a step-by-step analysis of a switch cycle is made, noting the changes in carrier densities, as well as the electric field and its effects on the switch cycle. After a basic understanding is established, consequences of computational mesh density, light delivery, trapping levels, hold-off voltage, circuit values, and switch geometry on the switching cycle will be explored.

B. Switch Cycle

The bulk switch geometry shown in Figure IV-1 is modeled with a cylindrical mesh such that all values are constant with angle but vary with radius and contact separation. The simulated PCSS is doped 10^{10} cm^{-3} n-type with $N_{Si} \approx N_{Cu} = 10^{16}$ cm^{-3}. The light flux is applied uniformly throughout the device. The typical modeled device has 1.0 mm contact separation, a 2.0 mm radius, a peak on flux of 5×10^{25} cm^{-2}-s^{-1} ($\approx$ 9 MW/cm^2) and a peak off flux of 8×10^{25} cm^{-2}-s^{-1} ($\approx$ 9 MW/cm^2). Both the on and off laser are Gaussian in time with Δt = 2 ns. The circuit consists of a 3.3 pF capacitance in parallel with the switch, as well as a 20 nH inductance and a 100 Ω load in series with the switch. The current and voltage versus time for the typical device is shown in Figure IV-2. The shaded region begins at the peak of the on laser pulse (6 ns) and the region ends at the peak of the off laser pulse (16 ns).

The switch closes with the application of the on laser pulse peaking at 6 ns. The conducting state is achieved approximately a nanosecond before the peak of the on laser pulse with a closing time $\approx$ 1.5 ns. The voltage across the device drops from 3 kV to $\approx$ 35 V and is conducting 29.6 A of current of the 30 A circuit limit. The effect of the on laser pulse is to photoionize the electrons from the compensated copper traps to the conduction band. The increase in electron density between the contacts for various times in the closing phase of the switch cycle is shown in Figure IV-3. In the bulk of the switch, a general rise is seen in n_e for increased time (3-10 ns) as more photons are absorbed, which generates more carriers from the copper level. The rise in n_e near the anode during the later part of the

closing cycle is due to the electric field enhancement developing near the anode. The electron level near the cathode reflects the level of carrier injection supporting the circuit.

For example, at 6 ns assume the electric field levels are large enough for the saturation velocity to be reached, and the hole density is low enough not to contribute significantly to the particle current. With $I = qAn_e v_s = 29.6$ A, the area $A = \pi(0.2 \text{ cm})^2$ and the saturation velocity $v_s = 7 \times 10^6$ cm/s, the electron density required at the contact to sustain this current is $n_e = 2.1 \times 10^{14}$ cm^{-3}, which is near the value observed in Figure IV-3 at the cathode. The electric fields near the cathode in the closed stage of the switch are large enough for a saturation velocity approximation to be valid. This is apparent in Figure IV-4 for the closing cycle, which shows the variation of the electric field for various times. With the large hole cross section, the hole level is close to nil at switch closing, and the copper density N_{CU} is uniform throughout the switch as a consequence of the uniform application of light. The only varying charged particles across the switch are the electrons. As the applied light moves the electrons from the copper traps and makes them mobile, they move to the contacts. A result is the uncovering of the charge of the shallow ionized Si donors and a varying positive charge density throughout the switch. The general depletion of electrons near the cathode means a positive space charge at the cathode and, as a result, electric field enhancement near the cathode. Figure IV-5 is a plot of the variation between the contacts of the charge density and voltage at 4 ns and shows the trend toward positive space charge and its effect on the voltage across the switch. As time progresses and the device moves into the closed state, the enhancement at the cathode increases and the bulk electric field level decreases.

At 16 ns, the peak of the off pulse, the switch begins to open, with the device dropping $\approx$ 720 V and conducting $\approx$ 24 A (Figure IV-2). Only at 19 ns or 3 ns after the opening laser pulse, has the device finally leveled off to an opened state with an opening time of $\approx$ 3.0 ns. The effect of the off laser pulse is to ionize the neutral copper traps through hole emission. Figure IV-6 shows the variation of the hole density between the contacts at various times near the end of the switch cycle. When photoionized from the copper levels the holes either are trapped again by the copper due to the large hole capture cross section or they recombine with a mobile electron in the conduction band. These two reduction processes cause the rapid decrease in the hole density shown in Figure IV-6. In fact, n_p

continually decreases after reaching its peak nearly 2 ns before the off laser peak. As holes are introduced by the off laser pulse and recombine with electrons, n_c is reduced as shown in Figure IV-3 for the opening cycle. Also, as the switch opens, the amount of current injected into the switch decreases, which reduces the number of injected electrons and the density level near the cathode. The electric field decreases near the anode, and the electric field enhancement front near the cathode moves toward the anode as seen in Figure IV-4 for the opening cycle. The sharp reduction in electrons injected at the cathode as the switch opens causes an electron density gradient which moves toward the anode at the saturation velocity. The front moves by $\approx$ 0.005 cm from 18 to 19 ns, which corresponds to a speed of 5×10^6 cm/s, close to the saturation velocity.

It should also be noted that the opening phase is a slower process than the closing phase in the switching cycle. The mere introduction of mobile carriers that are collected at the contact decreases the conductivity of the device and closes the switch. To open the device, it is not the introduction of holes that lowers the conductivity but the holes recombining with the free electrons that have been maintaining the conductive closed state. The creation of holes followed by the recombination of electrons and holes is a more lengthy process than photoionizing traps alone. This results in a longer opening phase relative to the closing phase.

C. Mesh

With the spatially uniform initial conditions used for the simulations in this chapter, values vary little with radius. Thus a larger portion of the mesh variation is placed between the contacts with a typical mesh distribution of 4x256 used. The mesh is nonuniform, with the smallest dimension usually chosen as 5×10^{-4} cm at either contact, and if 256 mesh points separate the contacts, the largest mesh width is 1.37×10^{-3} cm. There is a dependence on the mesh size with these calculations. The mesh size was varied to test the effects of the mesh sizing on the results. Figure IV-7 shows the voltage cycle of the switch as a uniform mesh size becomes sparser. The result for the nonuniform mesh is included for comparison. As the mesh size increases or the number of mesh points is reduced, the closed state of the switch moves to larger voltage values and the ringing in the opening stage is diminished. The switching cycles also demonstrate the increase in accuracy with denser meshes. As the number of mesh points increases, sharper changes in the electric field can be resolved, which increases the numerical accuracy.

An important region to resolve is near the contacts where the electric field collapses as the switch closes.

D. Light

The level of laser flux applied to the switch controls the degree to which it opens and closes. If the threshold switching requirement for the laser flux is not met, the device will fail to open or close. Figure IV-8 shows the temporal development of current with the on laser flux Φ_{on} varied and the circuit limit at 30 A. If the flux is too low, ringing occurs with no distinguishable plateau. This flux level would be considered below the threshold for creating a discernible switching cycle since the switch never stays in a consistent closed or conducting state. As the on flux is increased, the rise time decreases and the degree of switch closure increases. Applying a large enough flux achieves 99.8% (3000 to 7 V) closure of the device. The threshold for switching this typical device is $\approx$ 2-4 x10^{23} cm^{-2}-s^{-1} ($\approx$ 35-70 kW/cm^2), when approximately 50% closure of the switch is achieved. As complete closure is approached, larger fluences of laser energy are required to close the switch by a smaller percentage.

The effect of Φ_{off} on the switch voltage is shown in Figure IV-9. As more laser flux is used, the device opens to a larger voltage, and the rise time becomes smaller. However the fluence is not large enough to completely open the switch. Very large fluences caused ringing. The difficulty in opening the switch by increasing the magnitude of the opening laser flux suggests that a degree of temporal development is necessary to aid the switch in opening. If a broader off flux is used so that, integrated over time, more holes are introduced, the device can close further as seen in Figure IV-10. Figure IV-10 shows the effect on switch closure when the temporal width of the off laser pulse Δt_{off} is increased from 2 to 4 ns and the off laser peak is shifted from 16 to 20 ns. As the off laser pulse is temporally widened, switch closure is increased.

The opening phase of most switches is achieved through electron hole recombination, with the exact time the switch opens relatively uncontrollable. With the BOSS, the opening time is controlled by the time the off light pulse is applied. Figure IV-11 shows the switching cycle for different off laser pulse application times, which demonstrates the controllability of the switching cycle width and, thus, the agility of the switch.

In results thus far, the light flux level is the same throughout the switch which is an approximation. In bulk switches the light is typically shone at one contact which is made transparent to the wavelength of light used. The absorption length of the light, however, affects the closing of the switch. If less light can penetrate into the switch, it becomes more difficult to form a conducting channel across the switch. Figure IV-12 shows the voltage cycle as the absorption coefficient of light shone through the anode is varied. In Figure IV-13 the light is shown through the cathode. The switch closes to larger voltage values at the anode as the absorption coefficient increases (absorption length decreases). Consequently, the switch has become less sensitive to the triggering light. The closing time increases with decreasing absorption length at the cathode, although the closing level is unaffected until $\alpha = 30.4\ cm^{-1}$. At this time the solution begins to swing wildly which is likely a numerical instability. Comparing anode vs. cathode, there is a slightly larger sensitivity for the light applied near the cathode.

E. Traps

The device trigger sensitivity is affected by the density of deep traps in the device. Figure IV-14 shows the effect of trap density variation on the voltage cycle. As the density is reduced, the potential number of free carriers is reduced independent of the laser flux applied since the trap level represents an approximation of the maximum usable electrons that can be contributed to a closing phase. Thus, as the trap density is reduced, the number of usable carriers is reduced, which inhibits the level to which the switch can close. At $10^{14}\ cm^{-3}$ the switch has become insensitive to the triggering laser, closing at most by 15 %. The density of deep level traps in the device has to be large enough to contribute the minimum necessary level of carriers for switch closure.

F. Voltage

The closing and opening times of the switch have a weak dependence on the voltage being switched as seen in Figure IV-15. The figure shows the current and voltage switching cycles when the hold-off voltage varies from 2 to 5 kV. In the closing phase, complete closure is slower as the voltage is increased, with the time of complete closure increasing with applied voltage. In the opening phase, the voltage is always 600 V away from complete closure regardless of the voltage being switched. The "excess" 600 V is the voltage dropped across the load resistor as the switch opens to approximately 6 A

in all hold-off voltage cases. When 5 kV is switched, slight ringing is observed at the end of the opening phase. As the switched voltage is increased to 10 kV, which is shown in Figure IV-16, the opening phase has become completely unstable. The unstable condition in large part is due to the negative differential resistance effect which introduces nonuniformity in the electric fields and voltages throughout the switch. It should be noted that the model has no formalism for determining the maximum hold-off voltage the device is capable of. Therefore, "real" devices may not exhibit this behavior because other effects, such as surface flashover, would have already caused a failure. In practice, great effort is expended in processing the surfaces of these devices in order that a semiconductor breakdown process limits the applied voltage and not a surface flashover affect or surface breakdown which can occur at lower electric field levels.

G. Circuit

The magnitude of capacitance and resistance in the circuit greatly affect the response of the switch. Increasing the capacitance parallel to the switch decreases the fall time to switch closure as seen in Figure IV-17. The results on the opening phase are mixed, and both the level the switch opens and the opening rise time are affected. The switch is opening to a larger level with a slight increase in opening rise time from 3 to 10 pF. As the capacitance is increased further, however, the opening rise time becomes much larger, approaching the RC time constant, and the switch opens to lower voltages. The larger the load resistance is, the smoother the closing phase of the switch and the lower the final opening voltage level, as shown in Figure IV-18. As the load resistance is decreased, a peak develops in the closing transition that becomes more pronounced as the resistance is lowered. The variation of this peak is as large as 500 V in the 25 Ω case, when 3 kV is being switched. At the opening phase of the switch with low load resistances, there is significant ringing at the end of the transition. At high resistances, the instability has moved to the beginning of the opening phase transition. All cases eventually open to the same current level, although in the closed phase the lower load resistance case conducts more switch current as the circuit current limit has been increased.

H. Geometry

The geometry of the switch also affects the operation of the switch. The contact separation determines the amount of voltage that can be held off, and the width of the contacts determines the

amount of current the switch can handle. The width of the contacts and the contact separation were varied with the mesh length held to a uniform size for all mesh points. Figure IV-19 shows the circuit response to changing the radius or increasing the contact area. For all the radius cases, a uniform 8x32 mesh was used. As the radius is increased the contact area increases as well. With the larger collection area the switch conducts more current, closing to a lower voltage level. Figure IV-20 shows the change in the voltage as the contact separation is varied. To keep the mesh length constant and thus exclude any mesh effects, the number of mesh points is increased as the length is increased. Thus, for the 2 mm case a 4x64 mesh was used, for the 3 mm case a 4x96 mesh was used, etc. As the length is increased, the resistance of the switch should increase. When the switching cycle is observed, there is only a slight increase in the closed switch voltage level, which indicates that the switch is a little more resistive in the closed state for the longer lengths. The slight effect increasing contact separation has on the voltage cycle suggests that a large portion of the switch resistance is located at the contacts which are not effected by the variation of the contact separation.

I. Summary

The model has been applied to the bulk GaAs(Si:Cu) bistable optically switched semiconductor to gain a basic understanding of the important mechanisms involved in a switch cycle. In the closing transition of the switch, the electric field collapses to the contacts with more significant enhancement observed at the cathode. A major mechanism of electric field enhancement is electron emission from compensated deep traps due to photoionization. As the electrons drift to other areas of the switch, they expose the positive charge of the shallow donors. Holes have little role in the closing phase of the switch due to the large hole capture cross sections of the deep acceptor traps. In the opening phase an electric field enhancement front progresses from the cathode to the anode. The electric field front forms as an impulse response to the opening laser pulse and to the reduction of injection of carriers at the cathode. The BOSS was shown to be agile and to require less optical energy to close than to open. When triggering is accomplished with a laser at either end instead of uniformly throughout the switch, the closure time increases. The geometry and circuit parameters were shown to have a large influence on the switching cycle.

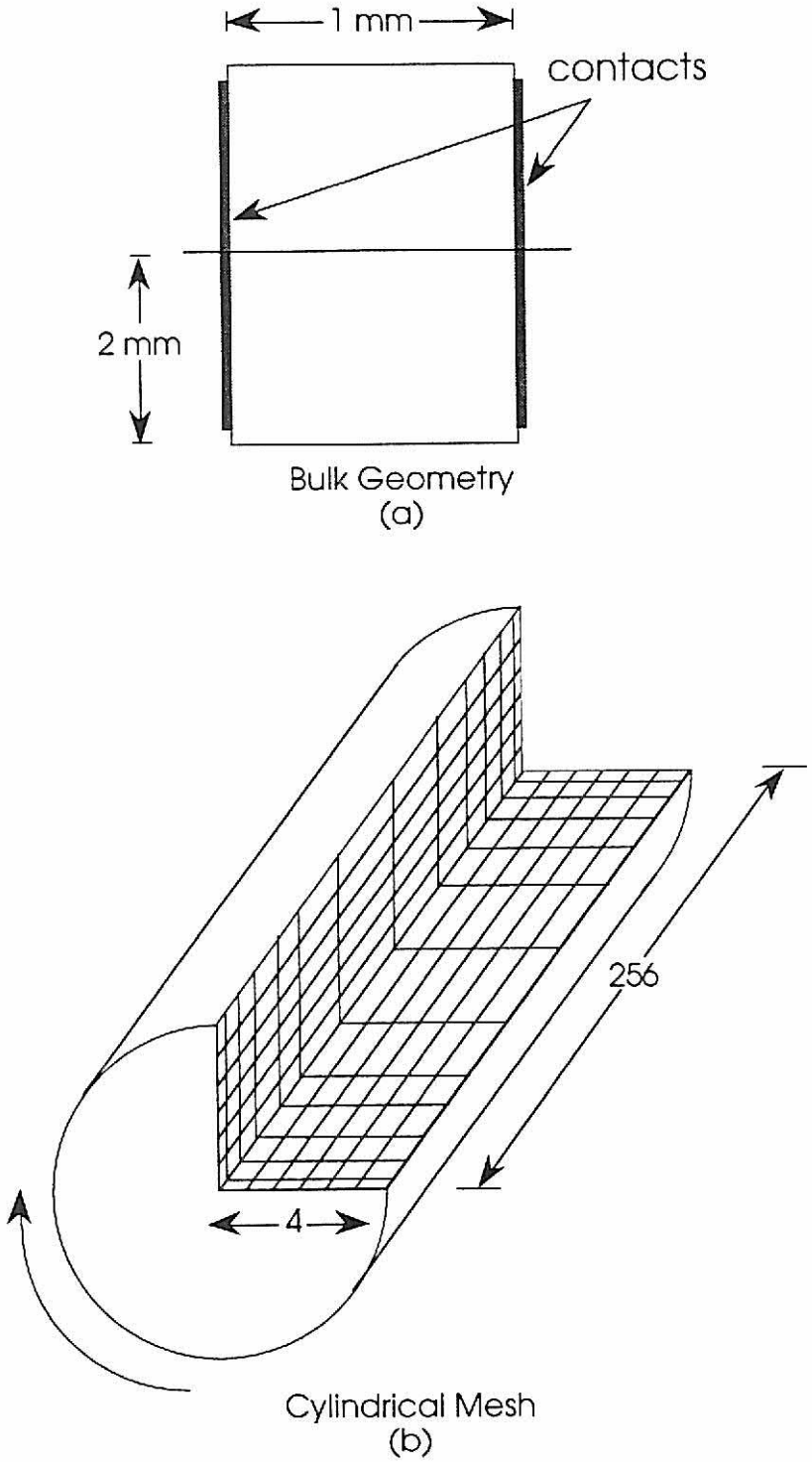

Figure IV-1. (a) The bulk switch geometry has contacts on either side of the semiconductor. (b) The mesh used for the finite differencing is cylindrical and is concentrated at the contacts with a typical nonuniform mesh dimension of 4 x 256. The dimensions used in the simulations are a 2.0 mm contact radius and 1.0 mm contact separation.

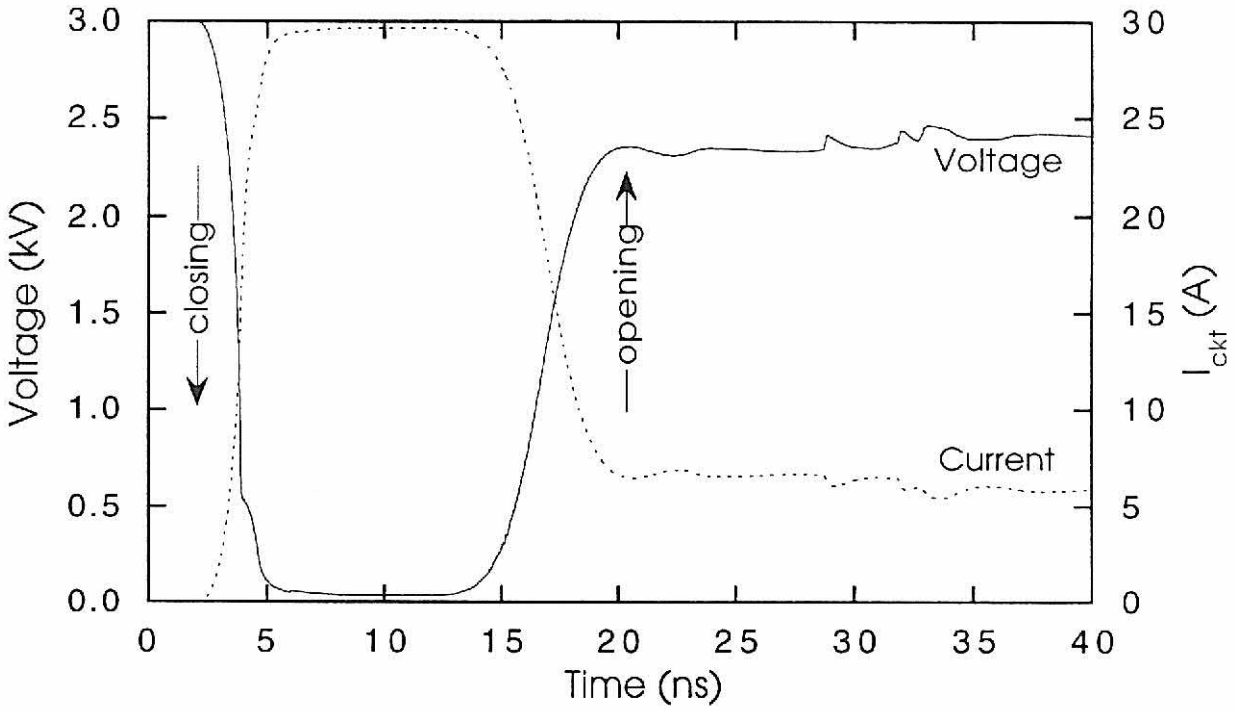

Figure IV-2. The current through and voltage across a typical PCSS. The shaded region begins with the peak of the on laser (6 ns) and ends with the peak of the off laser (16 ns). As the voltage across the switch is reduced and the current through the switch is increased, the switch is said to be closing, or on. As the voltage across the switch recovers and the current through the switch is decreased, the switch is said to be opening, or off.

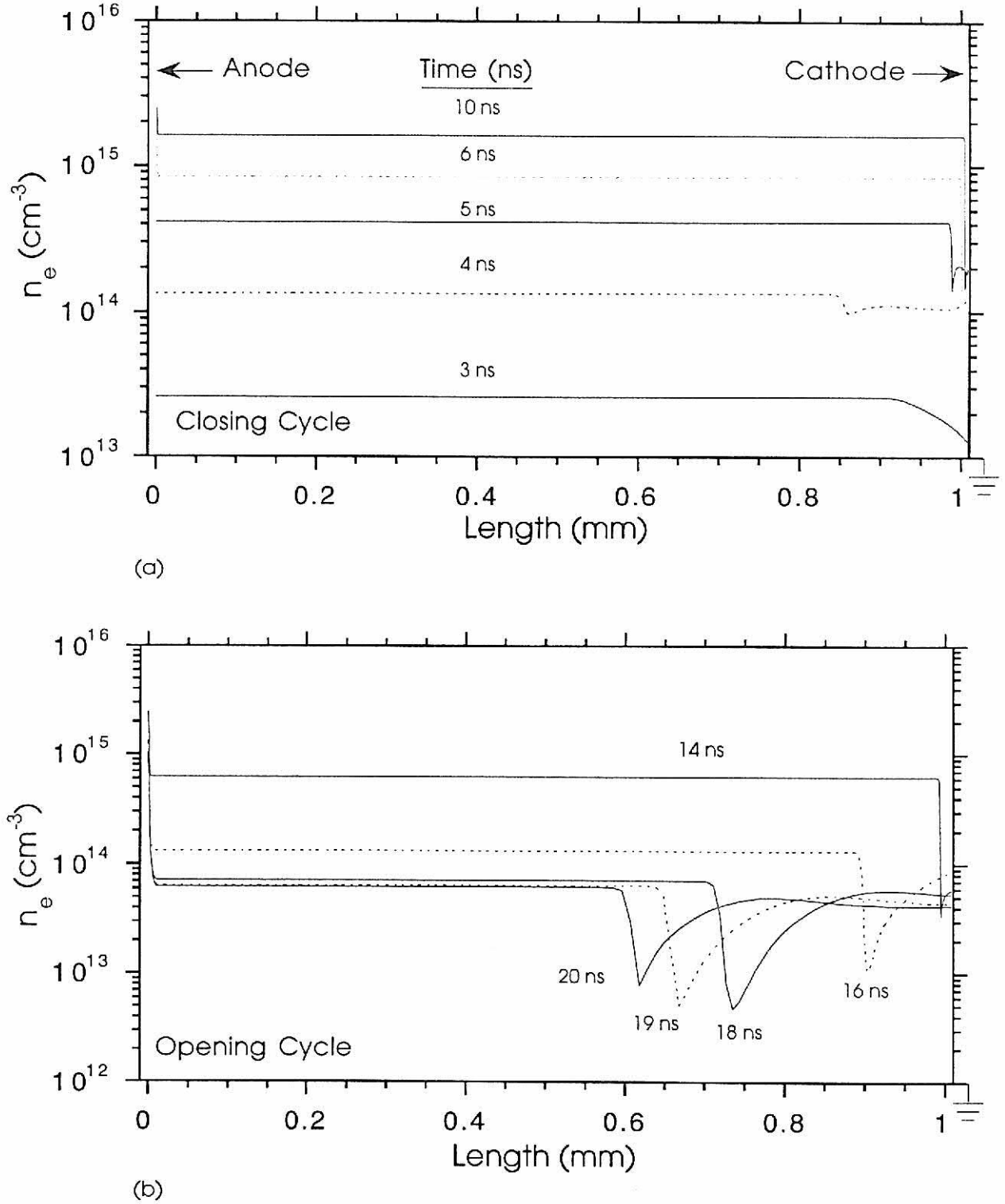

Figure IV-3. The electron density n_e across the switch for various times. (a) In the closing cycle, n_e is dominated by the uniformly applied laser light evidenced by the uniformity of n_e between the contacts. At the cathode, n_e is fixed at the injection level from the circuit, and at the anode it begins to rise later in the closing cycle due to electric field enhancement developing near the anode. (b) In the opening cycle, a pulse of low n_e is progressing from the cathode to the anode and is a result of the abrupt reduction of carriers in the bulk by the opening laser pulse and the sudden reduction in electron injection at the cathode.

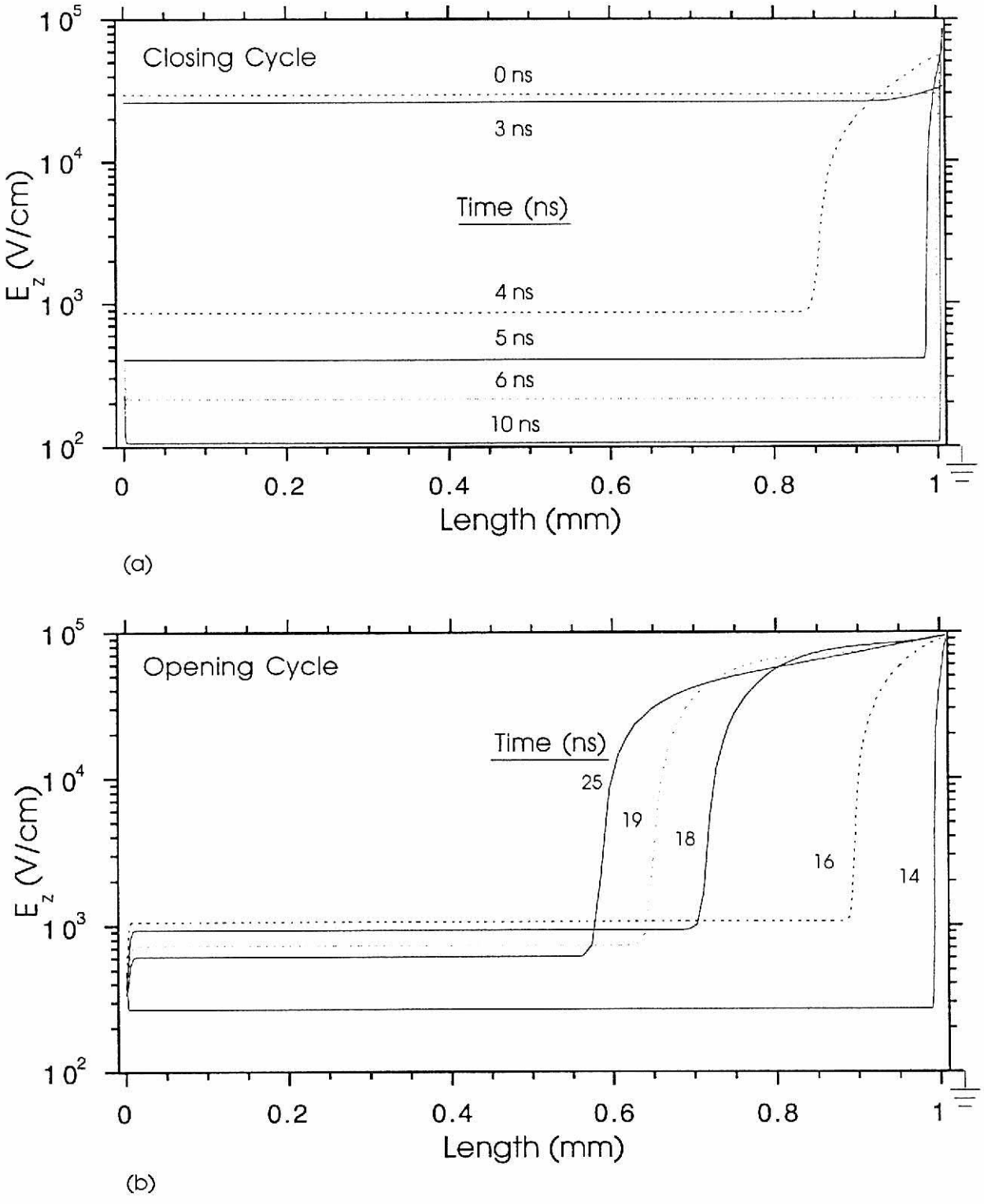

Figure IV-4. The electric field E_z across the switch for various times. (a) In the closing cycle, the electric field in the bulk is being reduced as the conductivity is increased by the closing laser pulse. The reduced number of electrons near the cathode uncovers positive space charge, enhancing the electric field in that region. The slightly negative space charge near the anode is causing less substantial electric field enhancement at the anode. (b) In the opening cycle, an electric field enhancement region is moving from the cathode to the anode at the electron saturation velocity. This front is a border for regions of high and low conductivity.

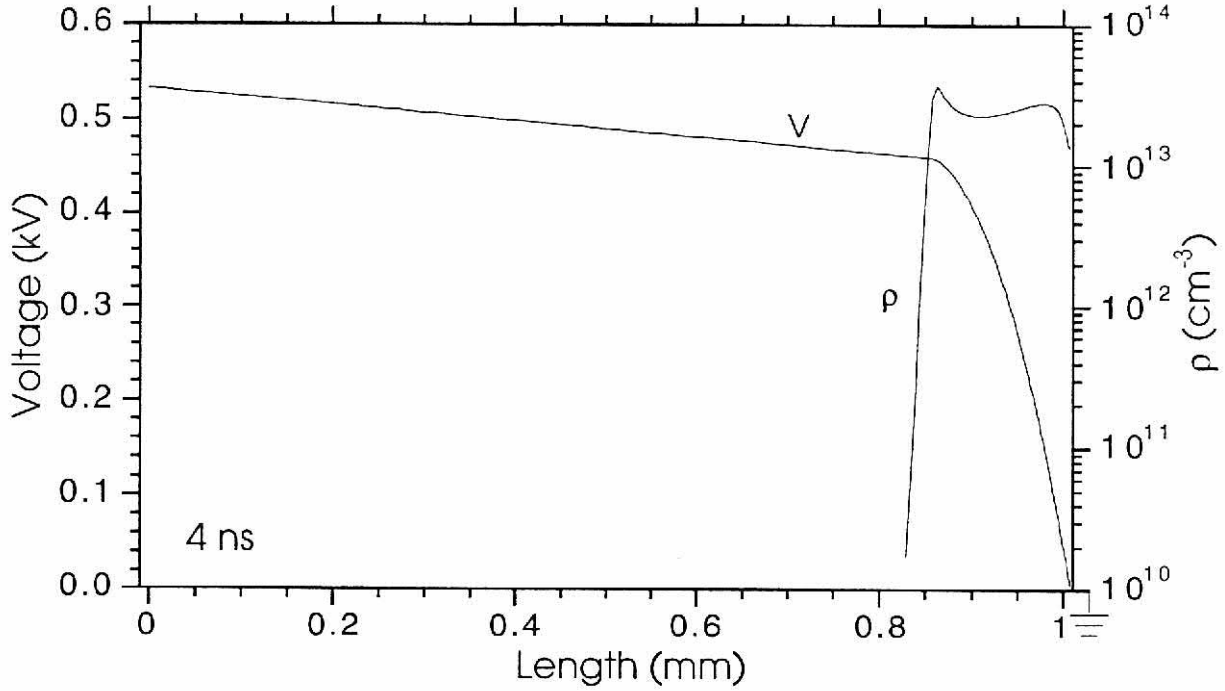

Figure IV-5. The space charge ρ and the voltage V across the switch at 4 ns. The general cause for electric field enhancement near the cathode is a reduced level of electrons causing the ionized donors to be uncovered and contributing to the space charge. As a result, a large portion of the voltage is being dropped near the cathode.

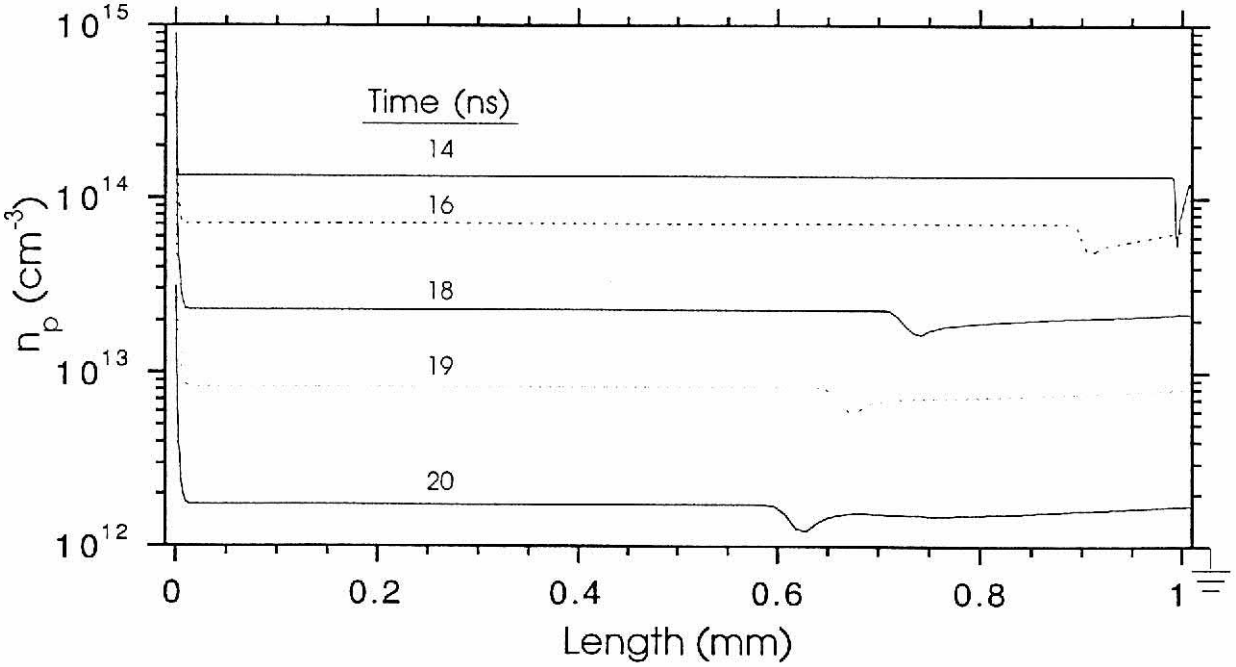

Figure IV-6. The hole density n_p across the switch for various times. In the closing cycle, the pressures on hole reduction are strong, resulting in below thermal levels of holes during the closing phase of the switch. In the opening phase the off laser is causing hole emission from the traps, which is increasing the level of holes in the bulk of the switch. The rapidity of hole reduction is evident when the hole densities in the bulk are reaching their peak values before the peak of the closing laser.

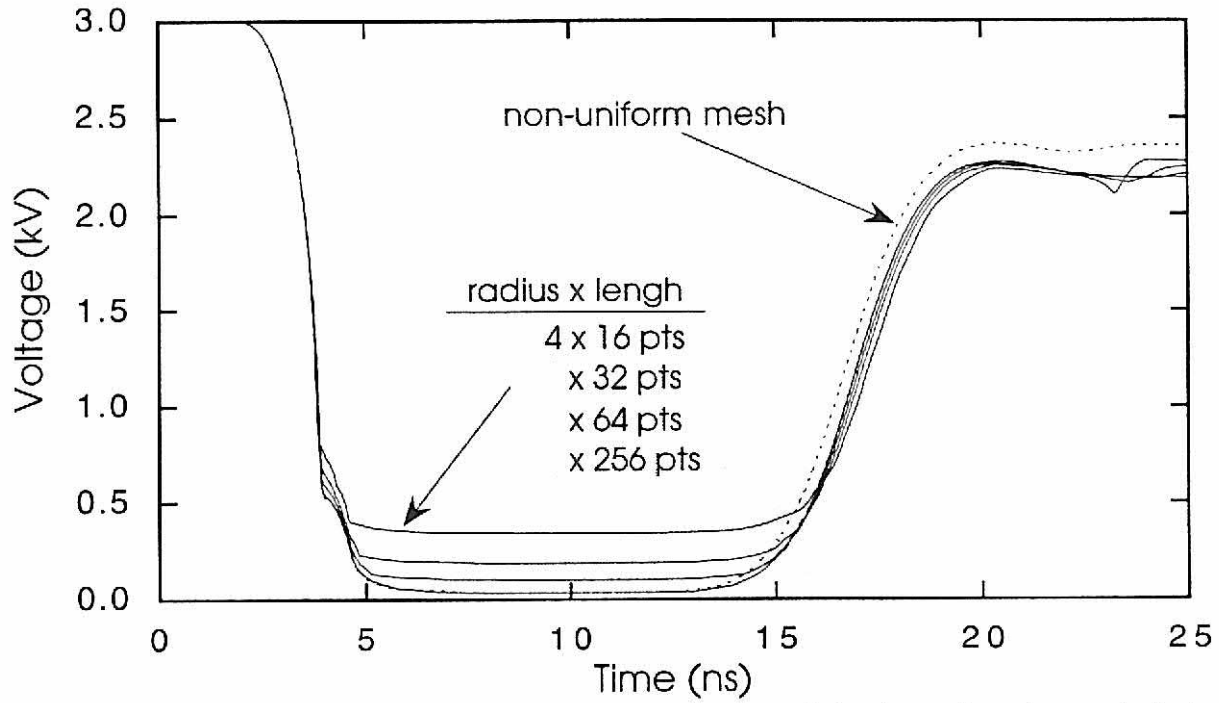

Figure IV-7. The voltage across a PCSS with the uniform mesh in the z-direction varied. As the resolution increases, more of the electric field near the contacts is resolved. Improved resolution at the contacts leads to a more accurate approximation as the closed voltage is seen to converge to a lower value as the number of mesh points increases. The 4x256 nonuniform mesh case (dotted line) is included for comparison.

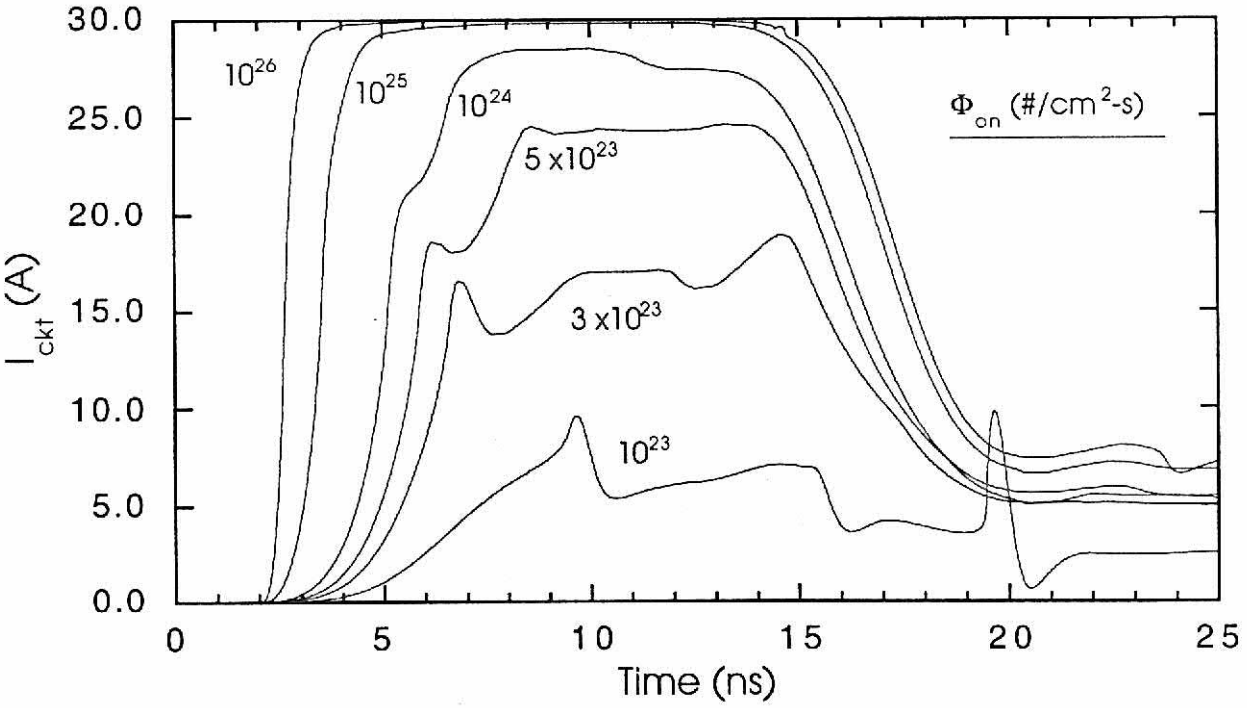

Figure IV-8. The current through a PCSS with the on flux Φ_{on} varied. As Φ_{on} is increased, the current through the switch approaches the circuit limit of 30 A (3 kV across a 100 Ω load). There is a threshold effect occurring with 50% switching achieved with a flux of 3 x10^{23} #/cm^2-s applied to the switch.

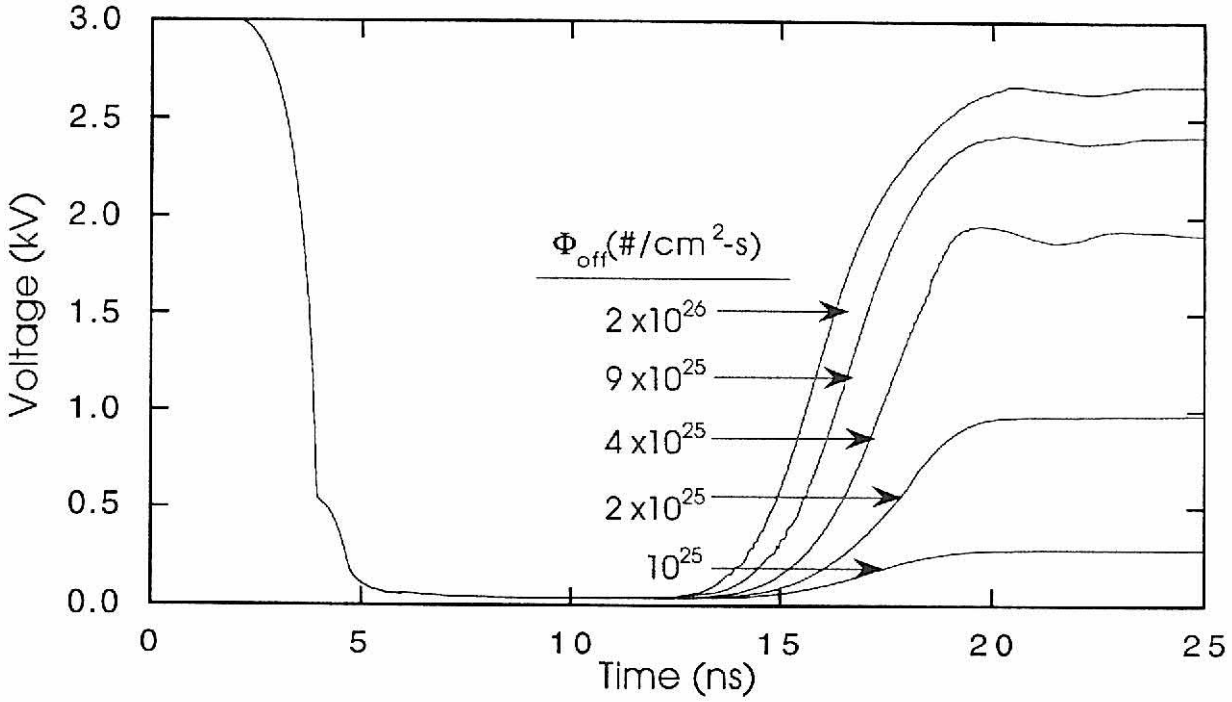

Figure IV-9. The voltage through a PCSS with the off flux Φ_{off} varied. As Φ_{off} is increased the level of opening increases. Compared to Figure IV-8, the opening laser fluence has to be larger to open the switch effectively than the closing laser fluence to close the switch.

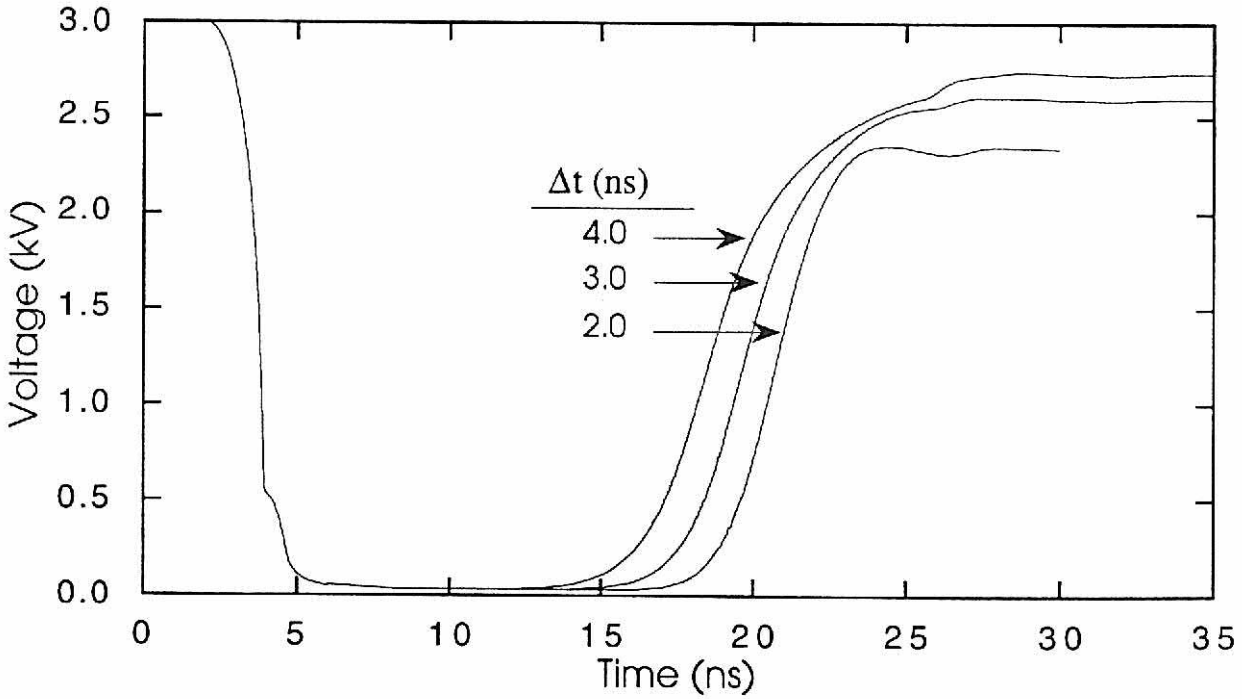

Figure IV-10. The voltage through a PCSS with Δt_{off} varied. As Δt_{off} is increased, the number of holes introduced into the switch integrated over time increases. With a larger number of holes with which the electrons recombine, the switch opens to a higher level.

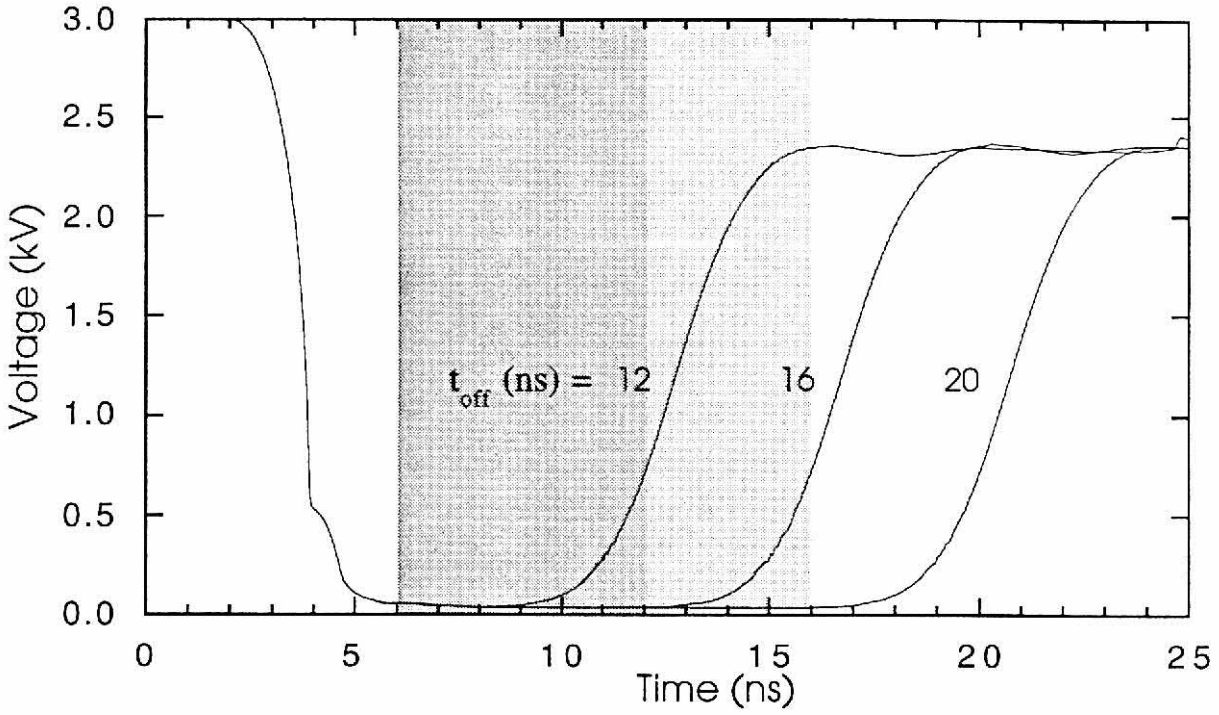

Figure IV-11. The voltage through a PCSS with t_{off} varied demonstrates the agility of the switch. The ability to choose the turn-off time is not typical of PCSS in general but is an advantage when using a BOSS.

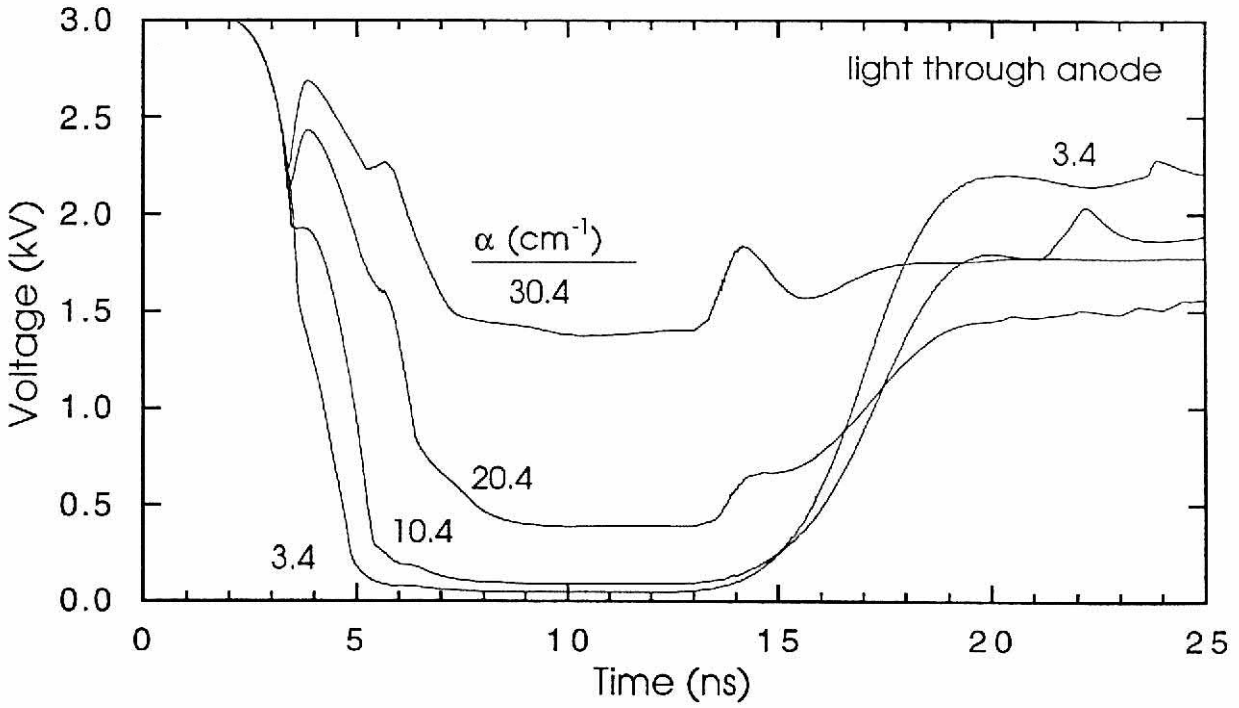

Figure IV-12. The voltage across a PCSS with the absorption length varied as the light is shone through the anode. As the absorption length is increased (decreasing absorption coefficient), the carriers penetrate further into the device and become more efficient at closing the switch.

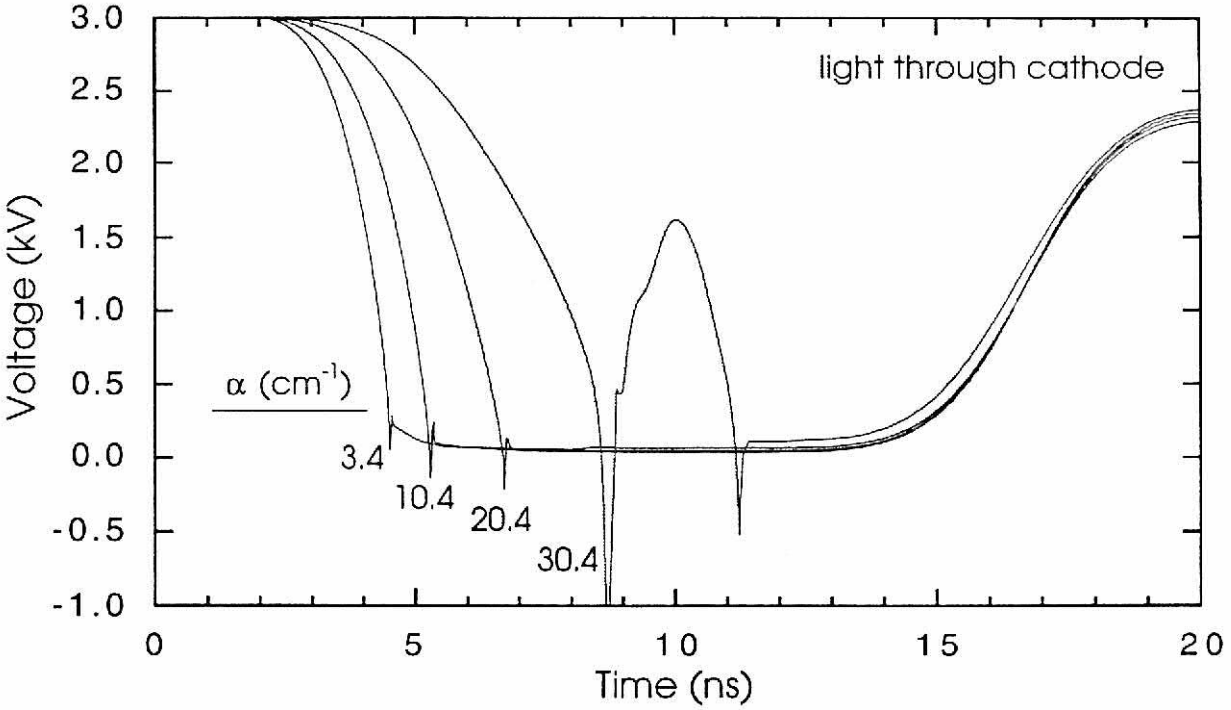

Figure IV-13. The voltage across a PCSS with the absorption length varied as the light is shone through the cathode. As the absorption length increases, the closure time decreases as the carriers penetrate further into the device.

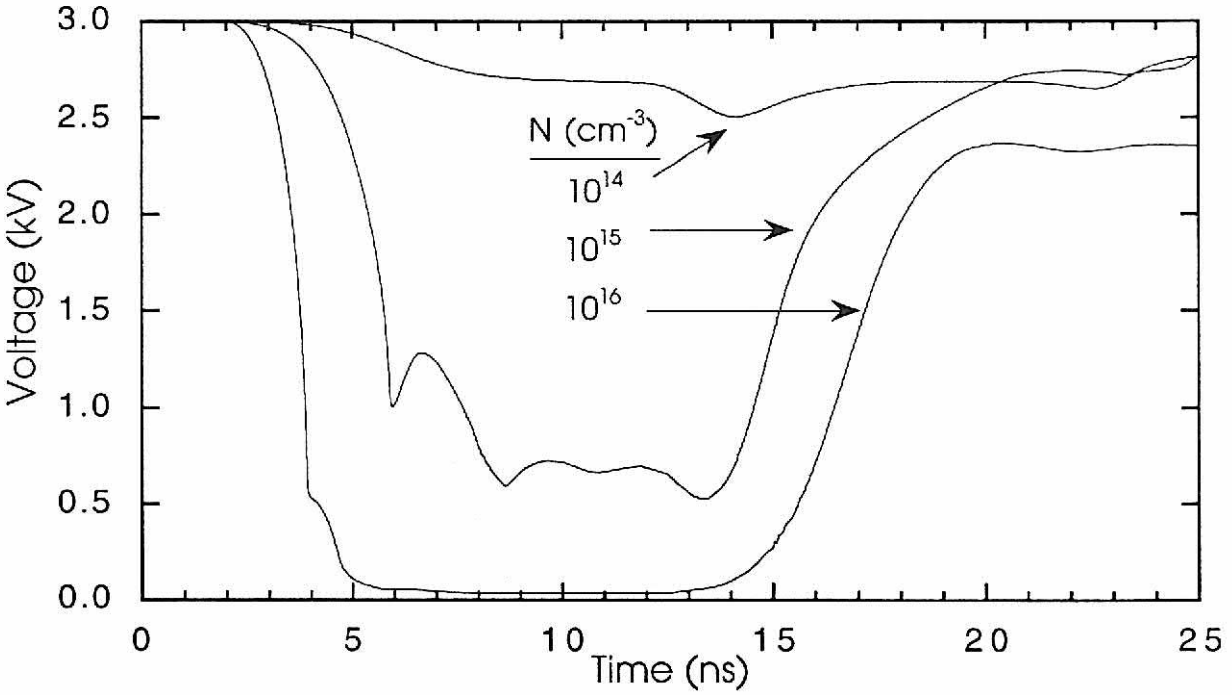

Figure IV-14. The voltage through a PCSS with N_{trap} varied. A minimal density of traps is required for the switch to be sensitive enough to the closing laser pulse. A smaller density would require a more powerful laser to close the switch. If the density level is too small to supply the minimal carriers necessary for switching, then even if a pulse energy was strong enough to completely emit all the electrons in the trap, the switch would still not be triggered.

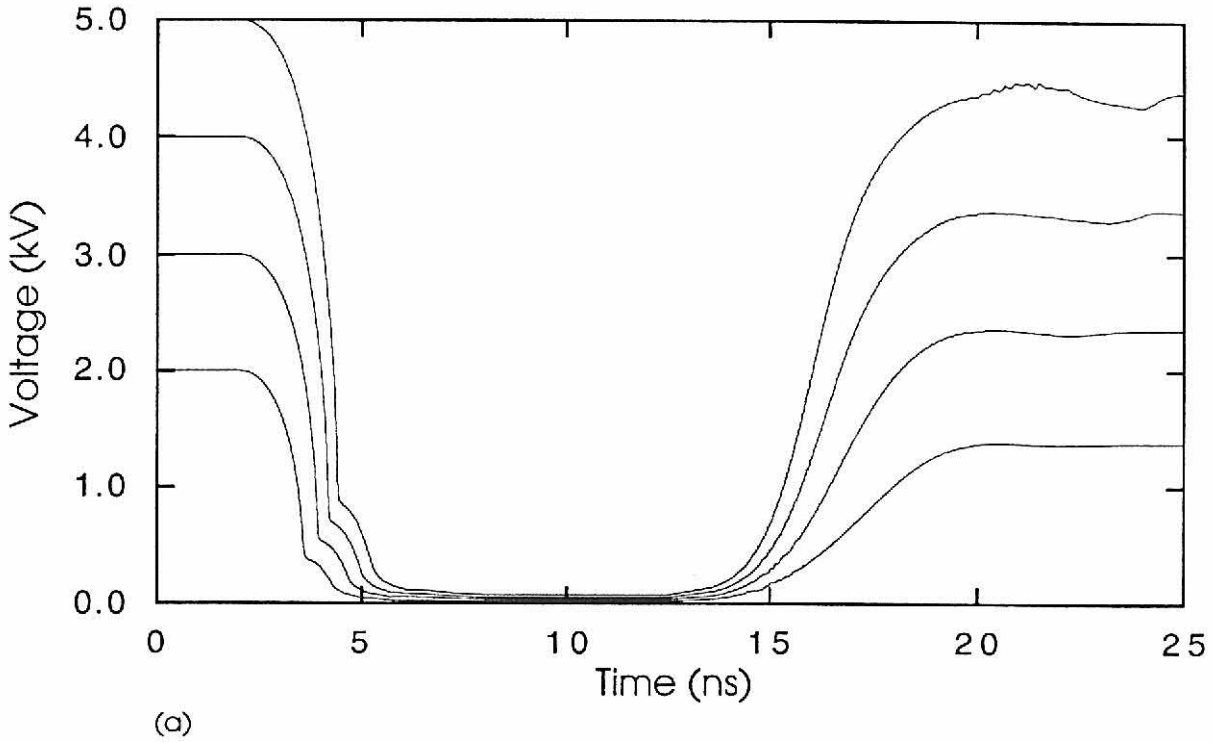

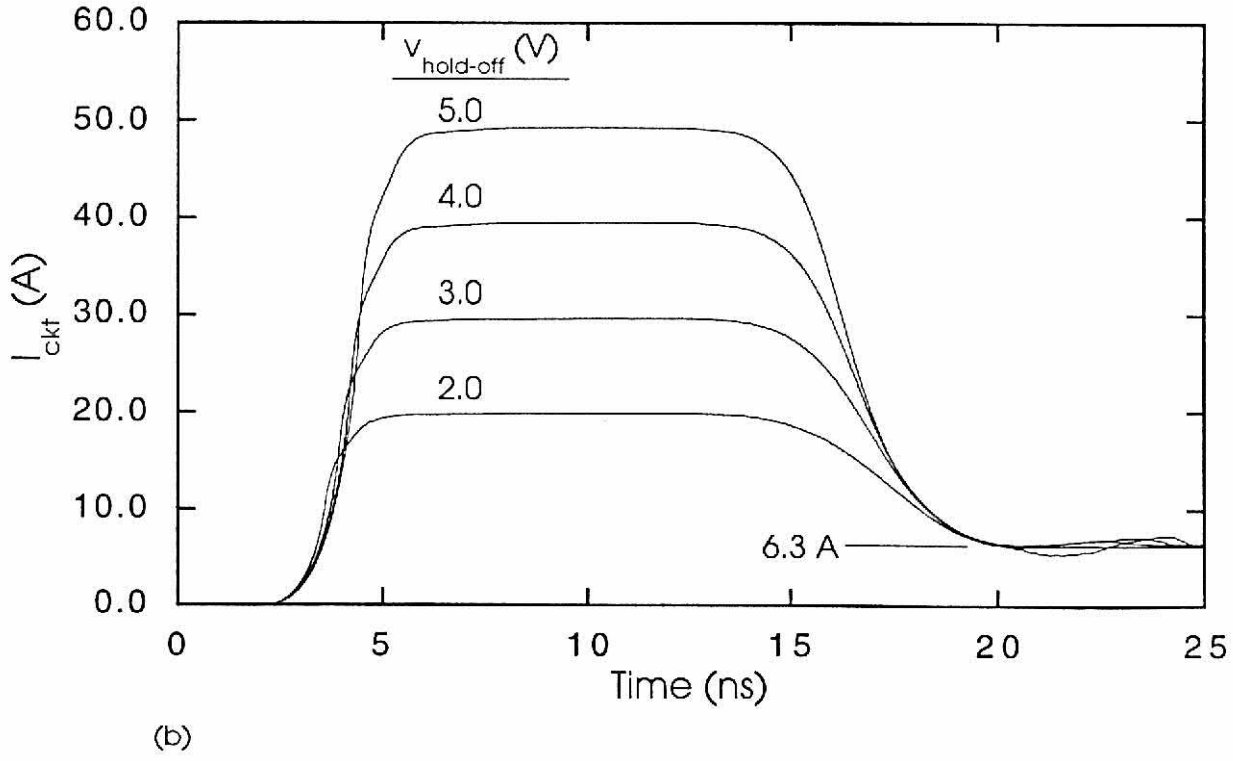

Figure IV-15. The (a) voltage and (b) current through a PCSS with the switched voltage varied. As the voltage is increased, complete closure takes longer to occur. The switch is consistently opening to ≈ 6 A independent of the applied voltage. As a consequence, the load is still dropping some of the applied voltage, and the switch voltage is ≈ 600 V from completely opening.

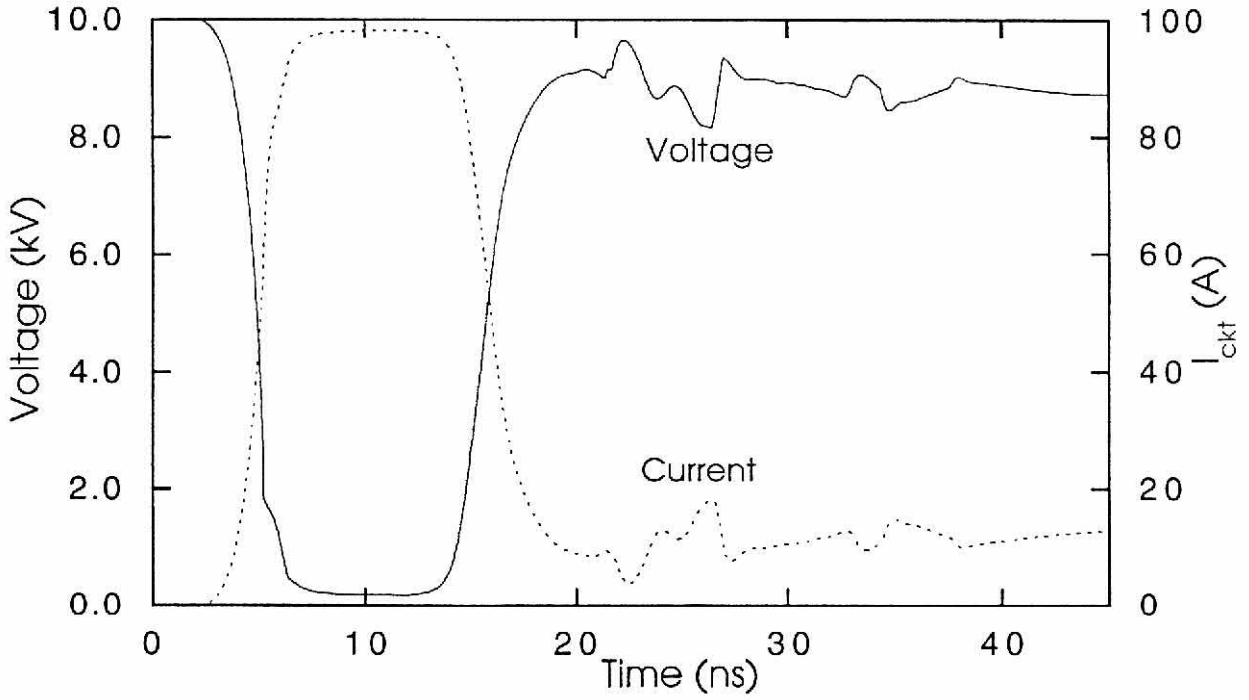

Figure IV-16. The voltage and current through a PCSS with the switched voltage V = 10 kV. The ringing at the off-state of the switch is due primarily to the electric field instabilities, which are a consequence of the negative differential resistance in the switch.

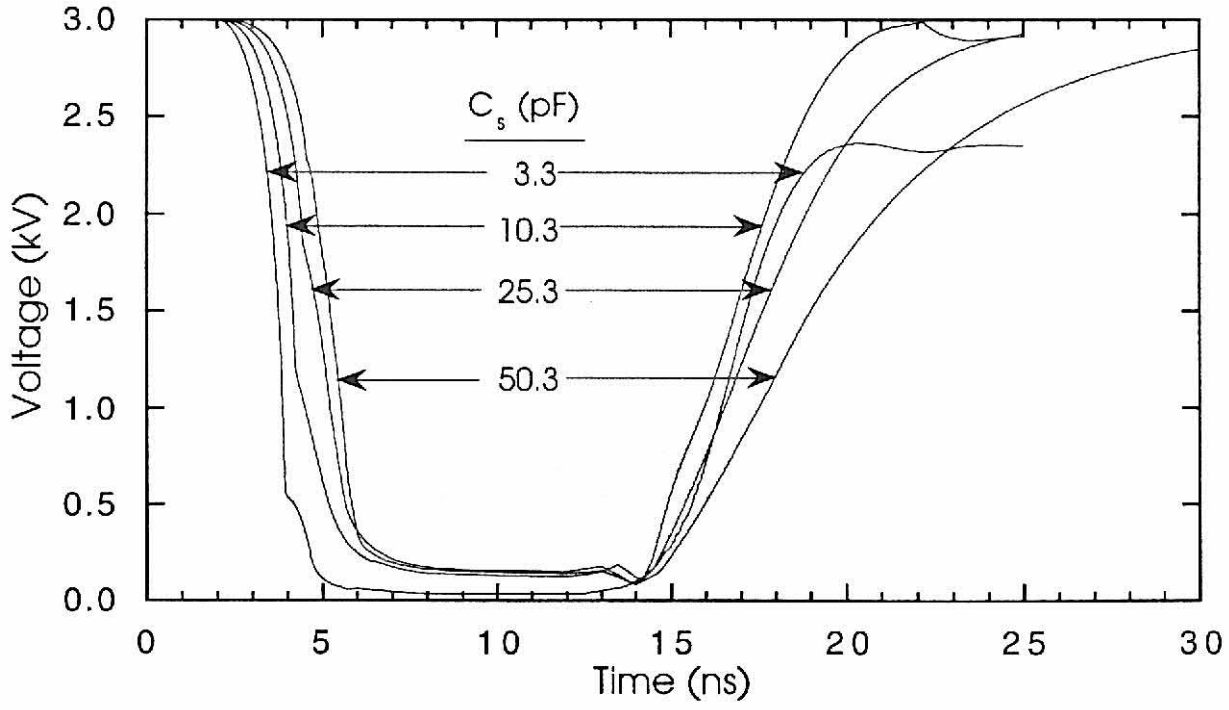

Figure IV-17. The voltage across a PCSS with the capacitance of the switch C_s varied. A larger capacitance in parallel with the switch leads to slightly reduced closing times. In the opening phase, the opening speed is dominated by the RC time constant when the RC time constant becomes greater than the characteristic opening time of the switch.

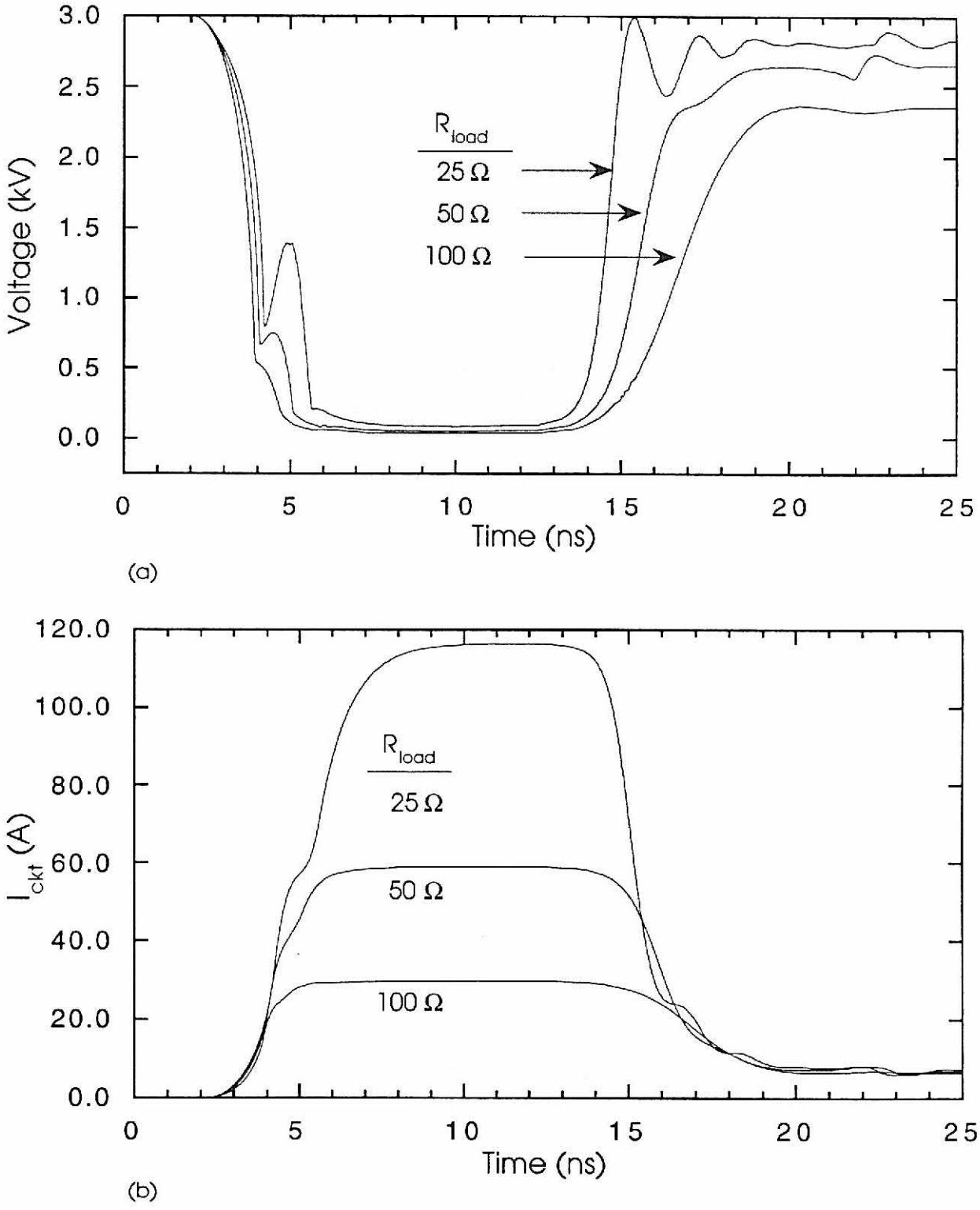

Figure IV-18. The (a) voltage across and (b) current through a PCSS with the load resistance R_{load} varied. As the load resistance decreases, the current limit of the circuit increases. Thus the reduced load resistance is increasing the current density flowing through the closed switch. When opening, the switch is more sensitive to the opening laser pulse when switched with a smaller load.

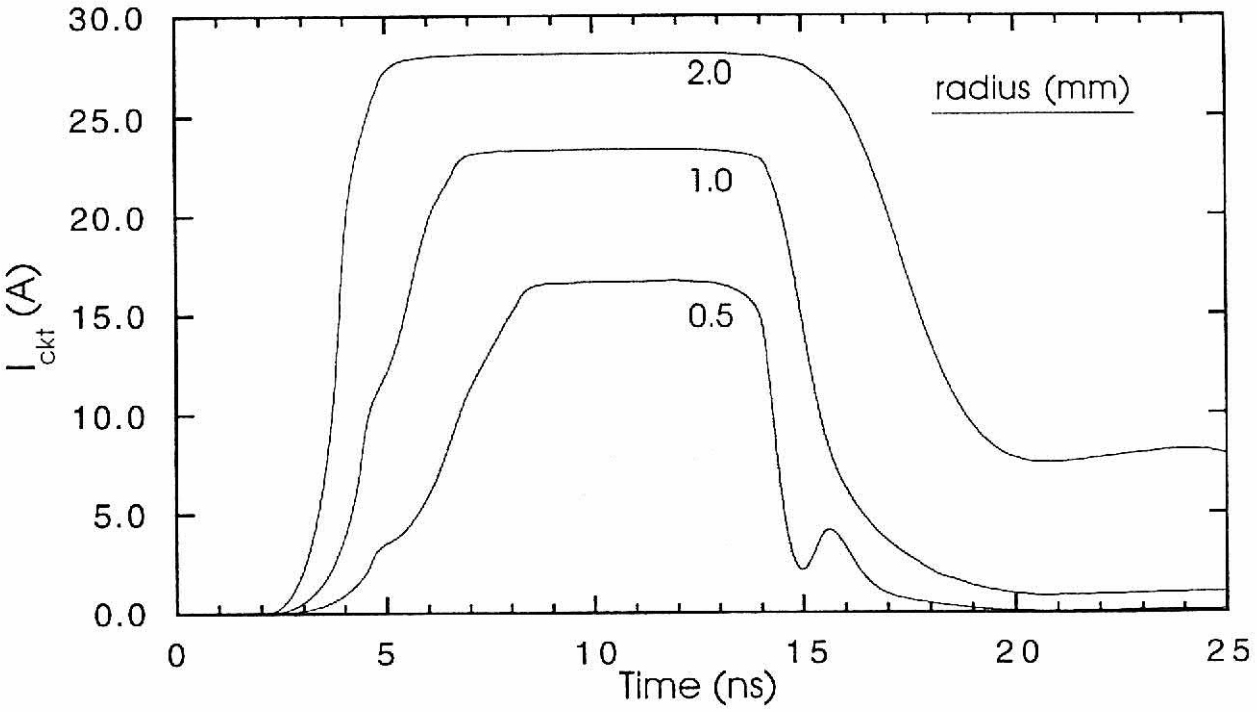

Figure IV-19. The current through a PCSS with the radius varied but on a uniform mesh with the mesh cells held constant. As the radius of the device is increased, the contact area increases, and thus the amount of carriers collected by the contacts increases. The result is an increase in the conducted current with an increasing radius of the switch.

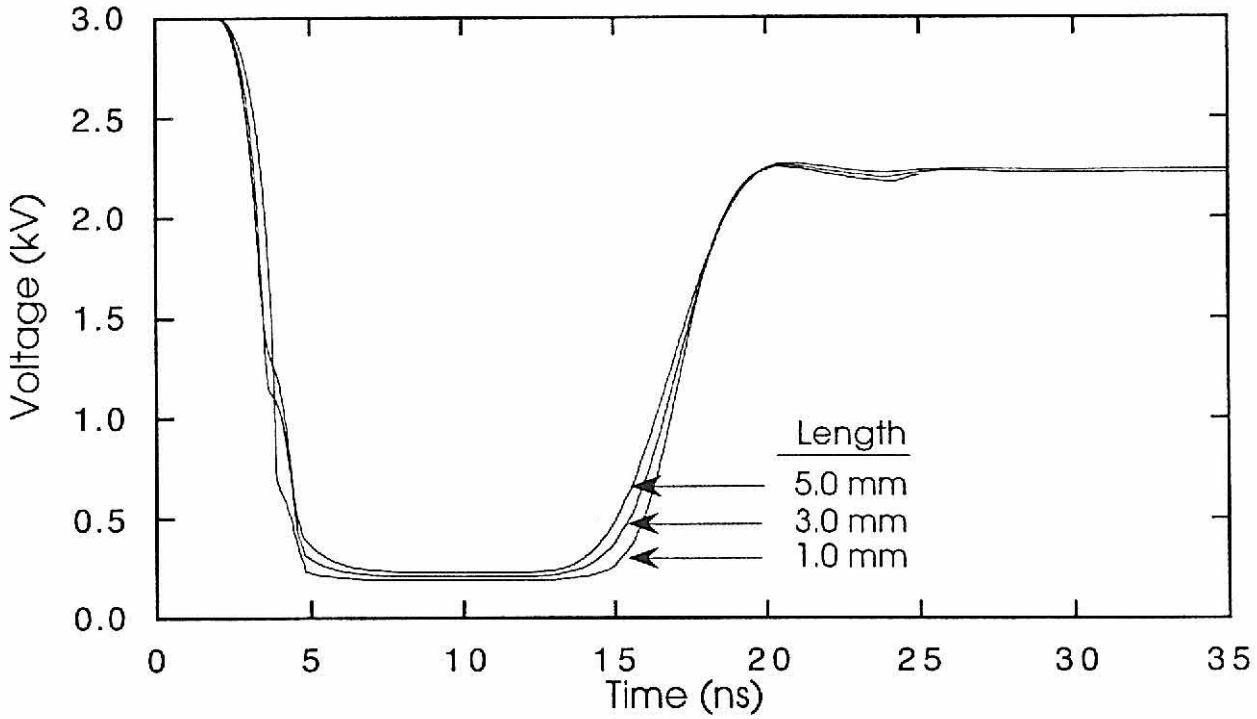

Figure IV-20. The voltage across a PCSS with the length varied but on a uniform mesh with the mesh cells held constant. Increasing the length of the device increases its resistance. Since most of the electric field is at the contacts in the closed state, the full effect of increasing the resistance cannot be resolved on the mesh near the contacts.

V. COPLANAR GaAs(Si:Cu) SWITCHES

A. Introduction

The model is applied to a coplanar BOSS device. The effect of the electric field on the I-V-t characteristics of the switch is established. Consequences of nonuniform permittivity, a grounded base, contact separation, nonuniform injection, laser pulse shape, embedded contacts, and light under contacts on the two-dimensional development of the electric field is analyzed. The effects of negative differential resistance and impact ionization on the switch cycle are established.

B. Switching

The coplanar switch geometry for the BOSS is modeled in the side view. The simulation geometry and mesh for a side view of the coplanar switch is shown in Figure V-1. The right side and bottom of the switch are treated as being either floating (isolated) or grounded. The anode and cathode, which can be embedded, are both current injecting. An embedded contact breaks the top semiconductor plane of the switch. Any boundary not set to a voltage has the electric field component normal to its surface set to zero. In the simulations, the PCSS is doped 10^{10} cm^{-3} n-type with $N_{Si} \approx N_{Cu} = 10^{16}$ cm^{-3}. The on laser pulse has a Gaussian temporal shape centered at 6 ns (FWHM = 2 ns) with a maximum intensity of $\approx$ 6 MW/cm^2. The off laser is centered at 16 ns and has a maximum intensity of $\approx$ 18 MW/cm^2. Typical switching parameters are $\Phi_{on} = 5 \times 10^{25}$ cm^{-2}-s^{-1} ($\approx$ 9 MW/cm^2), $\Phi_{off} = 10^{26}$ cm^{-2}-s^{-1} ($\approx$ 11 MW/cm^2). Both the on and off laser are Gaussian in time with Δt = 2 ns. The circuit parameters are a 3.3 pF capacitance in parallel with the switch, as well as a 20 nH inductance and a 50 Ω load in series with the switch. The laser pulses are spatially varied as a Gaussian distribution with a full-width-half-maximum (FWHM) of twice the contact separation and centered between the anode and cathode as shown in Figure V-2(c).

The current and voltage during a switching cycle for a switch with an ungrounded coplanar geometry are shown in Figure V-3. The dimensions are 5 x 0.64 x 4 mm, with abrupt contacts separated by 1.7 mm and embedded 0.1 mm into the semiconductor. A Gaussian distribution of light is used for the laser pulse. Upon application of the on laser pulse (6 ns), photodetachment of the ionized Cu acceptors introduces electrons into the conduction band. The applied voltage across the switch decreases from 3 to $\approx$ 118 V, with a closing time of $\approx$ 1.7 ns. The current is switched from mA's to

≈ 58 A, with a circuit limited value of 60 A. Upon application of the off laser pulse (16 ns), the Cu acceptors are reionized. This action produces holes in the valence band, which provides recombination partners for the conduction electrons. The result is that the switch almost completely opens, approaching 3 kV, with an opening time of ≈ 0.7 ns. As is seen experimentally (Figure II-3) the closing time is limited by the risetime of the closing laser pulse.[18,54] The switch will open to the line voltage slowly as the Cu acceptors trap the excess electrons on a microsecond time scale. The current density is maximum at ≈ 5 kA/cm^2, though it is spatially nonuniform. In general, experimental switches have spatially averaged current densities of ≈ 2 kA/cm^2.[18]

Electric fields in BOSS devices have been measured by Schoenbach et al. using a photoabsorption technique based on the Franz-Keldysh effect.[18] Transient nonuniformities in the electric field were observed for voltage pulses above a threshold value (above ≈ 3 kV in the coplanar geometry) with more severe nonuniformity as the voltage was increased. With the hold-off voltage slightly above threshold, photoabsorption is first observed near the cathode (indicating an increased electric field at the cathode). As the hold-off voltage is increased, electric field enhancement is observed near the anode as well (Figure II-7a). Eventually, at large enough hold-off voltages the high electric field at the cathode begins to merge with the electric field near the anode. The electric field is higher at the cathode region compared to the anode region before laser activation. After the switch is closed, the electric field in the cathode region breaks down (Figure II-7b). The electric field at the anode region is still rather large.[17] Falk et al.[23] have also made absorption measurements and have observed increased absorption at the anode that increases in width as the applied voltage is increased.

A time evolution of the electric field for the ungrounded abrupt contact case is shown in Figure V-4 for the same conditions as the abrupt case in Figure V-3. The electric field is initially enhanced at the sharp edge of the embedded anode and cathode (0 ns). As the on laser is applied (3 ns), the electric field enhancement increases at the contacts and is reduced in the center, where the carrier density has increased. As time progresses (4 ns), the electric field enhanced regions increase further as they are compressed toward the contacts. At the peak of the laser pulse (6 ns), the switch has been triggered to 118 V, which reduces the electric field enhancement in the bulk of the switch with the electric field collapsing to the cathode. This electric field configuration remains fairly static during the

closed phase. During the off laser pulse, the electric field at the cathode begins to increase due to the increasing hold-off voltage (14 ns). However, as the switch opens (16 ns), the region of electric field enhancement begins to move toward the anode at a speed of $\approx 7.8 \times 10^6$ cm/s. When Eq. (III.9) is used for the electron velocity as a function of the electric field, 80 kV/cm corresponds to a velocity of $\approx 7.6 \times 10^6$ cm/s. These trends concur with the experimental observations.[14,17,19]

The motion of the high electric field toward the anode results from excess electrons being swept out of the volume, trailing an interface between a high and low conductivity. Figure V-5 is a time evolution of the log of the electron density for the abrupt case. Near the peak of the closing laser pulse, electrons are the only mobile carrier. As the closing laser pulse is approached (4 ns), the large level of n_e introduced by the laser pulse is evident with some nonuniformity corresponding to the electric field enhancement observed near the contacts. At the peak of the closing laser pulse (6 ns), the large electron density mirrors the spatial distribution of the applied laser pulse which is dominating all the electron generation processes. At the peak of the opening laser pulse (16 ns), a reduced region of electrons has formed as a result of abruptly reducing the magnitude of electron injection that was occurring when the switch was closed and of the large reduction of electron density near the center of the switch through recombination with the holes introduced by the opening laser. The small electron density under the cathode is a reflection of the reduced injection. After the switch has opened (21 ns), the level of n_e has been lowered in the center of the switch where the holes were introduced and is higher near either side.

The evolution of the log of the hole density is shown in Figure V-6. In the closing phase, holes play a small role. Similar to the bulk switch, the Cu hole trapping cross section is large. Thus, any background holes are quickly trapped by the Cu. As the switch opens due to hole emission from the Cu traps, however, the hole density does become significant. The mechanisms for hole reduction are severe enough, however, that these holes remain mobile in the switch for only a short time. As the switch begins to open, the hole distribution reflects the laser flux distribution. At the peak of the closing laser pulse (16 ns), there is slight nonuniformity in n_p between the contacts where holes are recombining in proportion to the nonuniform electrons in the region. The two main mechanisms, Cu trapping and electron-hole recombination, are rapid enough that n_p decreases by two to three orders of

magnitude 2 ns after the peak of the closing laser pulse (18 ns). Some time into the opening phase of the cycle (21 ns), n_p is again at background levels.

The spatial distribution of Cu traps is dominated by the laser pulse spatial distribution. Figure V-7 shows the time evolution of the density of the neutral traps N_{CuB}. The copper density starts completely compensated or ionized. Therefore, the density of neutral traps is zero. When an electron is emitted from a copper trap or a hole is trapped, the neutral copper density increases. The positive charge on the shallow ionized silicon donor density N_{Si}^{+} is no longer shielded by the ionized copper acceptor density when the electron moves from the area. When a hole is emitted from a copper trap or an electron is trapped, the neutral copper density decreases, which shields more of the ionized silicon donors. As the switch closes (6 ns) and during the closing phase (10-12 ns), the spatial distribution of N_{Si}^{+} is similar to the laser pulse applied. The larger density is at the center top, where the laser flux and thus electron emission from the traps is the largest. In the opening phase (18 ns, 21 ns), the density varies by 9.1 $x10^{15}$ cm^{-3} to 8.8 $x10^{15}$ cm^{-3} over the bulk of the switch. The variation is due in large part to the uneven trapping of holes.

The electron, hole, and trap spatial distributions, in part, determine the space charge density. A time evolution of the log of the space charge density is shown in Figure V-8. A dashed line represents negative space charge and a solid line represents positive. Also note that even though the magnitudes of the density are shown, the contours show their log value. A circled positive sign represents a background of positive space charge, and a circled negative sign represents a background of negative space charge. A space charge at the background level is not sufficient to perturb the electric field. The zero density lines were smoothed. In general they are at the roundoff error level of the computer and are much rougher given the large dynamic range of the calculation. As electrons are emitted from the copper traps during the closing phase (4 ns) and drift toward the anode, they expose the positive space charge of the shallow Si donor. The electric field enhancement fronts are a consequence of positive space charge moving slightly ahead of negative space charge. This charge separation is a result of electrons in a smaller electric field drifting at greater speeds than the electrons near the electric field enhancement front. When the switch is closed (6 ns), the space charge variation is small, except near the contacts at which the large electron injection near the cathode is perturbing the electric field. After

the switch has opened (21 ns), again there is a plane of positive space charge moving ahead of a negative space charge. To get a better idea of the space charge variation and how it effects the electric field, a spatial slice under the contacts is taken from the 21 ns case and is plotted superimposed with the voltage in Figure V-9. The charge discontinuity between the contacts affects the concavity of the voltage and, consequently, enhances the component of the electric field parallel to the spatial slice taken. This discontinuity is set up with the abrupt decrease in electron injection at the cathode and the rapid recombination of electrons with the emitted holes in the center of the switch. The voltage under the contacts is dominated by the contacts' proximity. The region of positive charge under the cathode is due to the absence of electrons in the region relative to the rest of the device.

C. Nonuniform Permittivity

Electric field enhancement at the contacts can result in nonuniform carrier injection and can possibly provide end points for filaments to strike and degrade the contacts. One source of electric field enhancement is simply the sharp edges of the contacts. Grading the contacts by producing a smooth transition in permittivity (by, for example, ion implantation) will reduce the electric field enhancement at the cathode and displace the maximum in the electric field into the bulk semiconductor. Since injection at the contacts is generally a function of electric field, providing a more uniform electric field at the contacts will promote more uniform injection at the contacts and will thereby reduce the likelihood of filament formation.

To simulate graded contacts in the model, the electrical permittivity was exponentially varied from the edge of the contacts at which $\varepsilon/\varepsilon_0 = 83.2$ to the bulk value ($\varepsilon/\varepsilon_0 = 13.2$) over a distance of 0.1 mm. The time evolution of the electric field for the graded contact case is shown in Figure V-10. Initially (0 ns), the peaks of the electric field in the abrupt contact case occur at the corners of the contacts. However, the peaks in the electric field are displaced into the bulk semiconductor with the graded contacts. As the switch cycle progresses (4 ns), the switch with the graded contacts also has regions of electric field enhancement near the contacts which eventually collapse to the cathode (14 ns), then shift to the anode as the switch opens (21 ns). However, the graded contact case has lower electric field enhancement near the contacts throughout the switch cycle as compared to the abrupt contact case. The graded contact switch also closes to a lower voltage of ≈70 V compared to the abrupt contact case

(≈118 V), as shown in Figure V-3, when using the same amount of optical energy for the switching laser. Since the number of carriers produced is the same in each case, the higher conductivity of the graded contact case near the contacts results from a higher drift velocity. The higher drift velocity is a consequence of the lower average electric fields in the graded contact case compared to the abrupt contact case, as shown in Figure V-10 and Figure V-4, respectively (14 ns). Due to negative differential resistance, the mobility of electrons (and, hence, the collected current) is larger with the lower electric field, provided the electric fields exceed the electric field required for maximum velocity, which is approximately 3 kV/cm.

D. Grounded vs. Ungrounded Base

If the switch is integrated into a microelectronic circuit in a stripline fashion or is in contact with a heat sink to draw off the excess heat generated in the switch, then the "bottom" and "side" of the switch will most likely be grounded. Figure V-11 shows the voltage switching cycle for a grounded and ungrounded graded contact case. The main difference is in the opening phase, in which the grounded case is much less sensitive to the opening laser pulse. A time evolution of the electric field for the grounded, graded typical case is shown in Figure V-12. The initial electric field distribution (0 ns) shows large enhancement near the anode, with the peak displaced due to grading of the permittivity. The asymmetry is a consequence of grounding the side and bottom of the switch. This asymmetry is the cause of much of the preferential enhancement at the anode. The closing characteristics appear fairly similar between the grounded and ungrounded (Figure V-10) cases, except for the absence of an electric field enhancement plane near the anode (4 ns) in the grounded case. The differences begin when the switch is opened. In the grounded case, an electric field enhancement front has formed and intersects the anode. In the ungrounded case, the electric field enhancement front formed near the cathode is drifting to the anode but at 21 ns has yet to intersect it. The shape of the electric field enhancement in the grounded case differs as well. Included with the planar enhancement front there is a point of enhancement at the bottom. The bottom enhancement is a result of the stationary electric field near the anode that is sweeping carriers out of the region, exposing the shallow positive donors, and perturbing the electric field. Raising the electric field level at the anode, as in this grounded case, causes changes in the injection of electrons at the contact and also affects the collection of holes at the contact.

Figure V-13 is the log of n_e for the grounded, graded case. The increased electric field enhancement near the anode causes the avalanche of carriers, which results in a large collection of carriers at the anode and a reduced opening of the switch. This occurs even though the collection of electrons is limited to near the saturation velocity rate due to this same electric field. In the ungrounded case, the absence of the large enhancement front at the anode allows the electrons to drift with a larger velocity, but the densities are small enough that the current collected by the contacts decreases the opening of the switch.

E. Opening Laser Level

Figure V-14 is a plot of the voltage cycle as the magnitude of the opening laser is increased. If the opening phase is triggered hard enough, it opens to a higher level but it is still less sensitive to the opening laser than it is in the ungrounded case. Figure V-15 shows the time evolution of the electric field when $\Phi_{off} = 3 \times 10^{26}$ cm^{-2}-s^{-1} ($\approx$ 34 MW/cm^2). Comparing Figure V-15 to the $\Phi_{off} = 10^{26}$ cm^{-2}-s^{-1} ($\approx$ 11 MW/cm^2) case of Figure V-12, one can see the increase in electric field at the bottom plane of the switch as the laser flux is increased. A larger on flux causes a larger hole density, which means a larger level of recombination with electrons, which results in a faster opening time. The residence times of holes in this system is fairly short. It was observed earlier that the hole density reverts to background levels within nanoseconds after the peak of the on laser pulse which is supplying the holes to the system. The larger opening fluxes cause larger enhancement of the electric field, which reduces the velocity of the electrons further, lowering the amount of collected current at the contacts and allowing the switch to open to a larger level. The downward slope of the opening level implies that the opening voltage level will be reduced as time progresses. Therefore, eventually the electric field at the anode will inhibit the complete opening of the switch.

F. Contact Separation

The level of the voltage that can be held off when the switch is open depends on the contact separation. The farther apart the contacts are, the more voltage can be applied without exceeding some critical electric field level. Above this critical electric field, either breakdown or uncontrolled avalanching of the carriers will occur. Figure V-16 shows the effect of contact separation on the voltage cycle of the switch. The closing phase is relatively unaffected. In the opening phase the larger the

contact separation becomes, the more complete the opening of the switch. Figure V-17 shows the time evolution of the electric field for contacts 1 mm apart, and Figure V-18 shows the electric field for contacts 3 mm apart. The first factor to note is that the contact separation (1.0 - 3.0 mm) does not effect the electric field maximums occurring in the device as the device is being triggered. Therefore, even though larger contact separation means larger hold-off voltages, during switch operation the electric field maximums will be relatively unaffected. Second, one can see that the electric field enhancement occurring at the anode while the switch is opening, is independent of the contact separation. However, the presence of the front is not the only factor causing the reduction of sensitivity in the opening phase, given the larger levels of opening achieved as the contact separation is increased. Also, the area under the contacts is drastically reduced as it goes from 1 to 3 mm contact separation, yet the amount of carrier collection for the cases during the closed state is similar, which suggests that carrier collection under the contacts, at least for embedded contacts, is occurring largely near the corners.

There is more than just a change in contact separation in these cases. Other factors may be playing roles in the changes just discussed. The mesh becomes somewhat larger in the center as the contacts are widened. Thus, less resolution is possible there. However, the electric field collapsed quickly to the anode in the 1 mm separation case as well as in the 1.7 mm case. Therefore, the electric field collapse was not due solely to a lack of resolution of the electric field at the center between the contacts. The spatial distribution of the laser pulse is also widened to accommodate the larger contact separation. The widened laser pulse means more carriers are introduced into the semiconductor as the contact separation is increased. Some of the increase in opening sensitivity could be due to the larger number of holes introduced into the semiconductor as the switch is opened.

G. Nonuniform Injection

One method by which nonuniform electric fields and filaments could be developed is by nonuniform carrier injection at the contacts that result from, for example, surface roughness on the contacts producing electric field enhancement. To test this hypothesis, roughness was applied to the bottom surface of the cathode producing an electric field enhancement of 25% over a distance of 0.2 mm. The resulting electric field distributions at t = 0 and 8 ns are shown in Figure V-19. The area

of roughness on the contact has become a seed for electric field enhancement throughout the switch, which may lead to filamentation.

H. Laser Pulse Shape

A more realistic laser pulse shape than the Gaussian distribution for light applied from the top is shown in Figure V-2. This distribution is based on a point source of light a distance away from the switch. Figure V-2(a) shows the light flux level in the switch when the light source is 1.0 mm away from the switch surface, and Figure V-2(b) is a 0.1 mm case. The contacts block the incident light so that the light will no longer penetrate under the contacts. As the focused light moves closer to the switch, more of the laser light is absorbed under the contacts. A comparison of the voltage cycle for a Gaussian and a focused light pulse shape for light points two distances away is shown in Figure V-20. The Gaussian case of comparison is the graded ungrounded case, the electric field of which is shown in Figure V-10. The switch having the Gaussian pulses closes to a lower voltage level than either of the point-of-light pulsed switches. Varying the distance from the switch of the focused light by two orders of magnitude shows little difference in the closed and opened state. The closing time is shorter for the nearer light source spot, however. The main reason for greater switch closure in the Gaussian case is that the Gaussian pulse introduces more carriers directly under the contacts, which allows the carriers to be collected immediately into the contacts before charge gradients form and electric field nonuniformities begin to take shape.

The differences in the two focused light cases arise from an electric field enhancement region which forms at the transition between a region where the laser light is being absorbed and a region of the semiconductor which is not being illuminated. The transition region separates high conductivity where the laser is introducing electrons to low conductivity where the laser introduces no carriers. This produces electric field enhancement at the boundaries. The location of this transition region depends on the location of the light source. Figure V-21 shows the electric field development for a point 0.01 mm from the switch, and Figure V-22 shows the electric field development for focused light 5 mm from the switch. In the respective cases at 14 ns, this transition region is evident at the collapsed electric field near the cathode. This enhancement compounds that already seen near the sharp corners of the embedded contacts. For the case in which the focused light is relatively distant, the proximity of the

corner electric field enhancement to the laser boundary enhancement is sufficient to delay the progression of the electric field front as it moves toward the anode. Figure V-23 further illustrates the delay of the electric field progression as the light source spot is pulled farther from the switch. Figure V-23 is the electric field at 18 ns for a switch triggered with light sources various distances from the switch. As the focused light is moved closer to the wafer surface, more light flux is absorbed under the contacts, and the electric field front progresses farther. The closer the light spot source moves, the switch response resembles more the case using Gaussian pulses. In fact, the characteristics associated with the closer focused light sources merge toward a Gaussian case. The boundary enhancement under the cathode as the switch is conducting in the closed state is the only difference.

The planar shape of the electric field enhancement is an artifact of the spatial distribution of the laser intensity being applied. The intensity of the laser pulse varies by only 20% from the top (contact plane) to the bottom of the switch with a 3 mm absorption length.[83] Altering the spatial distribution of the laser pulse in order that it penetrates only halfway into the switch (Figure V-24(a)) changes the character of the electric field enhancement as shown in Figure V-24(b). The electric field enhancement resulting from the "cropped" laser pulse does not penetrate through the switch. The electric field enhancement is larger in the center of the switch than with a penetrating laser intensity. Also the depth of these devices is 0.64 mm with a width of 5 mm, an order of magnitude difference. The aspect ratio in the figures is significantly altered and, as a result, may emphasize a planarity to the enhancement.

I. Nonembedded Contacts

Embedding contacts into the device moderates the electric field enhancement at the corners of the contacts but makes the switch manufacture more complicated then a direct deposition of the contacts on the flat surface. Therefore, shallower contacts are typical of the switches under development. The effect of a 5 μm contact depth compared to a 100 μm depth on the voltage switching cycle is shown in Figure V-25. The more deeply embedded contacts close to a lower voltage than do the shallow contacts. The shallower contacts have less surface area to collect current. Collecting less current raises the closed voltage level. Figure V-26 shows the electric field for the 100 μm embedded contact, and Figure V-27 shows the electric field for the 5 μm embedded contact. As is evident from the initial electric field, these are seen to be graded contacts. The main consequence of the shallower contact is an

increase of the electric field enhancement at the corner of the contact compared to that observed in the more penetrating contacts. The electric fields below the contacts, however, are relatively unaffected by the contact depth change, and the voltage cycle is similar.

When grounding the base of a shallow contacted switch and triggering with a point source, there is no severe reduction in the sensitivity to the off laser pulse like that observed for the Gaussian triggered embedded contact switch (Figure V-11). Figure V-28 is the voltage switching cycle for the (un)grounded shallow contacted graded switch. The grounded switch is shown to open to nearly the same voltage level as the ungrounded switch, although it opens slightly less. Figure V-29 shows the electric fields for the grounded switch with shallow contacts. The electric fields are similar in character to the grounded case with embedded contacts previously encountered in Figure V-12. Although Figure V-12 is a case with embedded contacts, the previous discussion showed that the only significant consequence of the embedded contacts is a moderation in the electric fields near the contacts. Also, the character of the applied light that is used as a trigger is different in these two electric field distributions. The case in Figure V-12 uses a Gaussian distribution, and the Figure V-29 case uses focused light. As the switch begins to close (6 ns) using focused light, the transition region between penetrating light and no light causes electric field enhancement which is not evident in the Gaussian pulsed grounded case of Figure V-12. The focused light case does exhibit large electric field enhancement near the anode during the opening of the switch that is also seen for the Gaussian triggered case. This difference implies that the enhancement at the base of the switch under the anode is a consequence of the grounded base plane geometry and not of the character of triggering light. Also, the enhancement front at the anode is not the direct cause of drastically inhibiting the opening level of the switch.

The electric field at the anode near switch closure takes longer to collapse to the cathode in the grounded case than it does in the ungrounded case with shallow contacts. Eventually, however, the electric field collapses to the cathode in both cases. As the switch begins to open, an electric field enhancement front begins to form at the cathode (16 ns) for both cases. As time progresses, the front dissipates in the grounded case. The enhancement of the electric field near the anode continues unabated. The electric field at the bottom ground plane also increases as the exposed positive charge of

the shallow donor is uncovered when the electrons are swept out of the region by the stationary electric field enhancement at the anode. Grounding the base plane compresses the electric field toward the anode and, as a result, causes larger enhancements near the anode for most of the switch cycle. In the ungrounded case, the symmetry of the electric field gives no preferential location of the electric field enhancement. As a consequence, any electric field nonuniformity is dominated by mechanisms other than the grounding geometry of the device.

J. Light Under Contacts

The importance of getting laser light under the contacts is the increase in the closing level for the same amount of light. This effect is seen in Figure V-20 when the voltage cycle of a switch triggered with a point source of light which does not penetrate to areas under the contacts is compared to a switch triggered with Gaussian light which does. Applying light from the bottom of the switch under the contacts would give a similar result. Introducing the light under the contacts leads to less electric field enhancement under the contacts. Figure V-30 shows the voltage cycle when triggering is done under the contacts of a graded shallow contact switch. The dotted line is the graded shallow contact case triggered by focused light over the switch. The effect is expected and is an increase in the closing level. The carriers introduced directly under the contacts minimize the electric fields under the contacts, increasing the electron and hole fluxes collected by the contacts. Figure V-31 shows the electric field for the ungrounded graded contact case with light applied at the bottom. Applying the light under the contacts leads to electric field characteristics similar to a Gaussian distribution, namely, collapse of the electric field to the contacts as the closing light pulse is applied and the eventual collapse of the electric field to the cathode as the on-state of the switch is reached. Also, in the opening phase an electric field enhancement front forms at the cathode and moves toward the anode. Having the light under the contacts, however, has an additional electric field front that forms in the center of the device as the switch opens. It also progresses toward the anode. This effect is not seen in the ungrounded Gaussian triggered cases (e.g., Figure V-4). The Gaussian application of light can thus approximate illumination under the contacts.

K. Negative Differential Resistance

The electric field enhancement front that progresses across the switch when the opening laser is applied is not evident when the overshoot character of the electron velocity is removed. Eliminating the negative differential resistance eliminates the formation of these mobile electric field enhancement fronts. Figure V-32 shows the electric fields of the shallow graded contact switch of Figure V-27 without the negative differential conductivity included. The electric fields in the closing phase for the two cases are essentially the same. In the opening phase, the electric field front does not develop in the case excluding negative differential resistance. The electrons in the large electric field enhanced regions drift with a faster velocity than electrons in less enhanced regions. Therefore, a high electric field enhancement front has no mechanism to travel toward the anode.

Excluding the negative differential resistance term reduces the number of electric field instabilities observed in the switch. A consequence of this effect should be a smoother voltage switching cycle that no longer has any Gunn type ringing or instability. Comparing the voltage cycle with negative differential resistance excluded and included (dotted line) in Figure V-30, one observes a smoother closing transition and much less ringing in the opening phase for the case in which negative differential resistance is excluded. Therefore, much of the ringing for the previous cases shown is due to the Gunn instabilities formed as a consequence of negative differential resistance.

L. Impact Ionization

Band-to-band impact ionization occurs at high electric fields. Given the rates of ionization in Eqs. (III.9) and (III.11), the electron density will change 1% per ns at an electric field of 1.38×10^5 V/cm. The consequence of including and excluding the impact ionization term in the model is shown in Figure V-33. Here the electric field is shown for an ungrounded switch with shallow graded contacts. Excluding impact ionization results in a significant increase of the electric field enhancement near the cathode. The lack of impact ionization of carriers removes a carrier generation process which can moderate the electric field enhancement due to the separated charge. It is also a process that is important in closing the switch, as seen in Figure V-30. The voltage is reduced during the on laser trigger. However, it quickly recovers and never sustains a closed state. Similarly, the introduction of holes during the opening laser trigger briefly increases the conductivity of the switch before the holes are

trapped, raising the resistivity of the switch. The enhancement of the electric field near the contacts creates carriers that are important in sustaining the closed state of the switch.

M. Heating

High electric field regions with high carrier concentrations can cause substantial joule heating. Severe local heating can damage the switch, particularly at the contacts. A consequence of a moderate local increase in temperature is a decrease in the band gap. The decreasing band gap causes the intrinsic carrier concentration to increase and increases the rate at which electrons and holes are emitted from the traps. These increases result in larger local rates of joule heating, which leads to higher temperatures. Highly nonuniform heating rates of 2×10^6 K/A-s near the anode and cathode have been simulated. A short voltage pulse (20 ns duration) produces only nominal increases in local temperature. However, long current pulses (100s ns to a few μs) coupled with high frequency repetitive switching will result in large temperature excursions. For example, a 2 μs current pulse with the abrupt contact switch will produce local temperature increases of 200 K over ambient.

N. Summary

The model has been used to investigate electric field nonuniformities in a coplanar GaAs(Si:Cu) photoconductive switch. Results from the model show that electric field enhancement in the switch is dependent on the geometry of the switch as well as on the type of laser activation used. In all geometries, the electric field completely collapses to the cathode at the on state with a more expedient collapse of the electric field for the ungrounded base switch geometry. For an ungrounded base, the opening laser pulse perpetrates the creation of an electric field enhancement plane at the cathode which progresses toward the anode at carrier drift velocity speeds. The opening phase of a grounded switch is dominated by electric field enhancement near the anode, which reduces the switch's sensitivity to the opening laser pulse. The mobile electric field enhancement planes observed when the switch is triggered are a consequence of negative differential resistance. Intrinsic avalanching of carriers plays an important role in closing the switch. When focused light is used to trigger the switch, the absorbed-light to no absorbed-light transition is a region of increased electric field. Grading near the contacts causes the electric field peaks to occur in the bulk of the switch rather than at the contacts, which results in more uniform injection of the carriers at the contacts. Embedding the contacts into the bulk of the

switch reduces the electric field enhancement observed at the corners of the contact when the device is holding off large voltages. Roughness at the contacts creates local charge excess, which generates local peaks in the electric field that are probable precursors to filamentation.

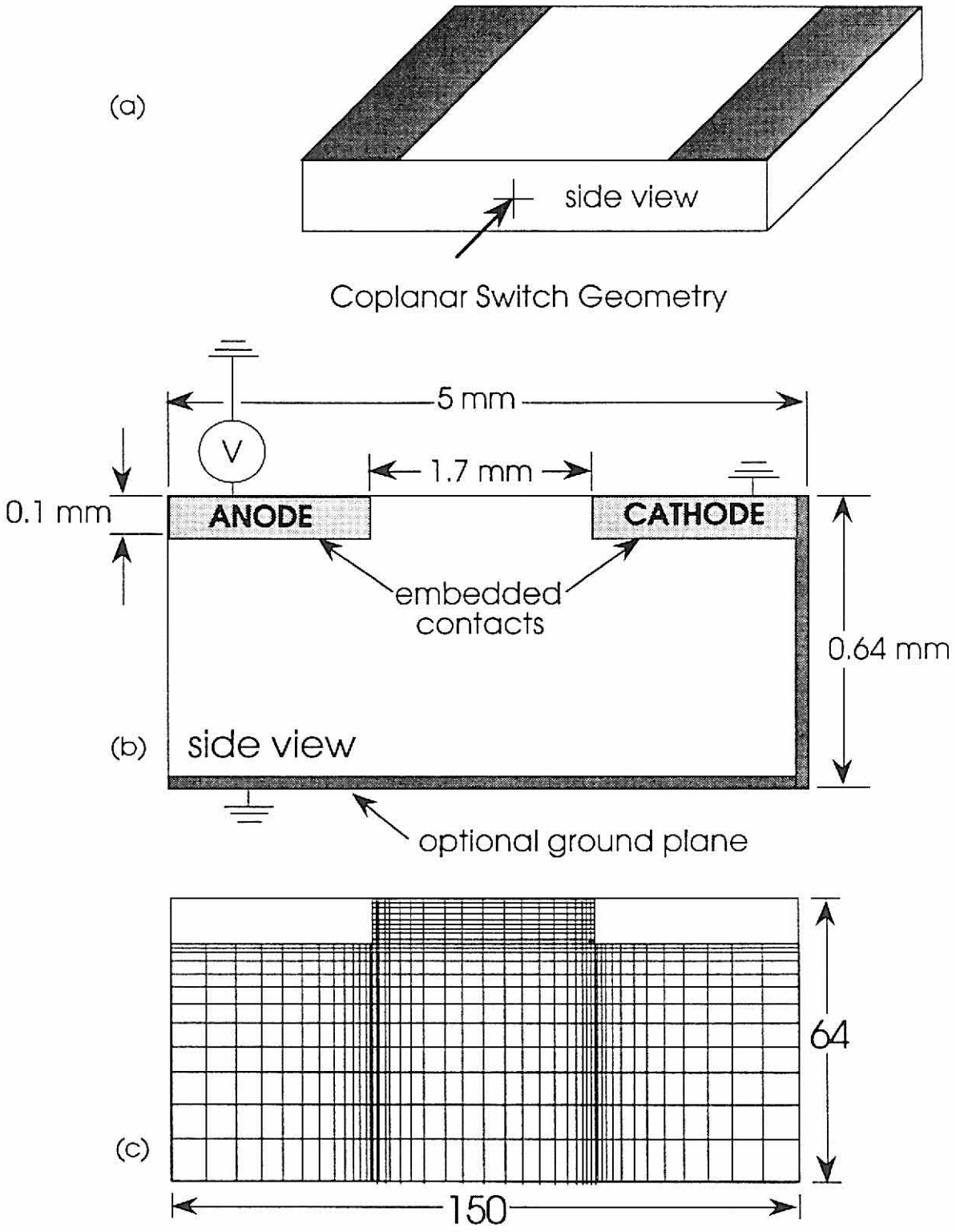

Figure V-1. Coplanar switch geometry: side view. (a) A photoconductive semiconductor switch using the coplanar geometry has both contacts on the same plane. (b) The typical dimensions used when simulating the side view of the switch are 5 x 0.64 mm, with a depth of 4 mm. The ground plane and embedded contacts are optional in the model. (c) The mesh used for the finite differencing is a nonuniform rectilinear mesh concentrated at the corners of the optionally embedded contacts.

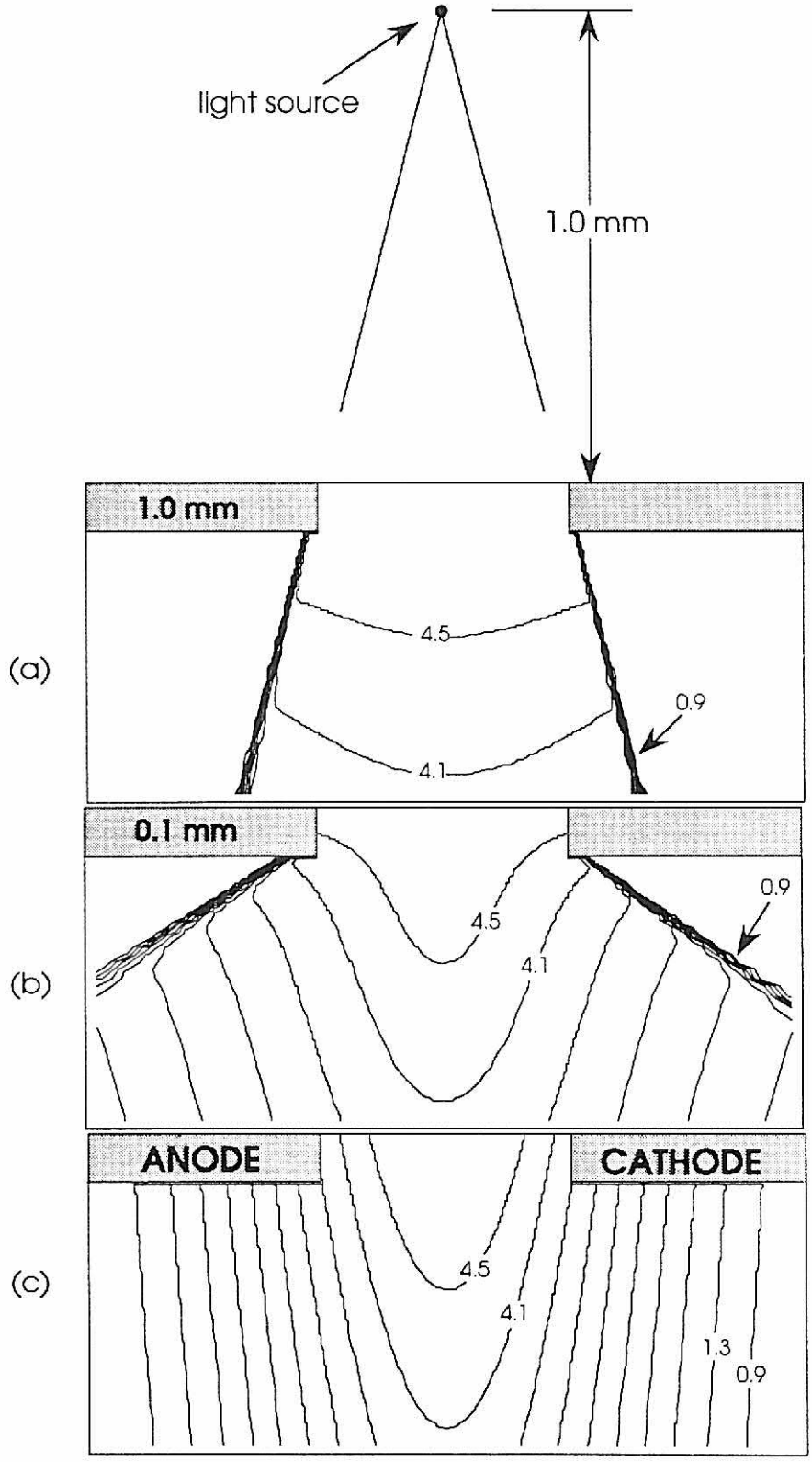

Figure V-2. Photon flux distributions. Photon flux $\left(\frac{10^{25}}{\text{cm}^2\text{-s}}\right)$ applied to the switch as (a) focused light centered between the contacts and 1.0 mm from switch, (b) focused light 0.1 mm from switch, and (c) a Gaussian spatial distribution with a FWHM equal to twice the contact separation.

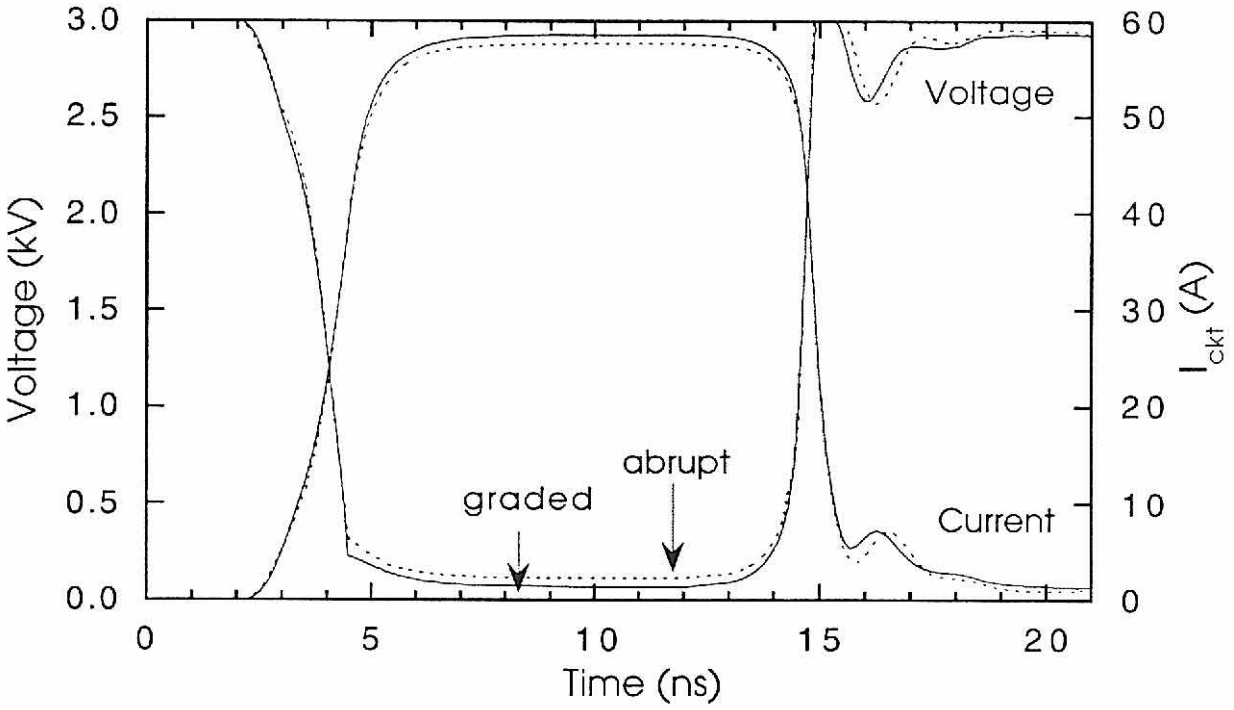

Figure V-3. The current and voltage characteristics for the abrupt and graded cases. The on laser pulse peaks at 6 ns. The off laser pulse peaks at 16 ns. The graded contact case closes to a lower voltage, given less severe velocity overshoot for electrons near the anode.

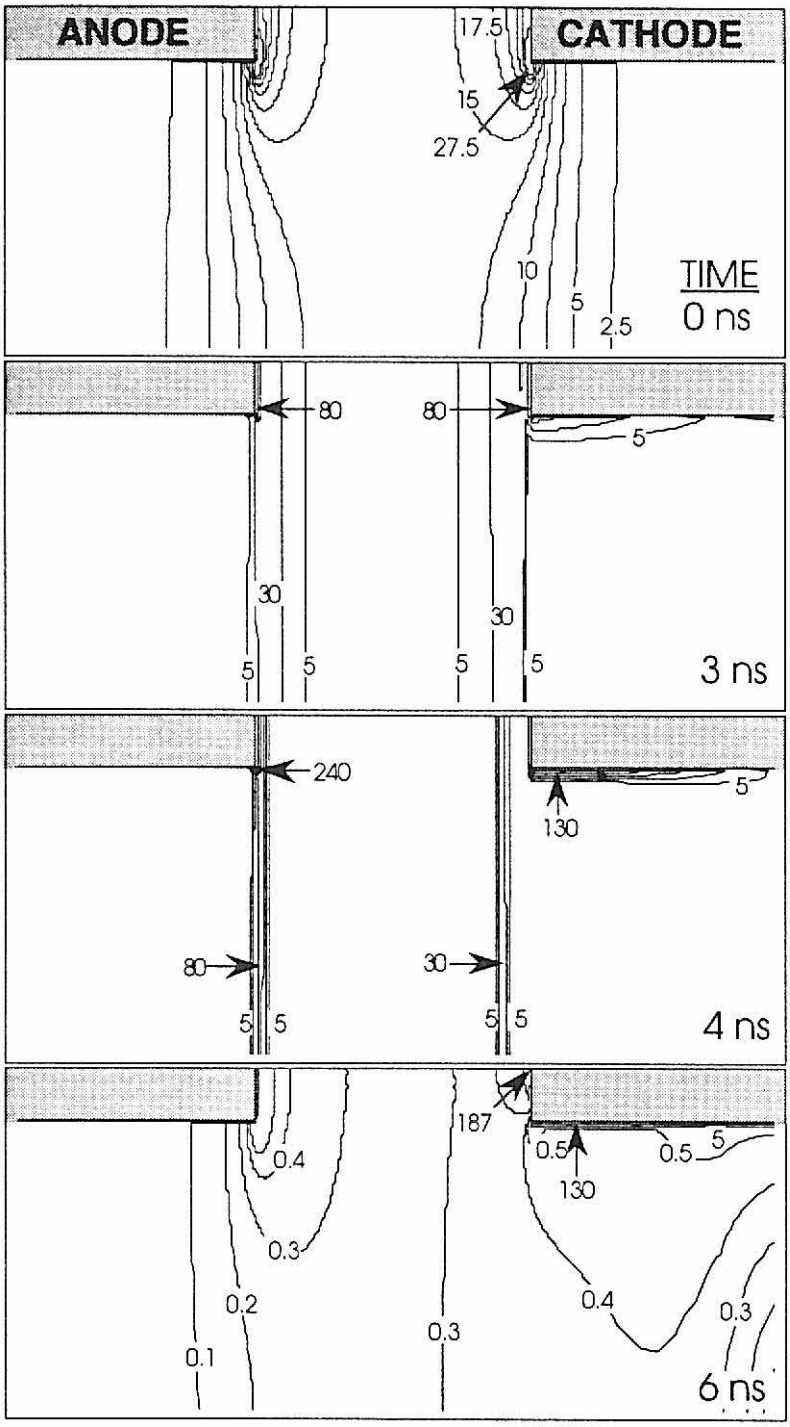

Figure V-4. Time evolution of electric field (kV/cm) for the ungrounded abrupt contact case for the conditions of Figure V-3. At t=0, electric field enhancement at the contacts are geometrical and symmetrical. During the on laser pulse, the electric field enhancement is being compressed to either contact as the conductivity in the center of the switch is increasing. Near the peak of the laser pulse the switch collapses to the cathode.

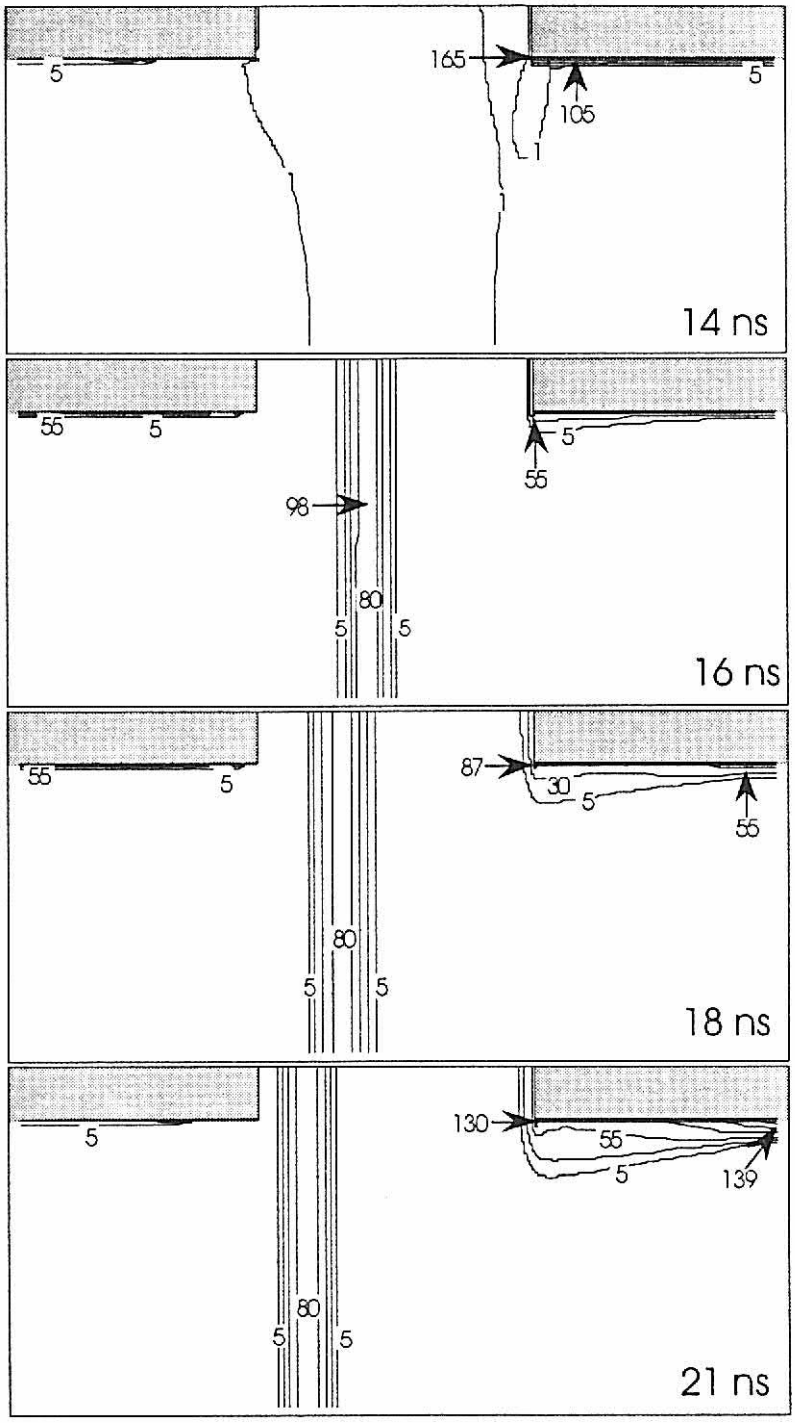

Figure V-4 (cont.) Time evolution of electric field (kV/cm) for the ungrounded abrupt contact case for the conditions of Figure V-3. During the off laser pulse, the region of electric field enhancement migrates to the anode as residual carriers are swept out of the bulk.

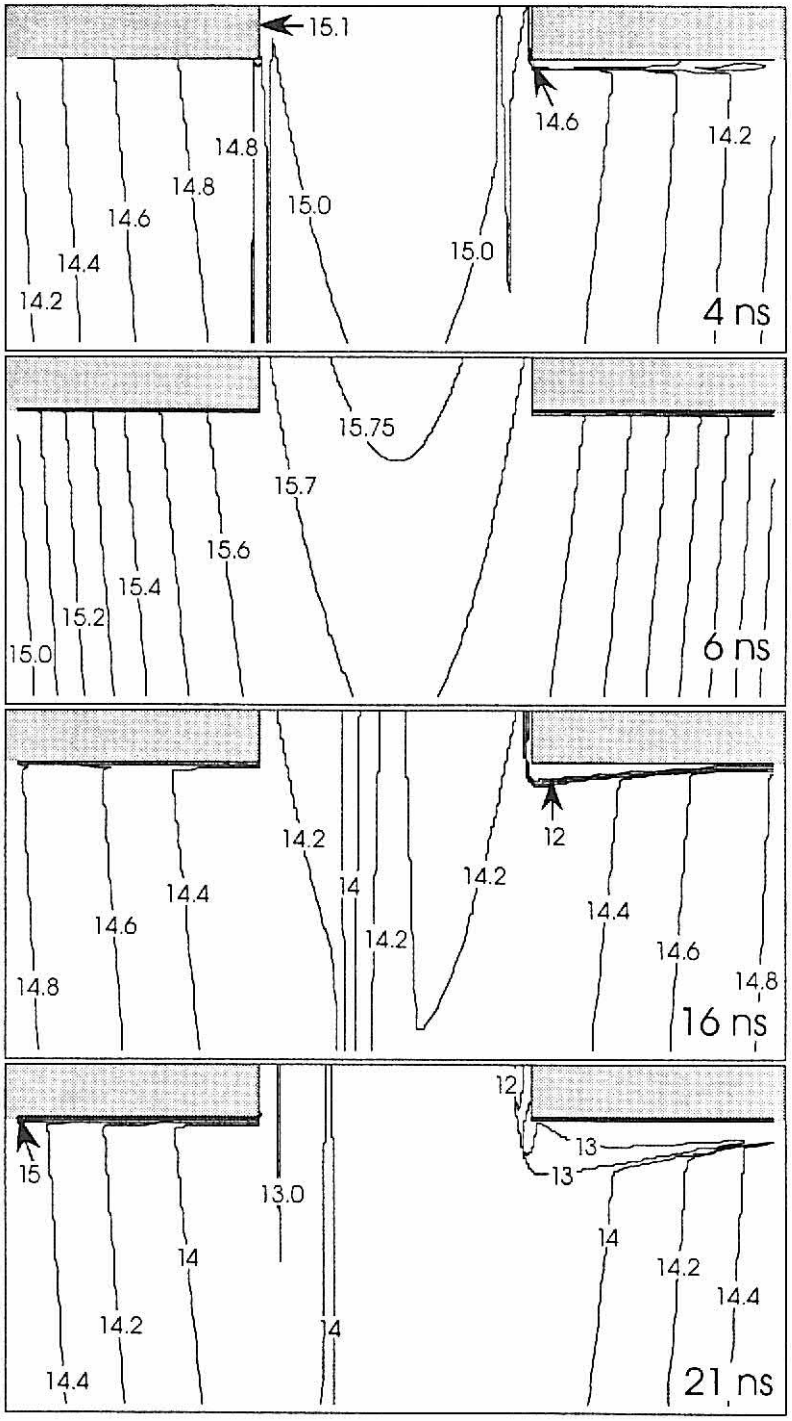

Figure V-5. Time evolution of the log of the electron density (cm^{-3}) for the ungrounded abrupt contact case for the conditions of Figure V-3. At the peak of the on laser (6 ns), n_e mirrors the Gaussian structure of the applied laser pulse. At the peak of the off pulse (16 ns), n_e is reduced at the electric field front as a consequence of carrier reduction on either side of the region.

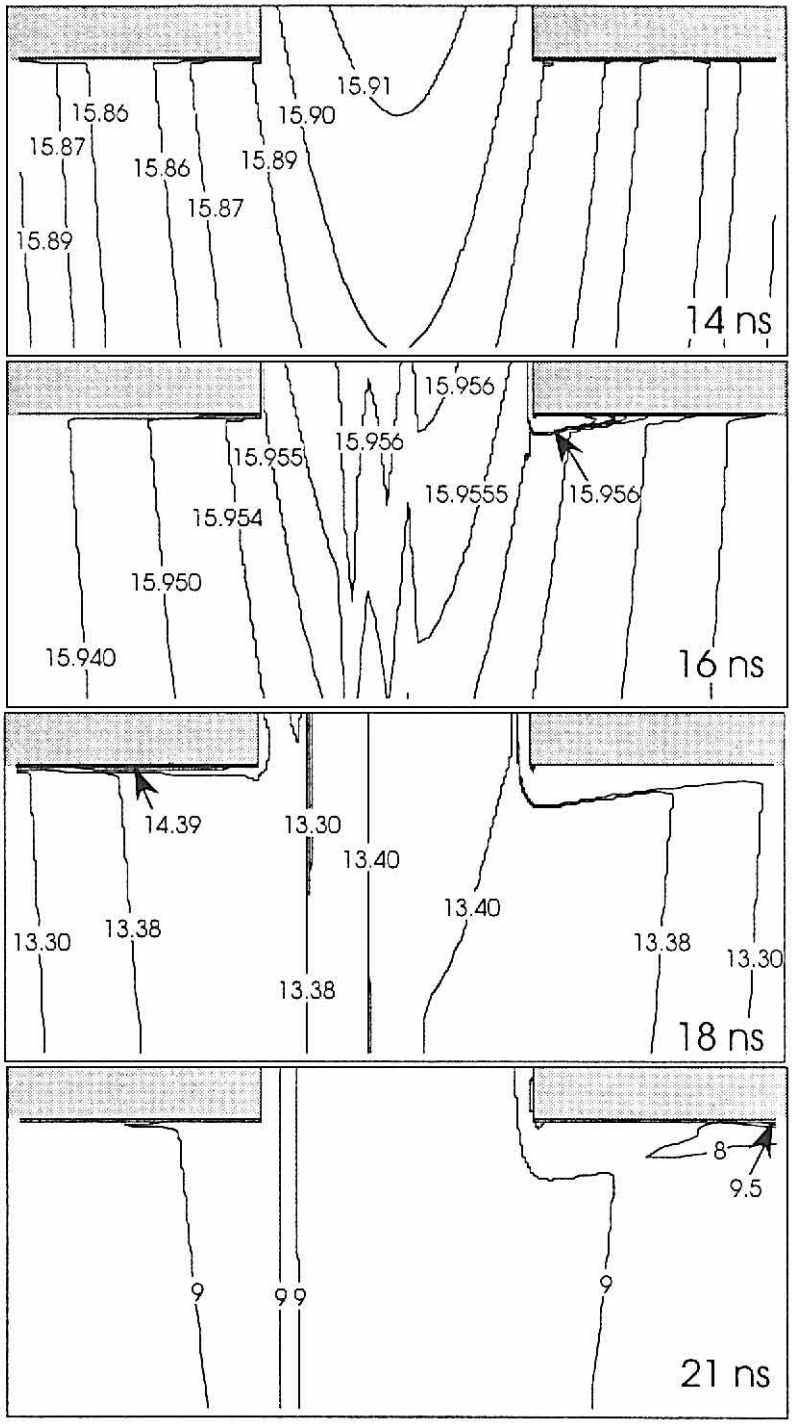

Figure V-6. Time evolution of the log of the hole density (cm^{-3}) for the ungrounded abrupt contact case for the conditions of Figure V-3. In the closing phase of the switch cycle, holes do not play a role, given the large trapping cross sections for holes. In the opening phase the hole trapping mechanisms are dominant enough that the hole density is quickly lowered soon after the peak of the off laser pulse.

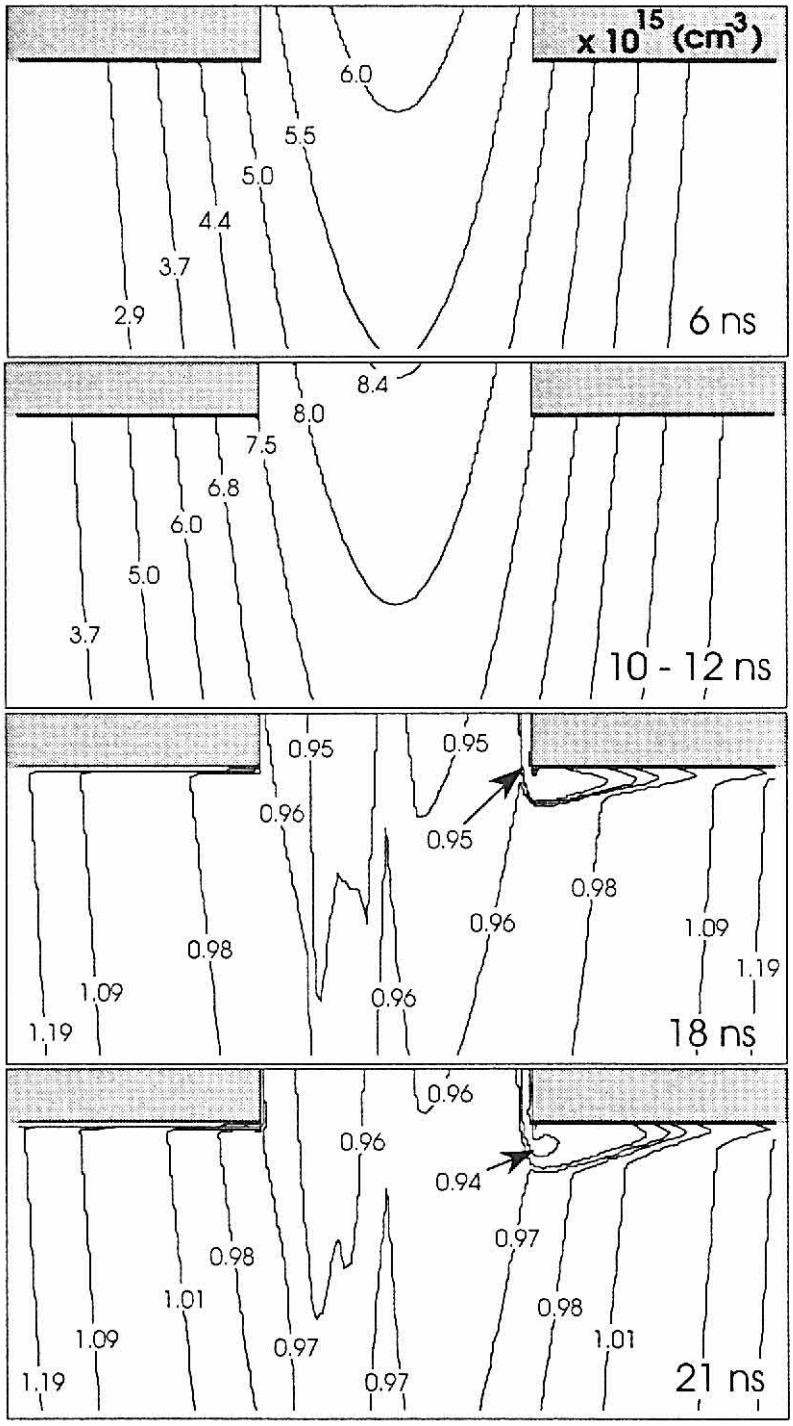

Figure V-7. Time evolution of the log of the neutral copper density N_{CUB} (10^{15} cm^{-3}) for the ungrounded abrupt contact case for the conditions of Figure V-3. Since the copper traps were completely compensated before switching by shallow donors, the N_{CUB} density gives the magnitude of N_{SI}^{+} charge that could possibly be exposed when the electrons drift from the area. In the closing phase, the high level of laser flux dominates the copper trap variation. In the opening phase, the variation is due in large part to the uneven recombination of holes.

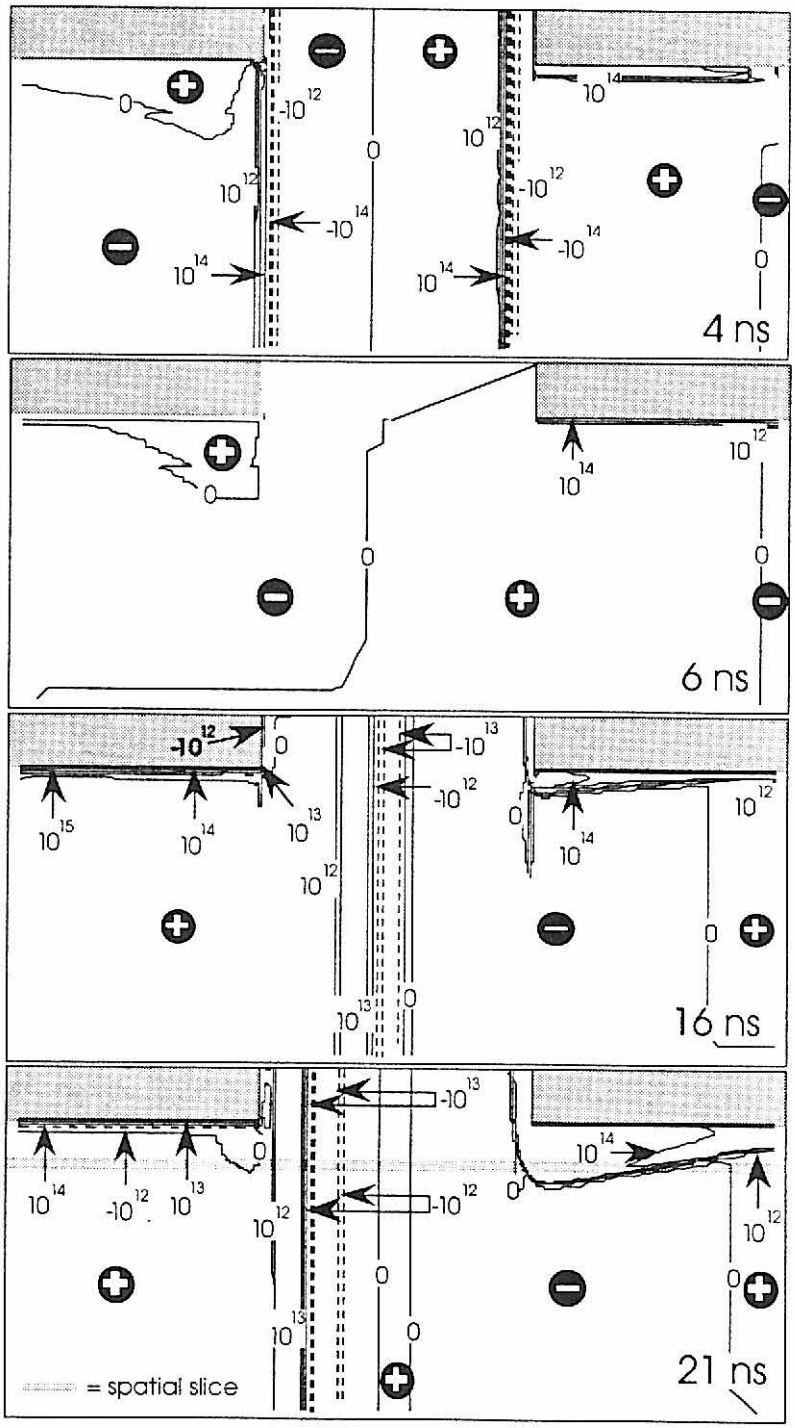

Figure V-8. Time evolution of the log of the space charge density (cm^{-3}) for the ungrounded abrupt contact case for the conditions of Figure V-3. The plus and minus signs indicate the charge of the background space charge. The zero lines were smoothed, given the large dynamic range in the calculation. The basic character of the enhancement fronts is a layer of positive and negative space charge, with the positive layer closer to the anode. At the point of enhancement, the electrons are drifting more slowly then away from the enhancement given the negative differential resistance of the material.

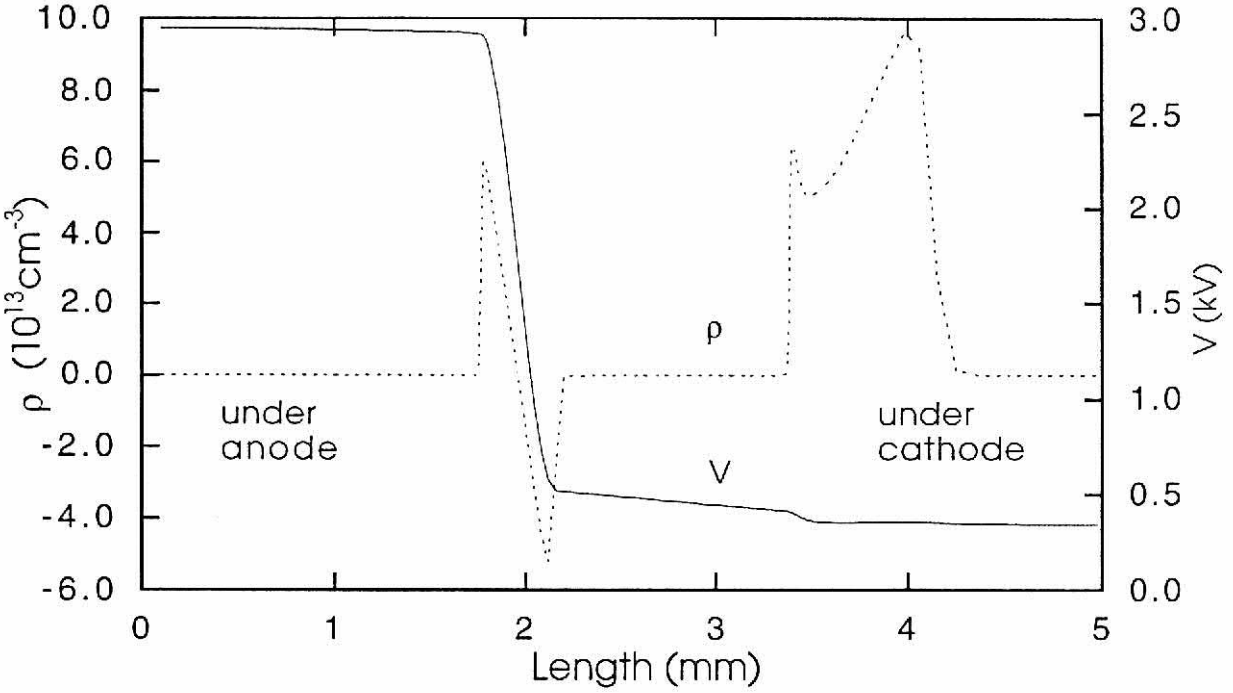

Figure V-9. Spatial slice at 21 ns of the voltage and the log of the space charge density (cm^{-3}) for the ungrounded abrupt contact case for the conditions of Figure V-3 with the exact position of the spatial slice shown in Figure V-8. The effect the space charge has on the voltage is shown. The enhancement front is a consequence of negative differential resistance, which slows electrons in the higher electric fields, increasing n_e in the area, and speeds up electrons in lower electric fields, reducing the n_e in the area.

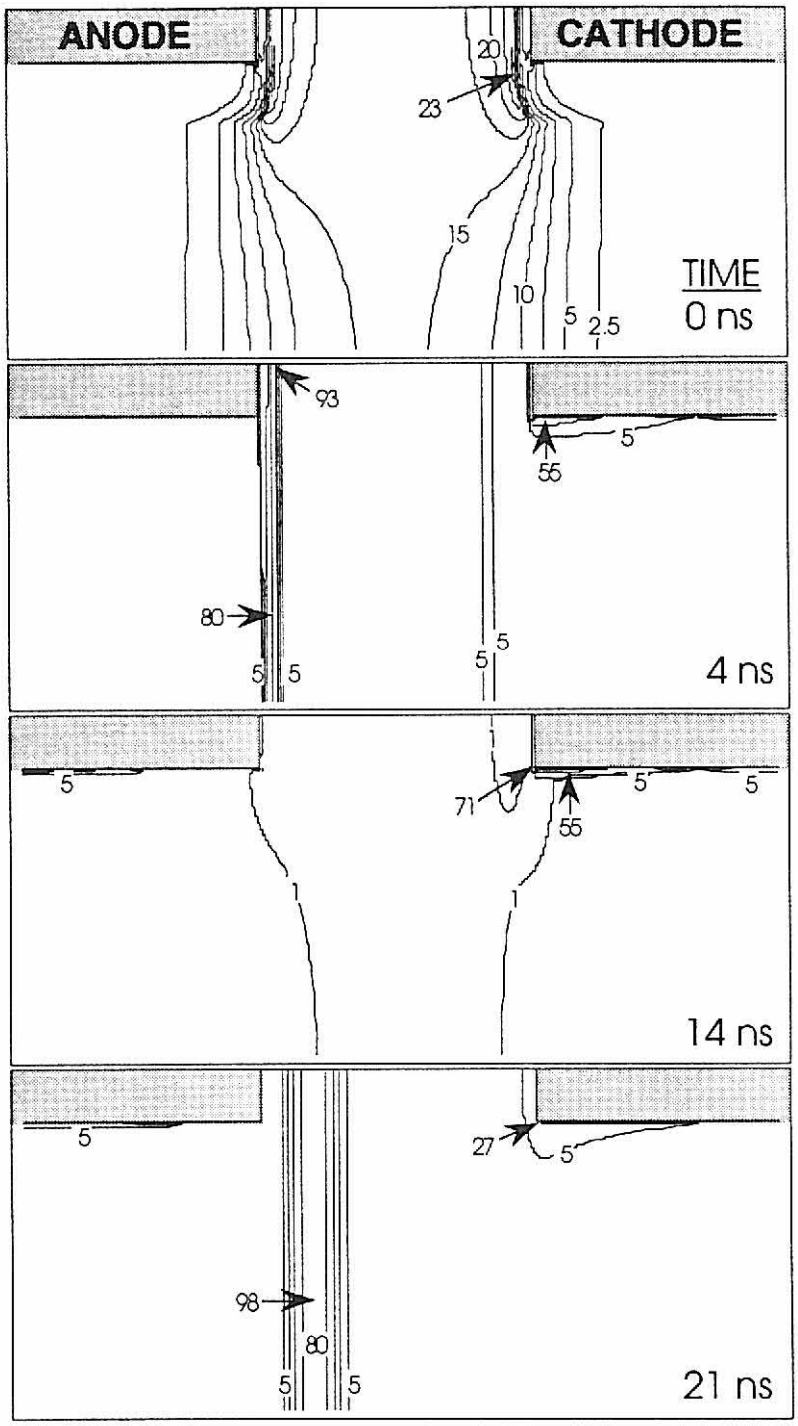

Figure V-10. Time evolution of electric field (kV/cm) for the ungrounded graded contact case for the conditions of Figure V-3. The grading that was introduced is evident in the initial condition with the electric field peaks displaced from the corners of the embedded contacts. Throughout the switching cycle there is a moderation of the high peak electric fields at the contacts. If there were no grading near the contacts, the peak electric fields at the contacts would be larger.

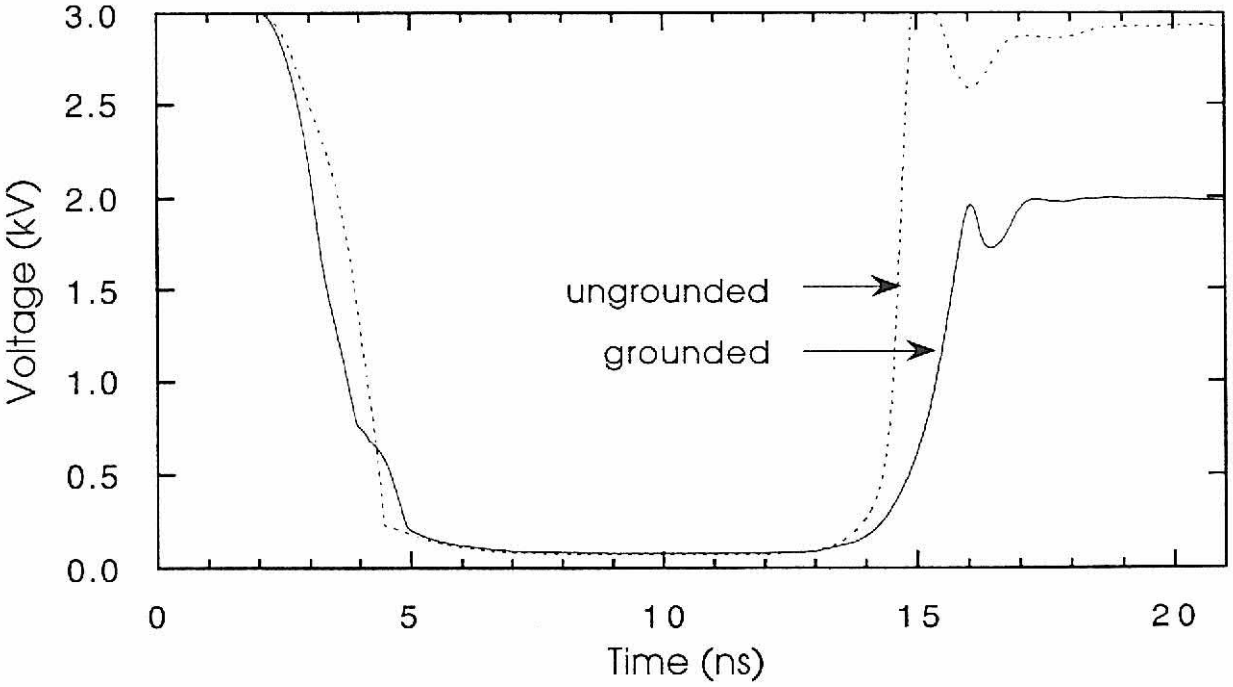

Figure V-11. The voltage characteristics for the grounded and ungrounded graded cases. The grounded case is much less sensitive to the opening laser pulse than the ungrounded case.

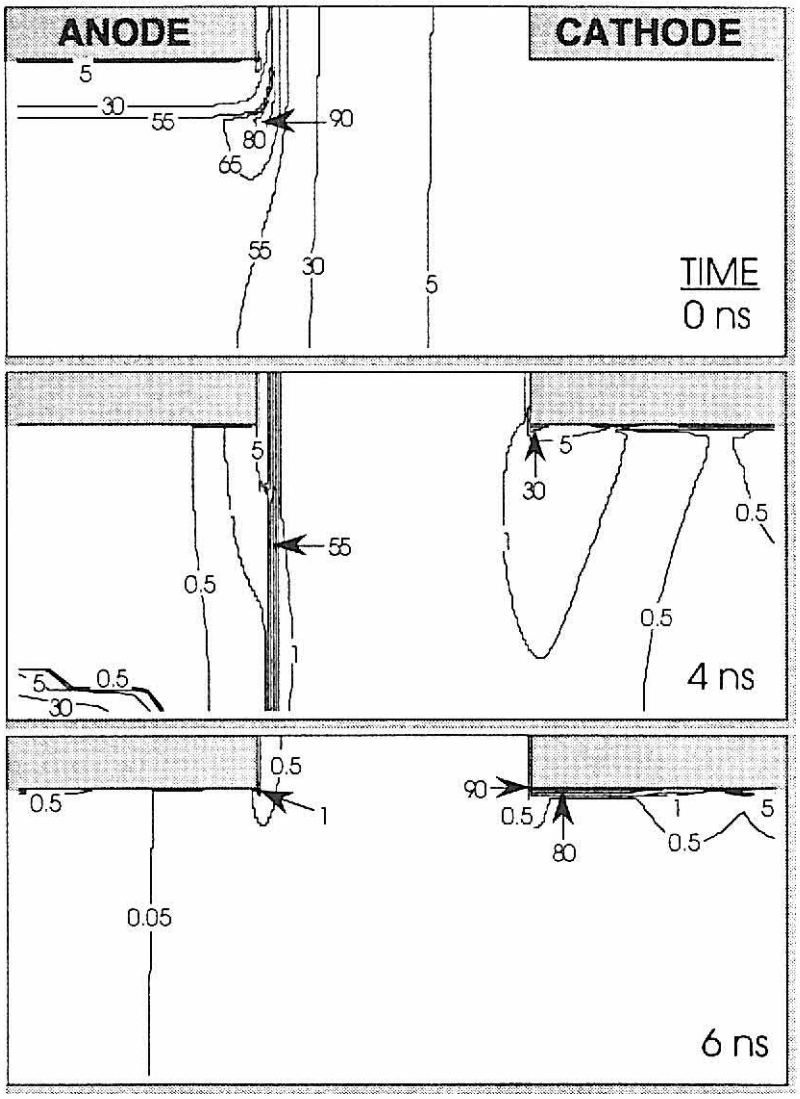

Figure V-12. Time evolution of electric field (kV/cm) for a grounded graded contact case. The result of a grounded side and bottom plane is the compression of the electric field to the anode (0 ns). Compared to the ungrounded graded contact case (Figure V-10), the closing transition is similar to the grounded case. There is less enhancement for the grounded case at the cathode near closure (4 ns). When the switch is in the on state the two cases are similar.

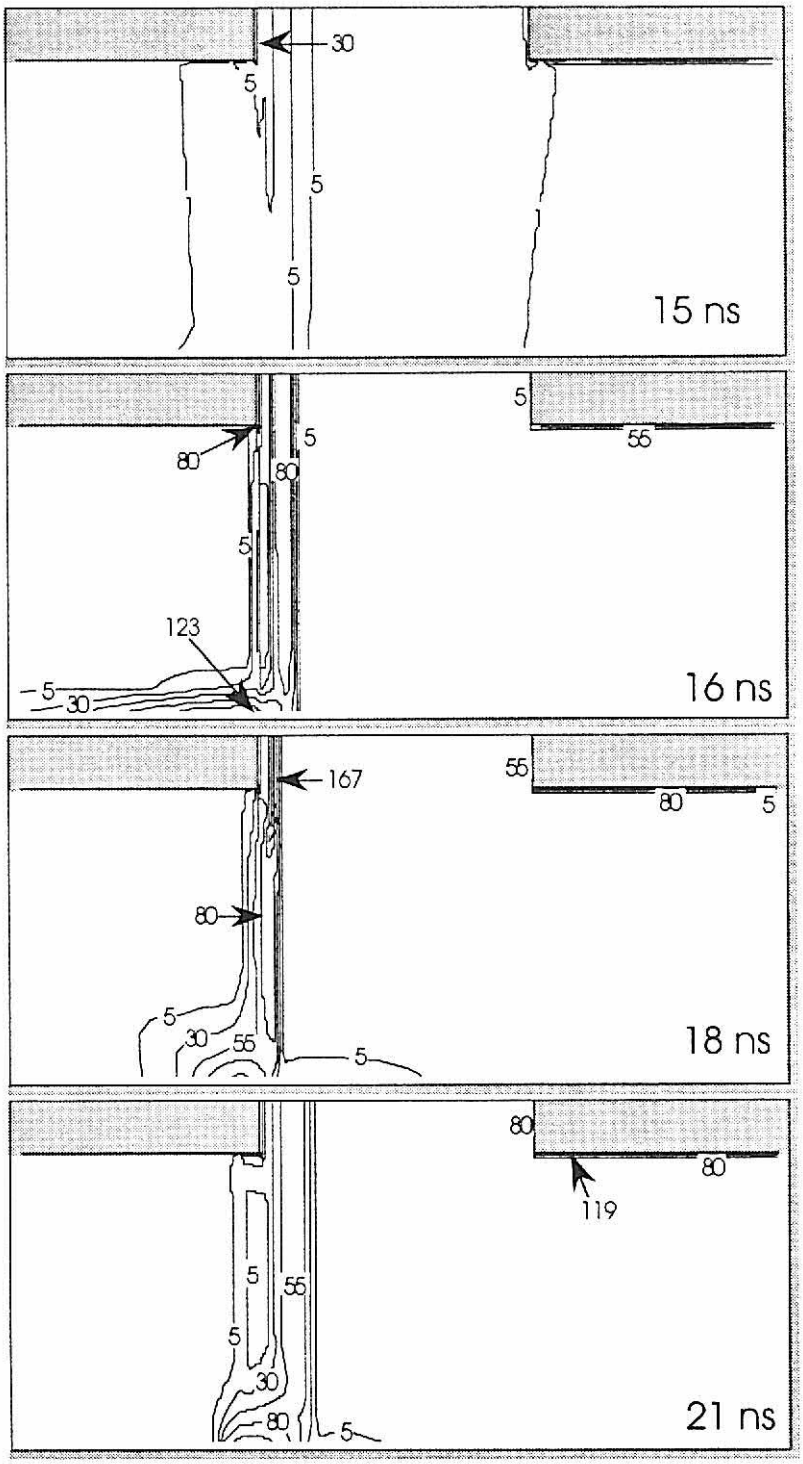

Figure V-12. (cont.) Time evolution of electric field (kV/cm) for a grounded graded contact case. In the opening phase there is immediate electric field enhancement near the anode. This electric field enhancement at the anode may be the cause of the reduced sensitivity of the switch to the opening laser pulse.

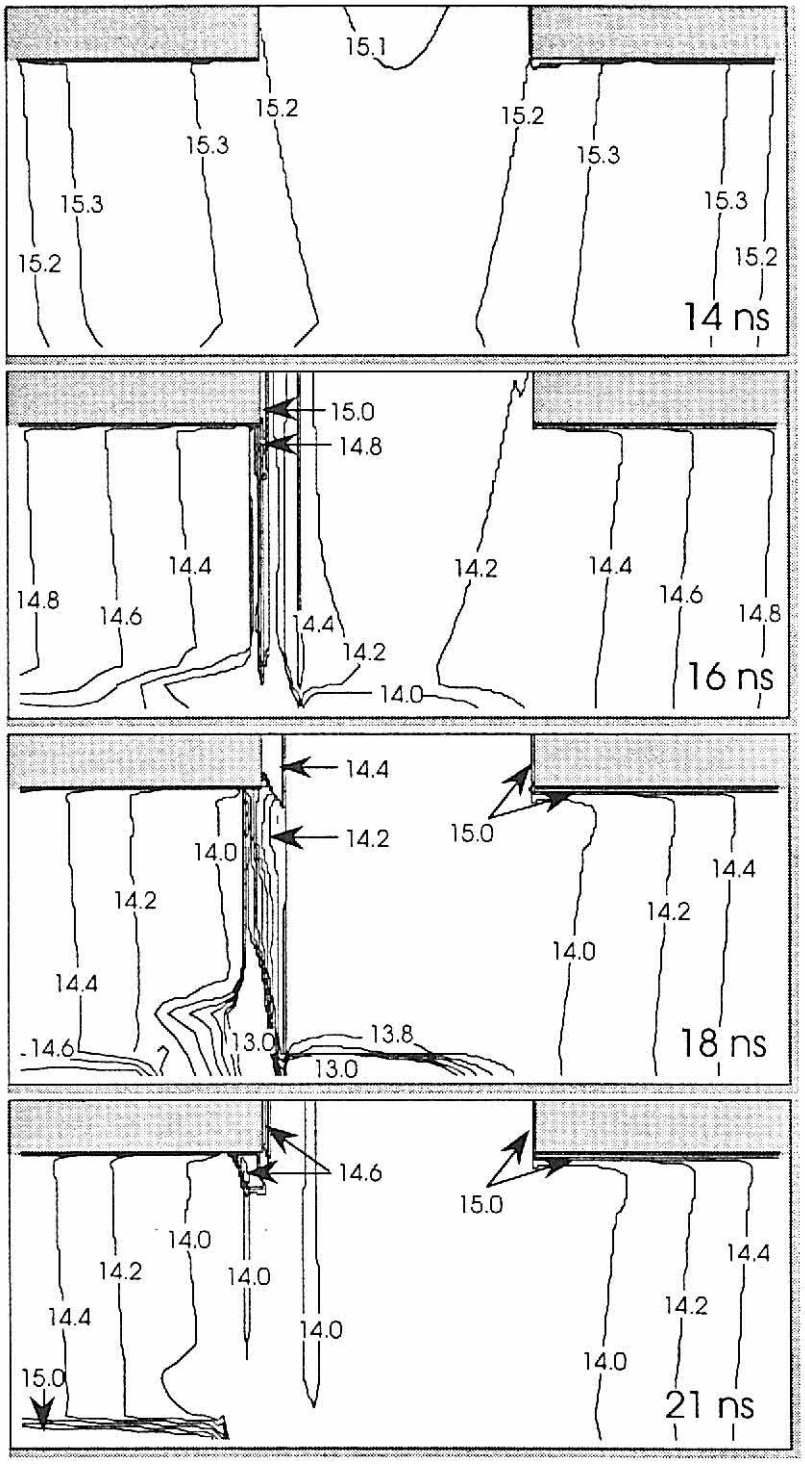

Figure V-13. The log of the electron density (cm^{-3}) for the grounded graded contact case of Figure V-12. With the increased electric field level at the anode, the number of carriers increases due to intrinsic impact ionization. The increase in carrier level increases the current collected by the contacts inhibiting the opening of the switch.

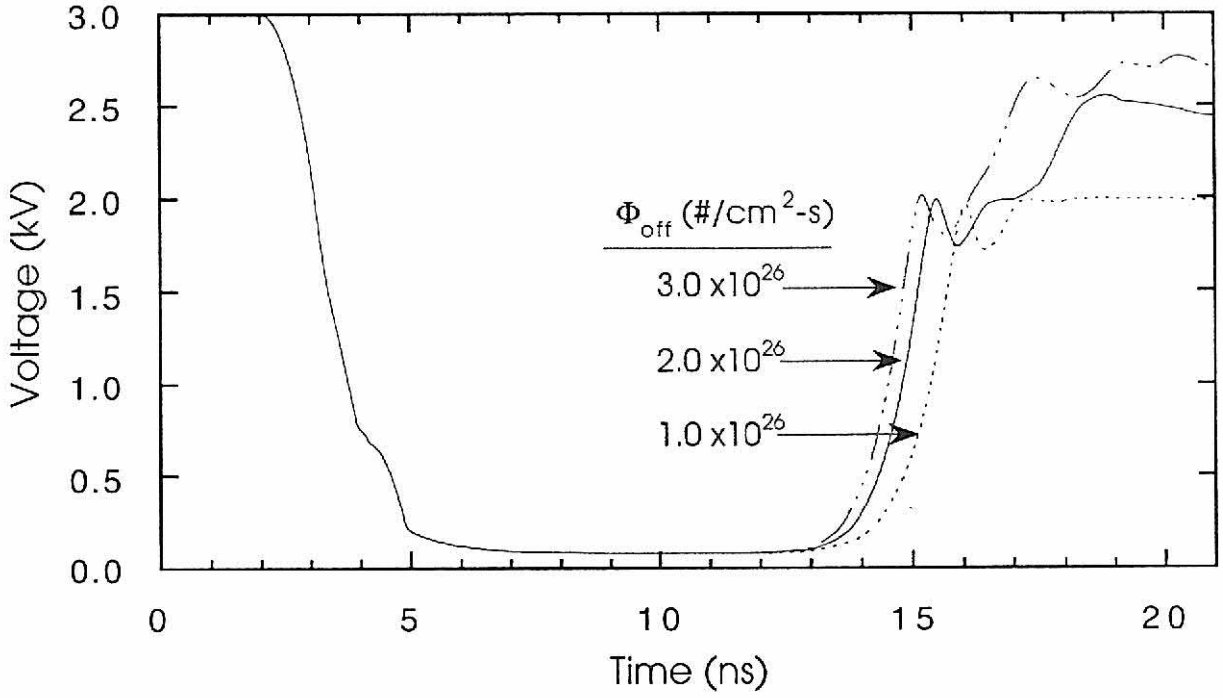

Figure V-14. The voltage characteristics for the grounded graded case with Φ_{off} varied. The larger the flux magnitude, the more the switch opens. Nonetheless, there is a negative slope for the larger flux levels which suggests that the switches may not completely recover but may stabilize to a lower voltage.

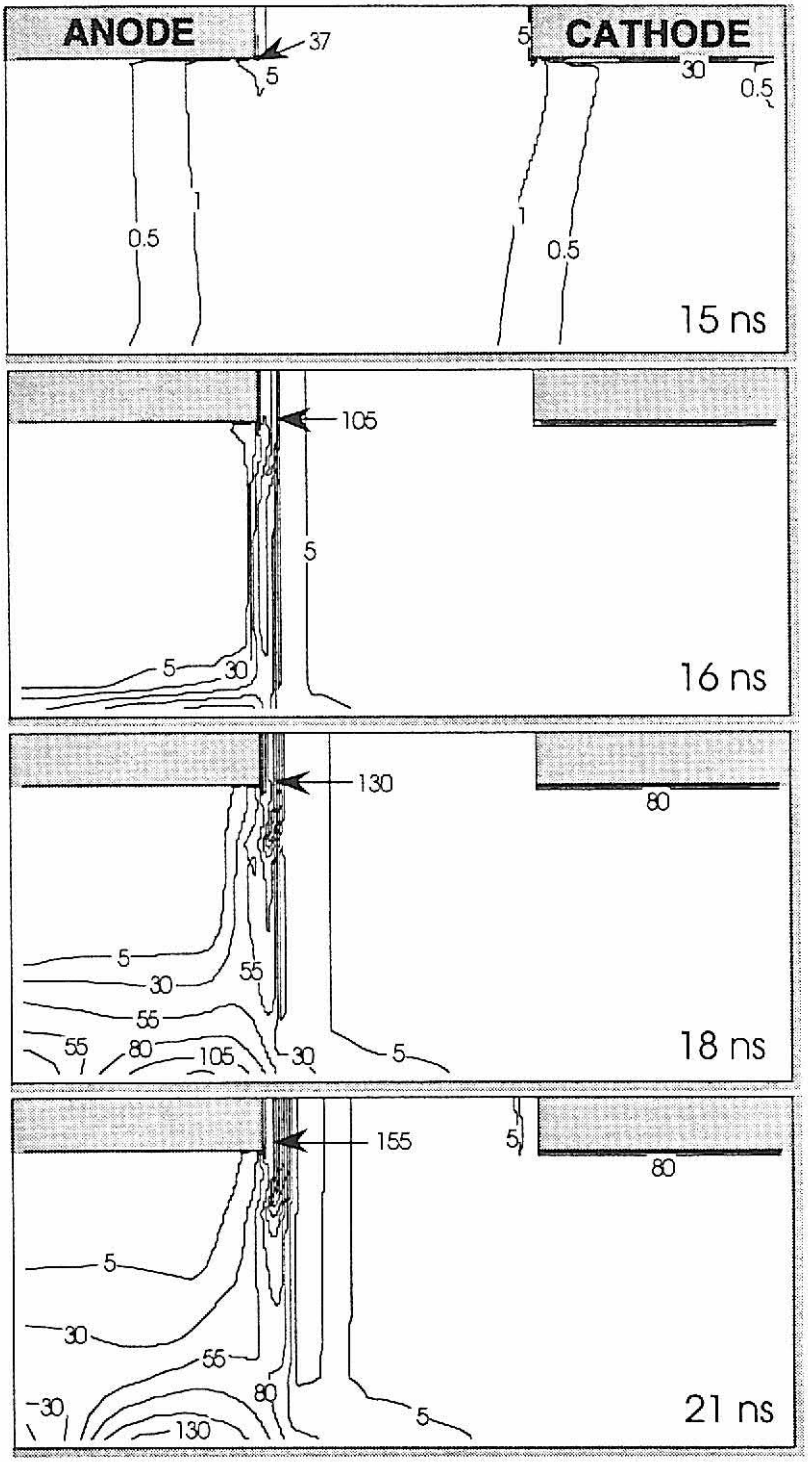

Figure V-15. The time evolution of the electric field (kV/cm) for a grounded graded contact case with Φ_{off} = 3.0 x10^{26} #/cm^2-s.

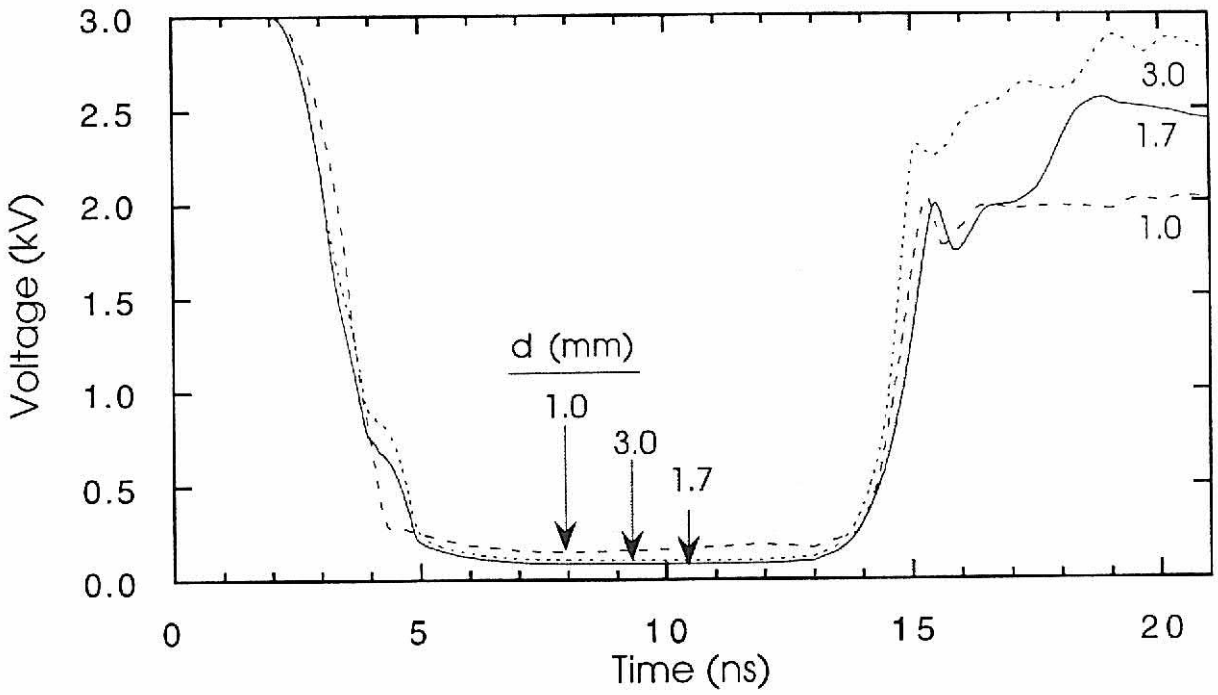

Figure V-16. The voltage characteristics for the grounded graded case with contact separation varied and $\Phi_{off} = 2 \times 10^{26}$ cm^{-2}-s^{-1}. The contacts farther apart open to a larger initial level than the 1 mm contact separation case. Although the two larger contact separation cases initially open to larger voltages, their voltage curves have negative slopes; therefore their final voltage levels are unknown.

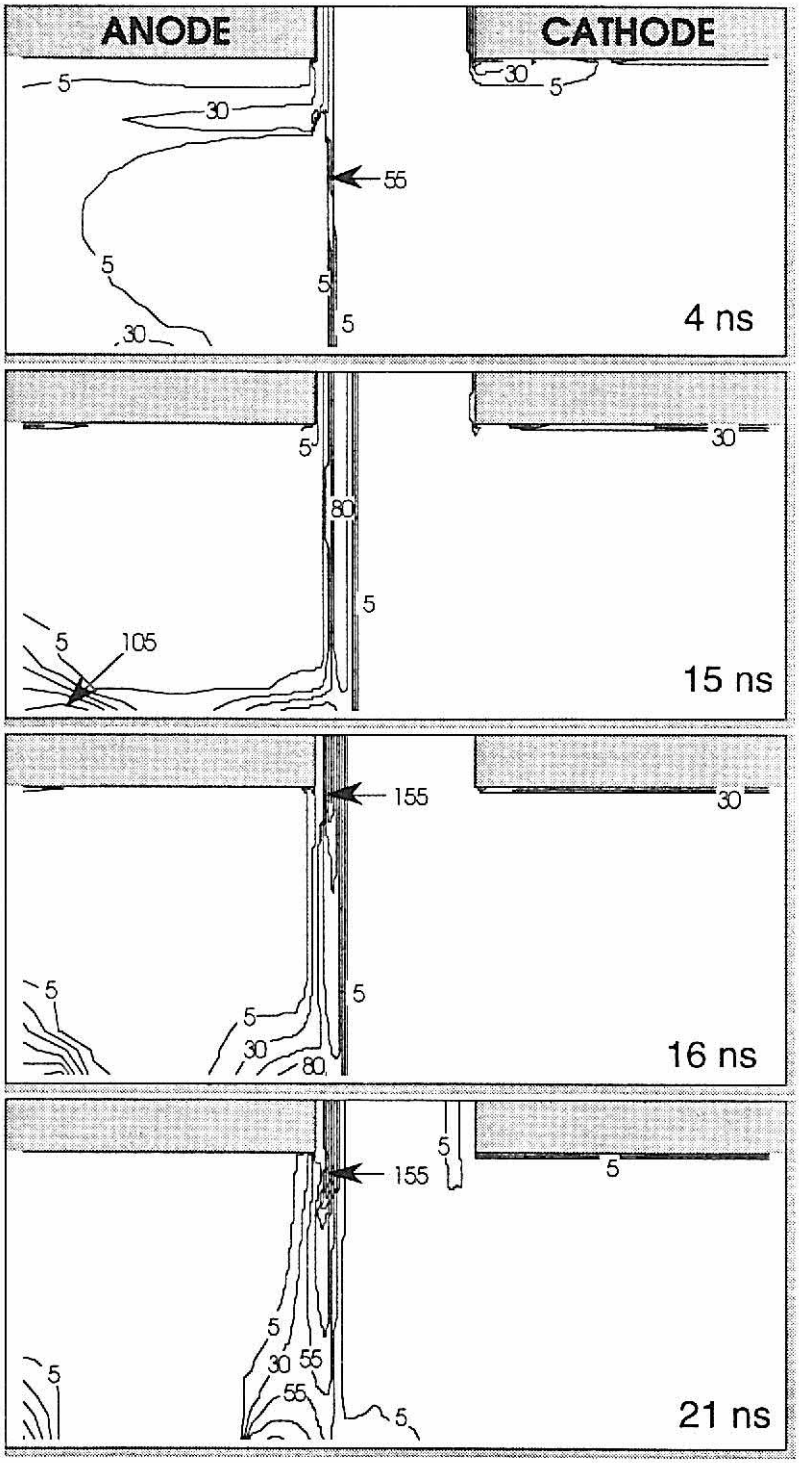

Figure V-17. The time evolution of the electric field (kV/cm) for a grounded graded contact case with $\Phi_{off} = 2.0 \times 10^{26}$ cm^{-2}-s^{-1} and a contact separation of 1 mm.

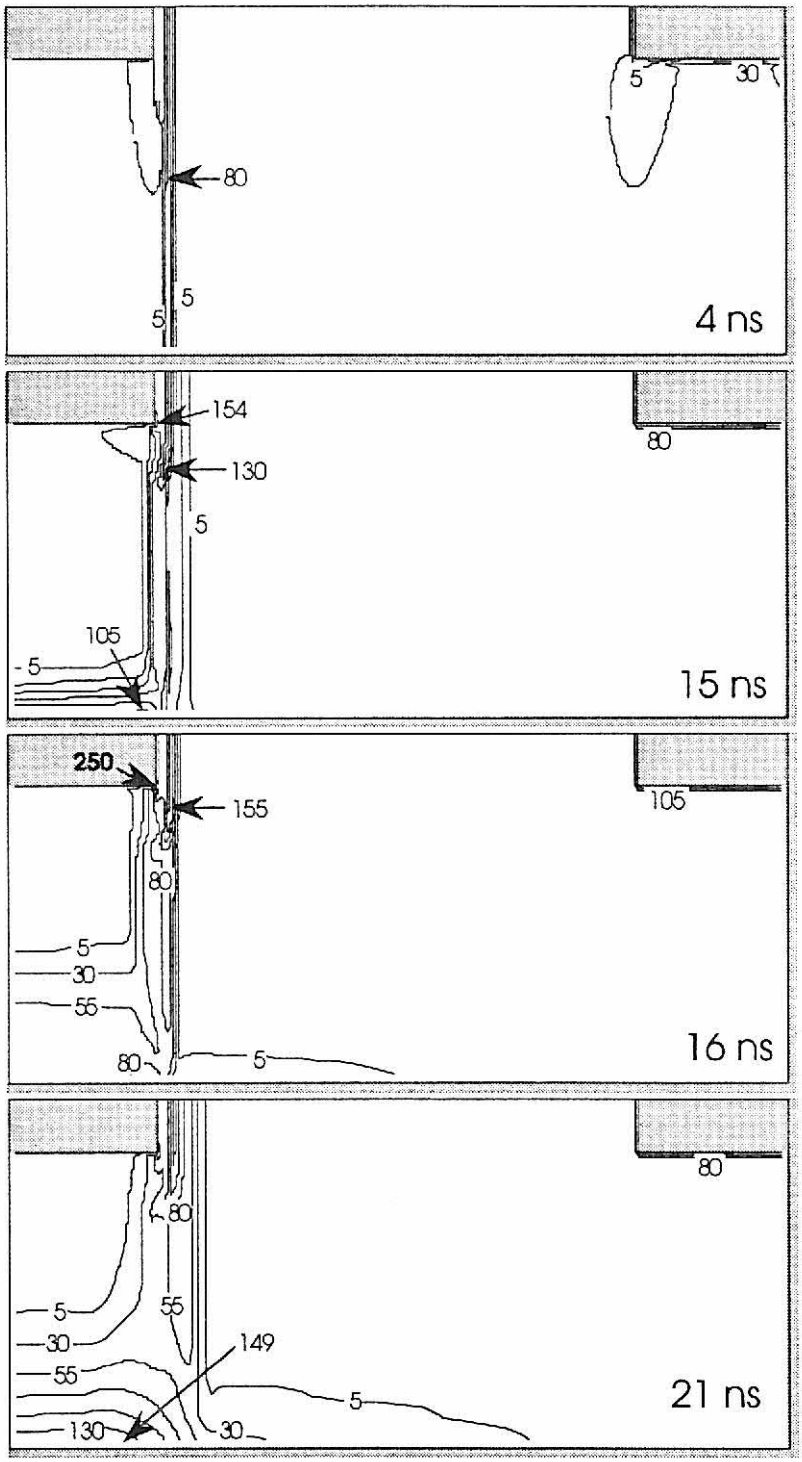

Figure V-18. The time evolution of the electric field (kV/cm) for a grounded graded contact case with $\Phi_{off} = 2.0 \times 10^{26}$ cm^{-2}-s^{-1} and a contact separation of 3 mm.

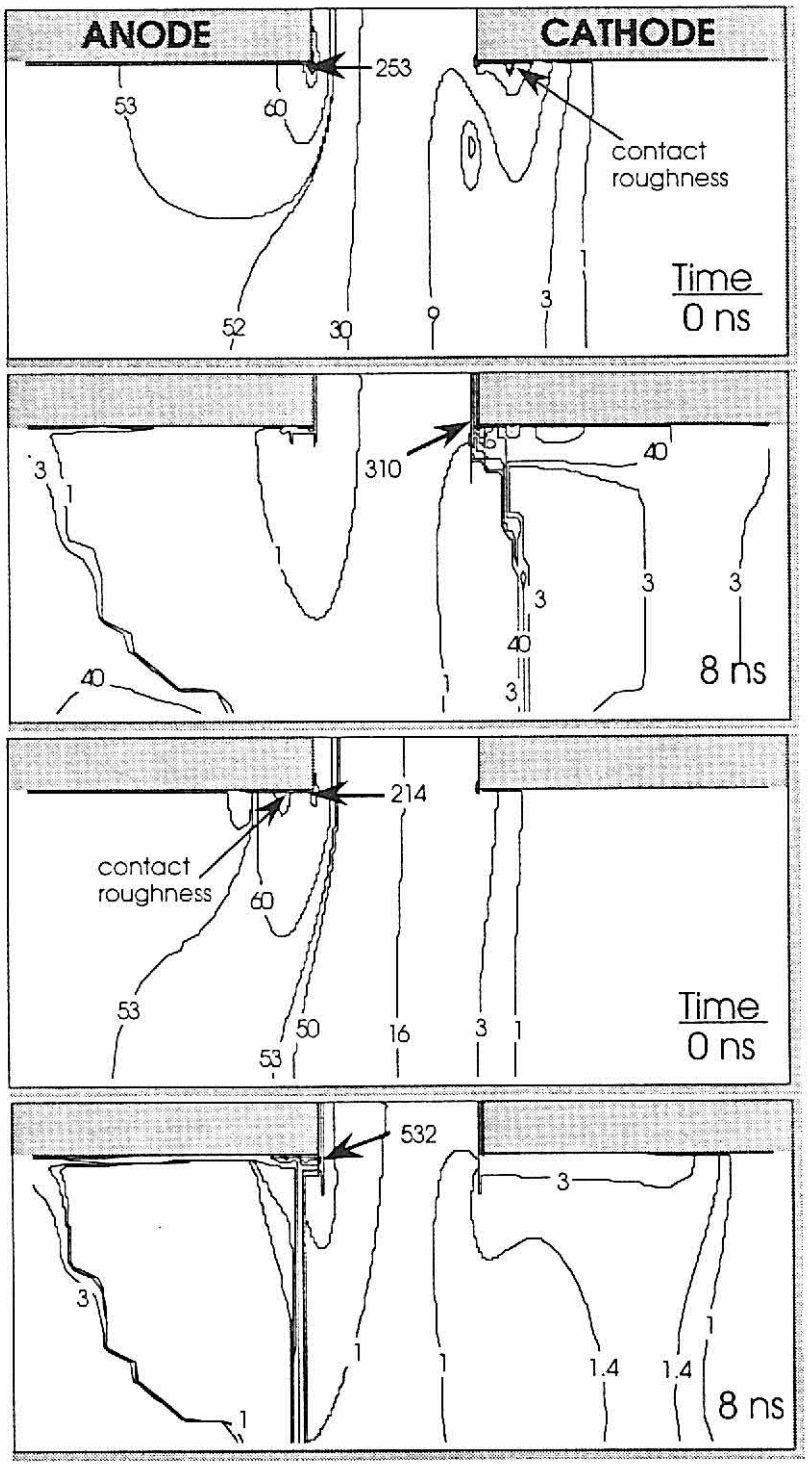

Figure V-19. The electric field (kV/cm) for the grounded abrupt typical case with contact roughness under the anode and the cathode. The increase in roughness under the contacts causes an increase in the electric field. The areas of roughness have become seeds for electric field enhancement.

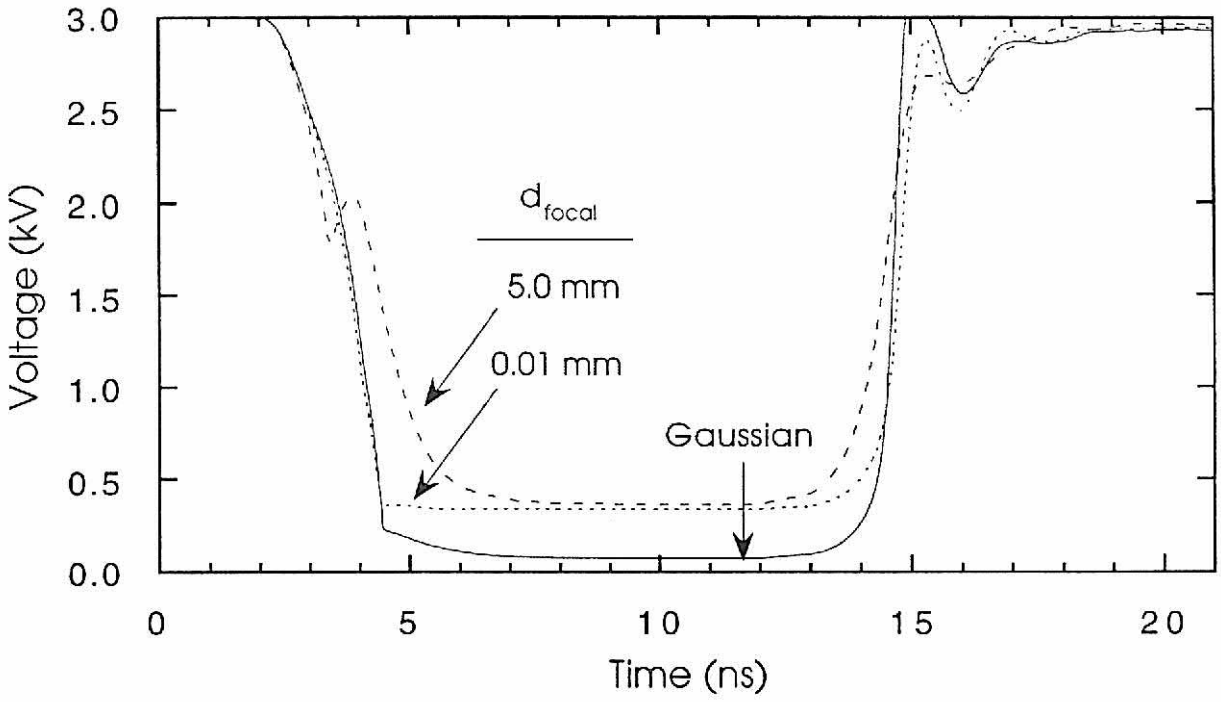

Figure V-20. The voltage cycle for the ungrounded graded case with a Gaussian laser pulse spread and a focused light laser pulse spread. When illuminating above the switch with focused light, less light is absorbed under the contacts, fewer carriers can be collected, and the switch closes to a higher voltage level.

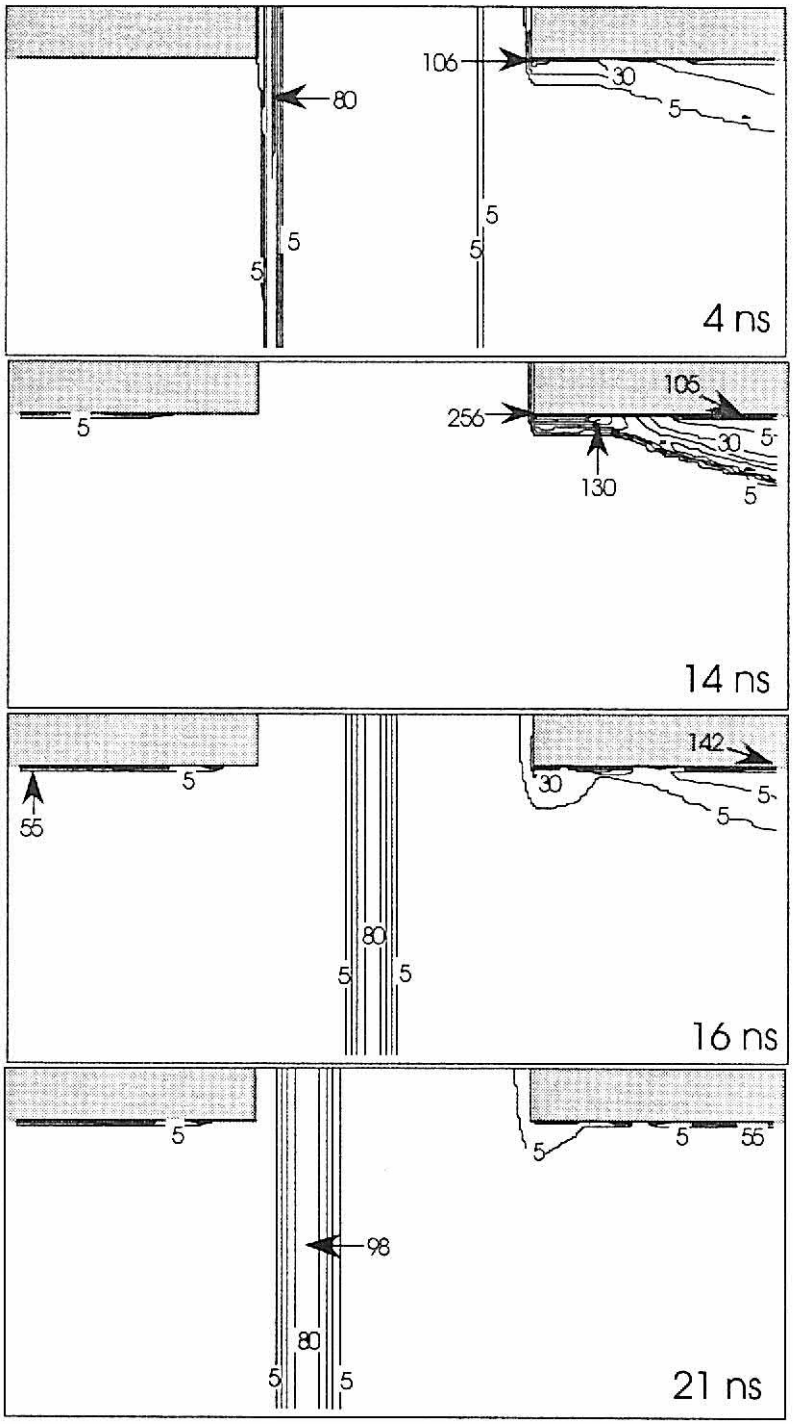

Figure V-21. The time evolution of the electric field (kV/cm) for the ungrounded graded contact case with focused light 0.01 mm away. The transition between light penetration and the point at which light no longer penetrates is marked by electric field enhancement. In the opening phase of the switch, the cathode-to-anode electric field enhancement front is similar to the Gaussian results (Figure V-10).

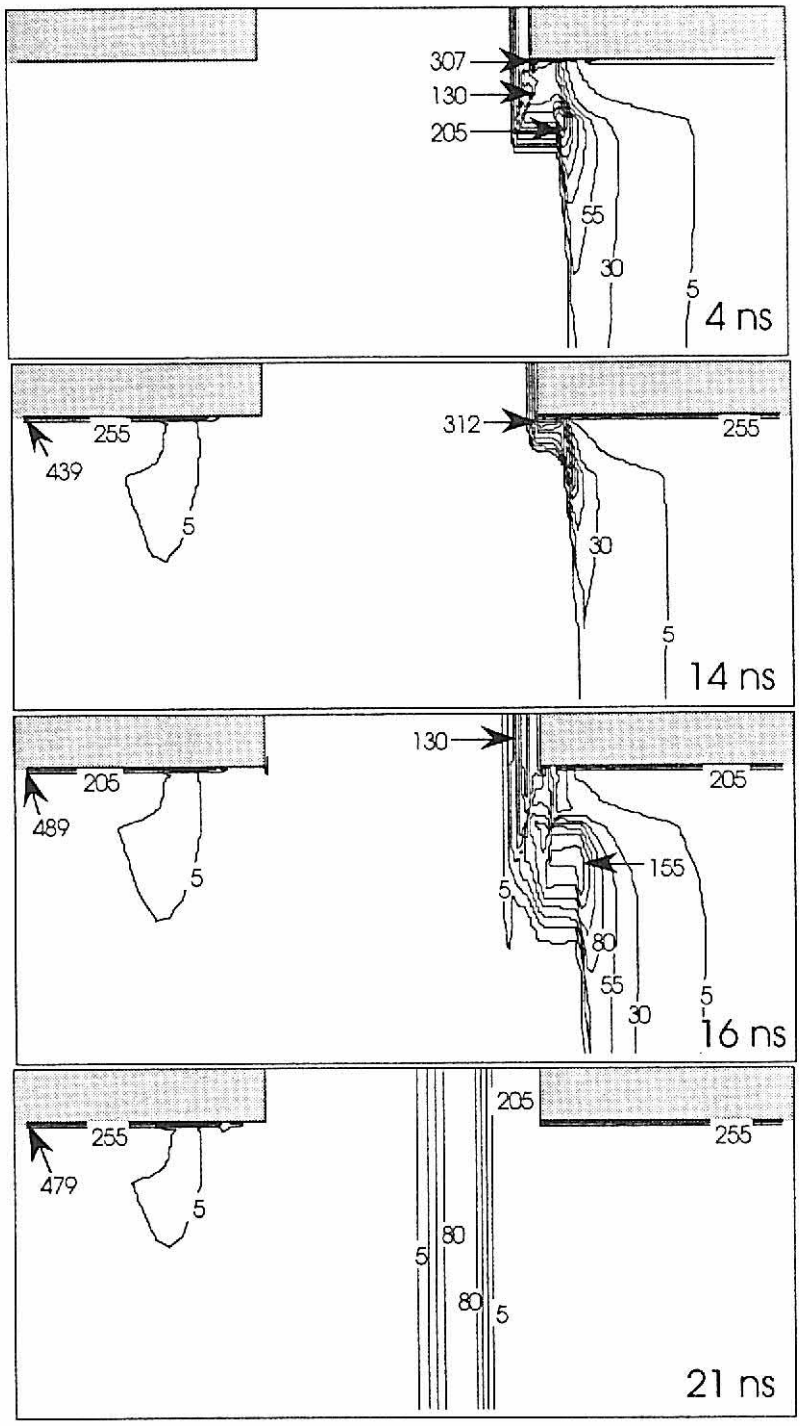

Figure V-22. The time evolution of the electric field (kV/cm) for the ungrounded graded contact case with focused light 5.0 mm away. The electric field enhancement due to the uneven focused light is close enough to the cathode contact to affect the formation of the electric field enhancement front that eventually progresses toward the anode.

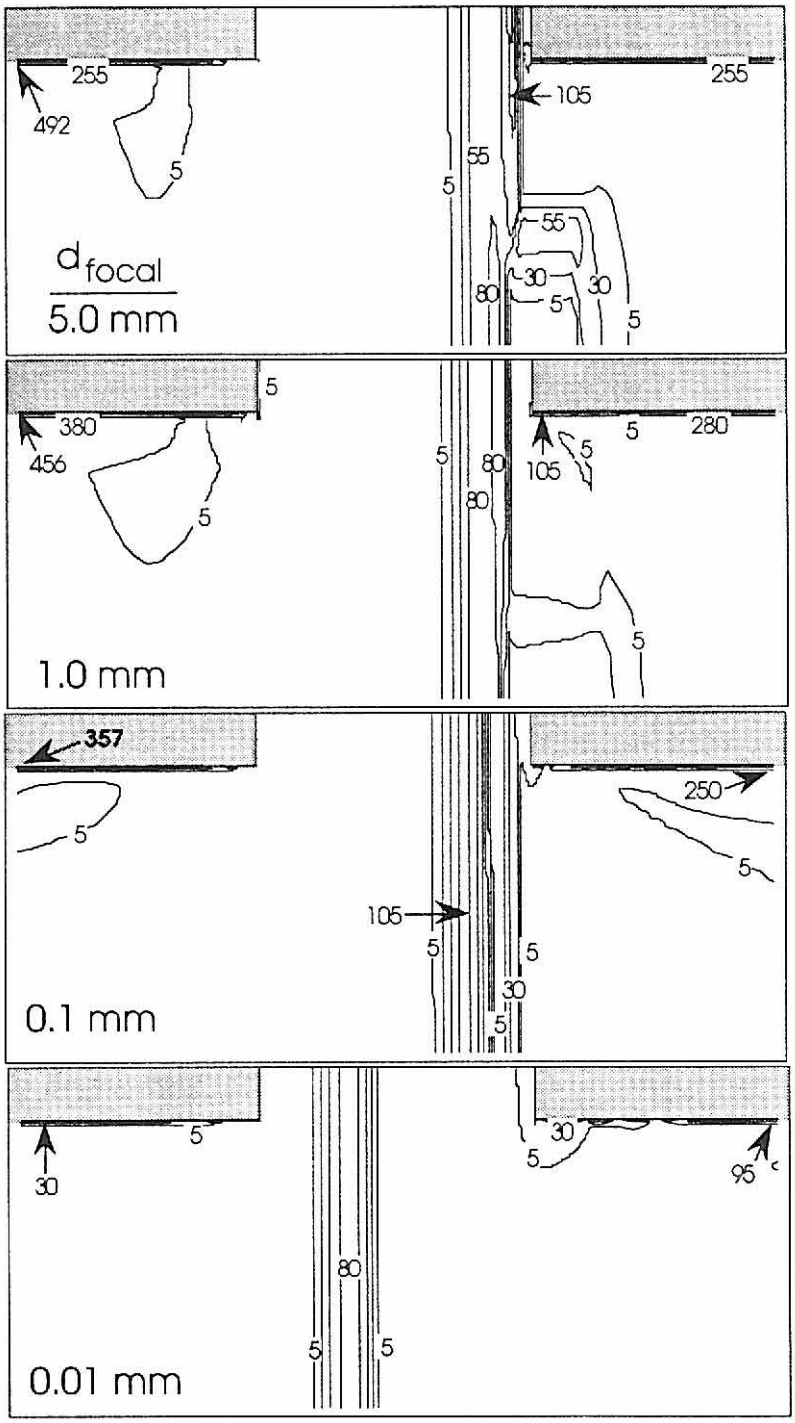

Figure V-23. The electric field (kV/cm) for the ungrounded graded focused light case at 18 ns with the focused light distance equal to 5.0 mm, 1.0 mm, 0.1 mm, and .01 mm. As the focused light is pulled farther away from the switch, the electric field enhancement introduced by the uneven focused light further delays the propagation of the electric field enhancement from the cathode.

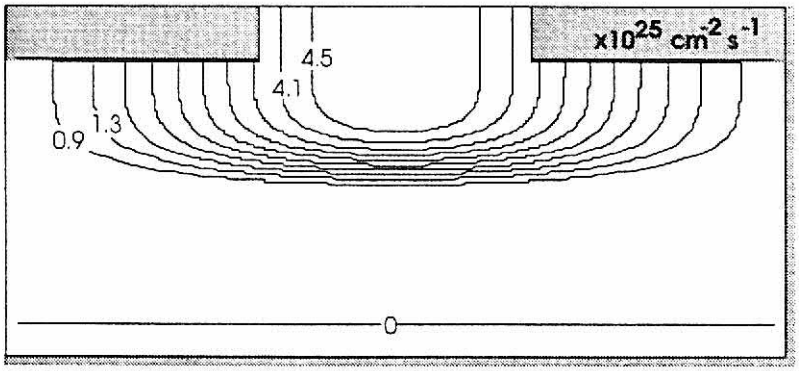

(a)

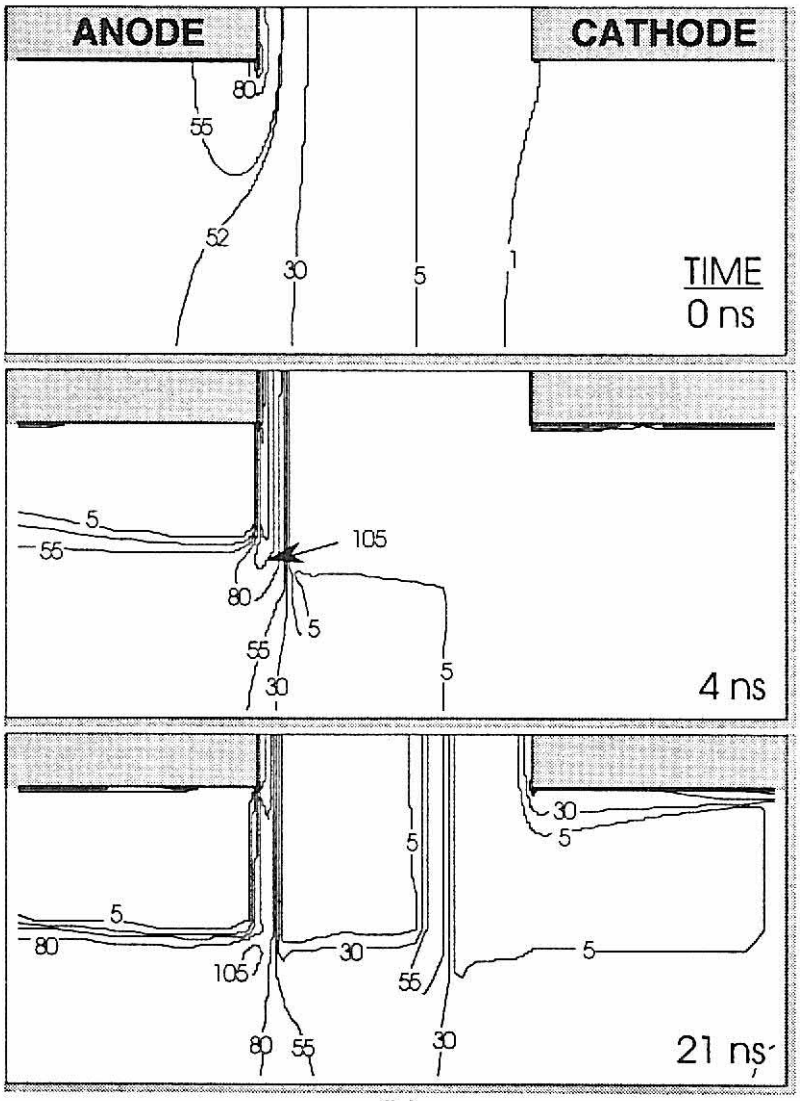

(b)

Figure V-24. The electric field (kV/cm) for the grounded abrupt cropped Gaussian light case. (a) The photon flux at the peak of the on pulse is shown cropped near the base of the switch. (b) The cropped light demonstrates that the planarity of the electric field enhancement fronts is partially a consequence of light that normally penetrates completely through the device.

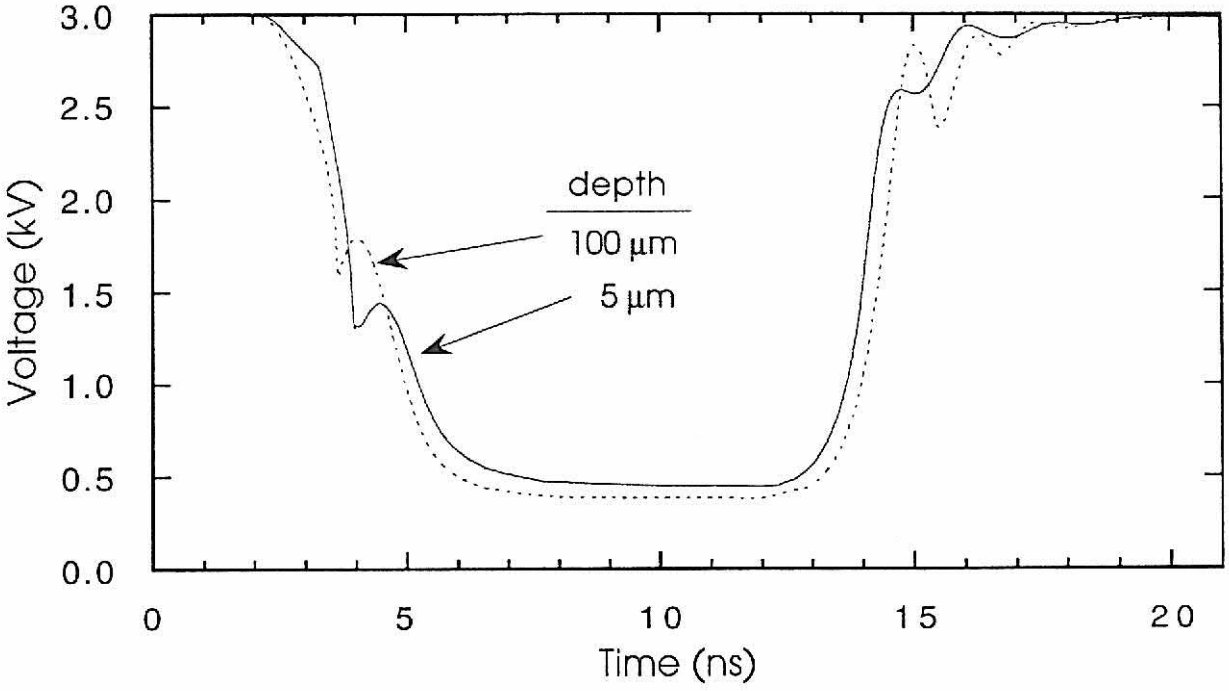

Figure V-25. The voltage characteristics for the ungrounded graded contact with focused light 1.0 mm away and the contact depth varied. The embedded contact case (100 µm) has more surface area to collect carriers, which enables it to collect more current and to close to a lower level.

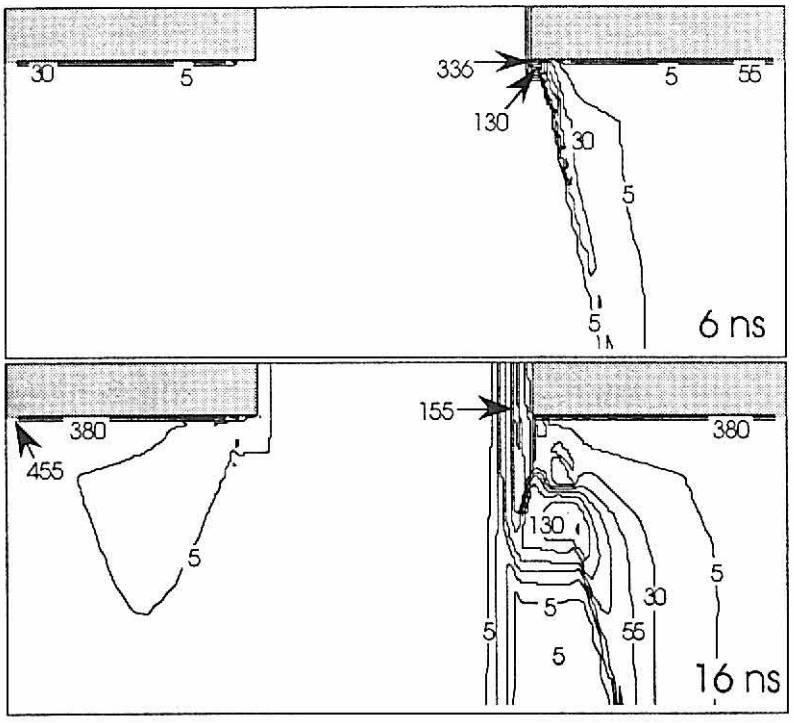

Figure V-26. The electric field (kV/cm) at 6 ns and 16 ns for the ungrounded graded contact case with focused light 1.0 mm away and with the contact depth = 100 µm.

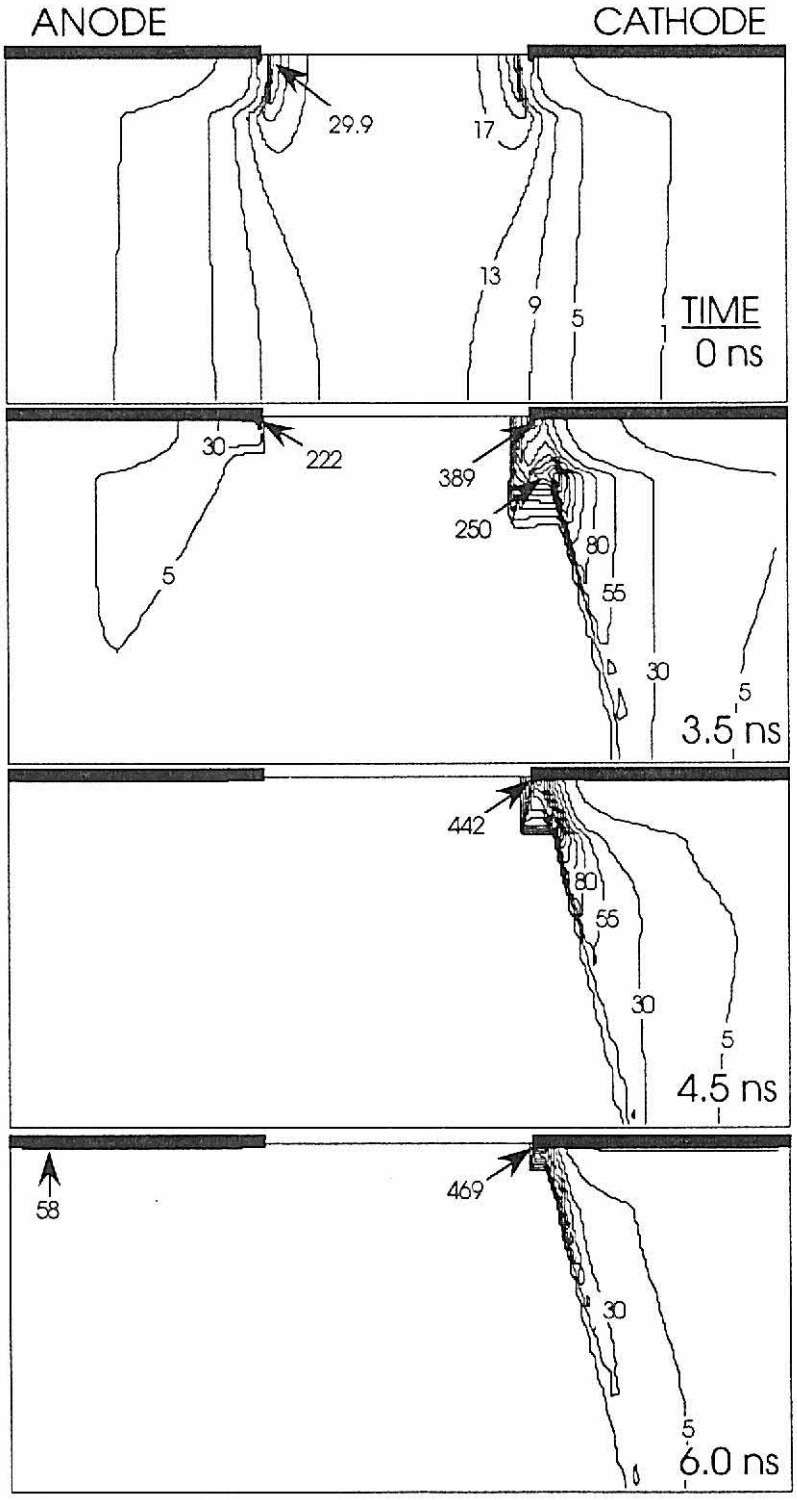

Figure V-27. The electric field (kV/cm) for the ungrounded graded contact case 1.0 mm with focused light 1.0 mm away and the contact depth = 5 μm. The electric field development is similar to that of the embedded contact case (Figure V-26).

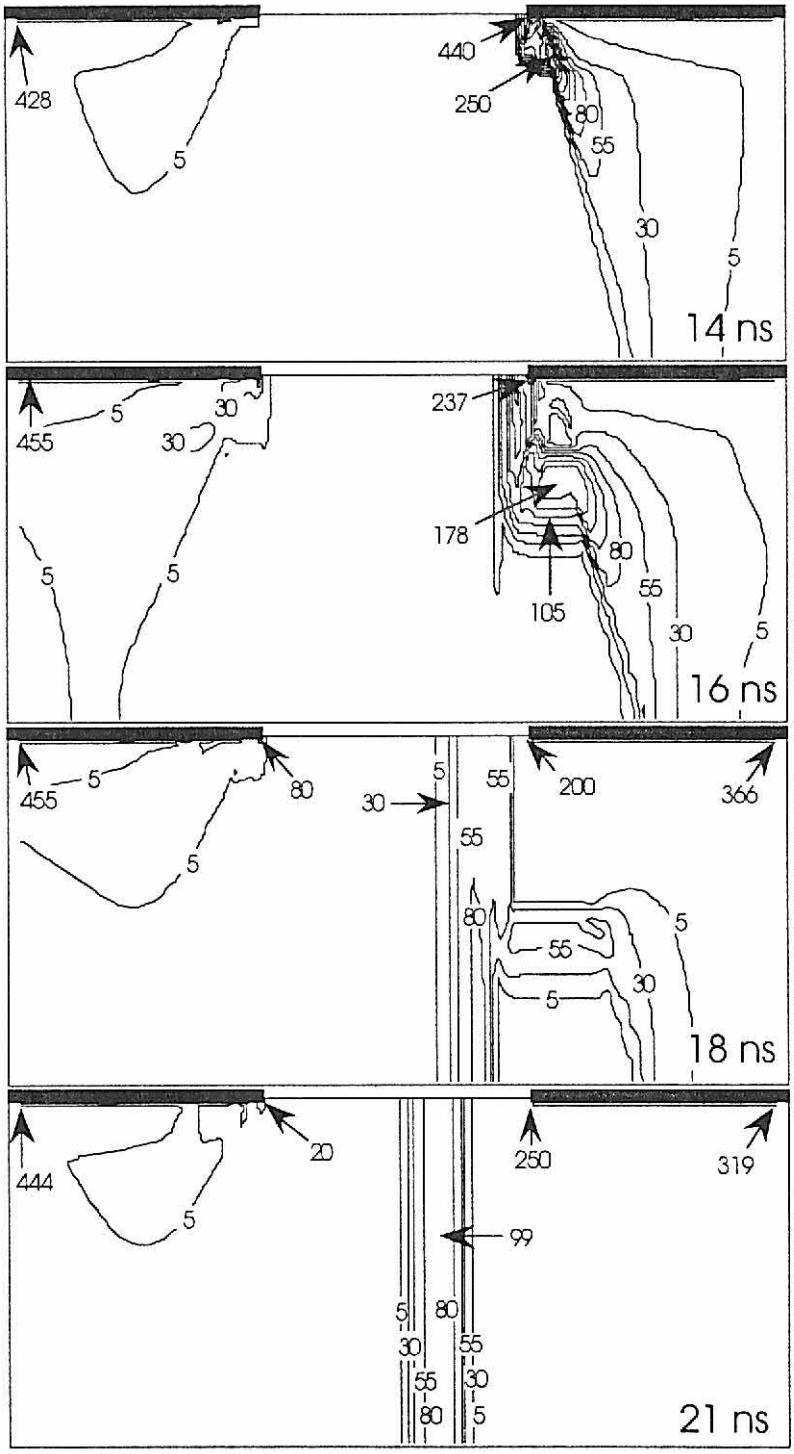

Figure V-27 (cont.) The electric field (kV/cm) for the ungrounded graded contact case with focused light 1.0 mm away and the contact depth = 5 μm.

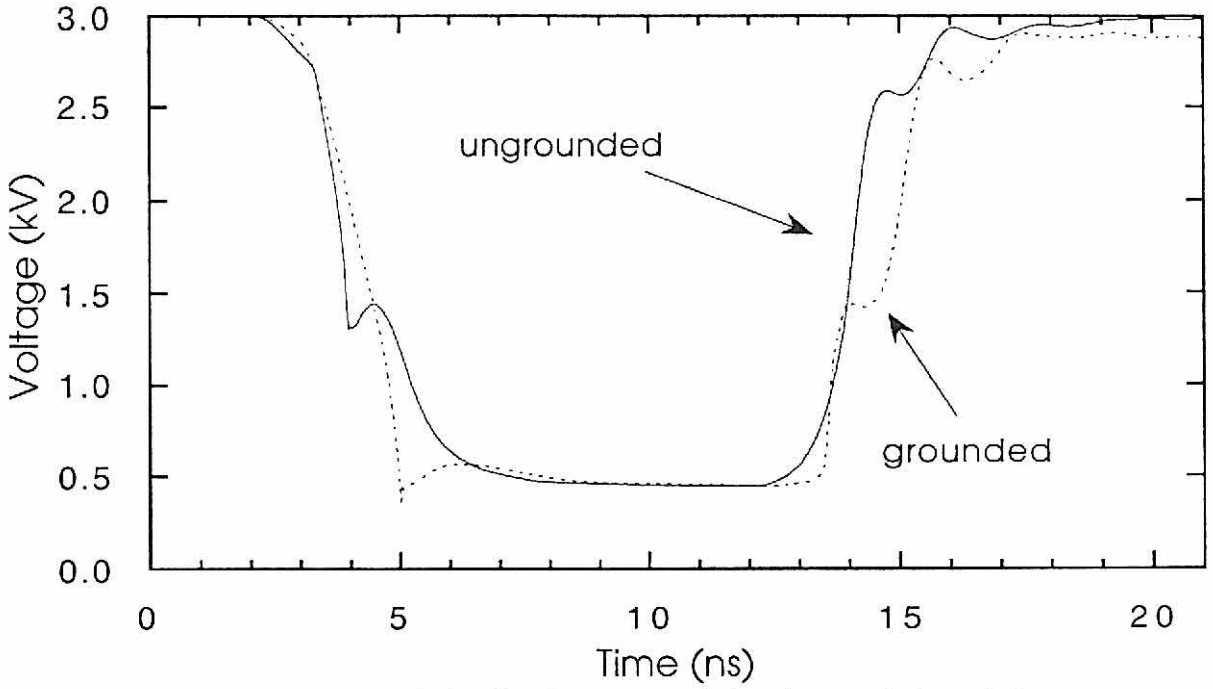

Figure V-28. The voltage characteristics for the ungrounded and grounded graded contact cases with shallow contacts and focused light. The voltage cycle for the (un)grounded cases varies little, although the grounded case opens to a smaller level. Comparing the opening level of the grounded case to the grounded embedded graded contact case with Gaussian light (Figure V-11), one sees that here the switch has opened much farther.

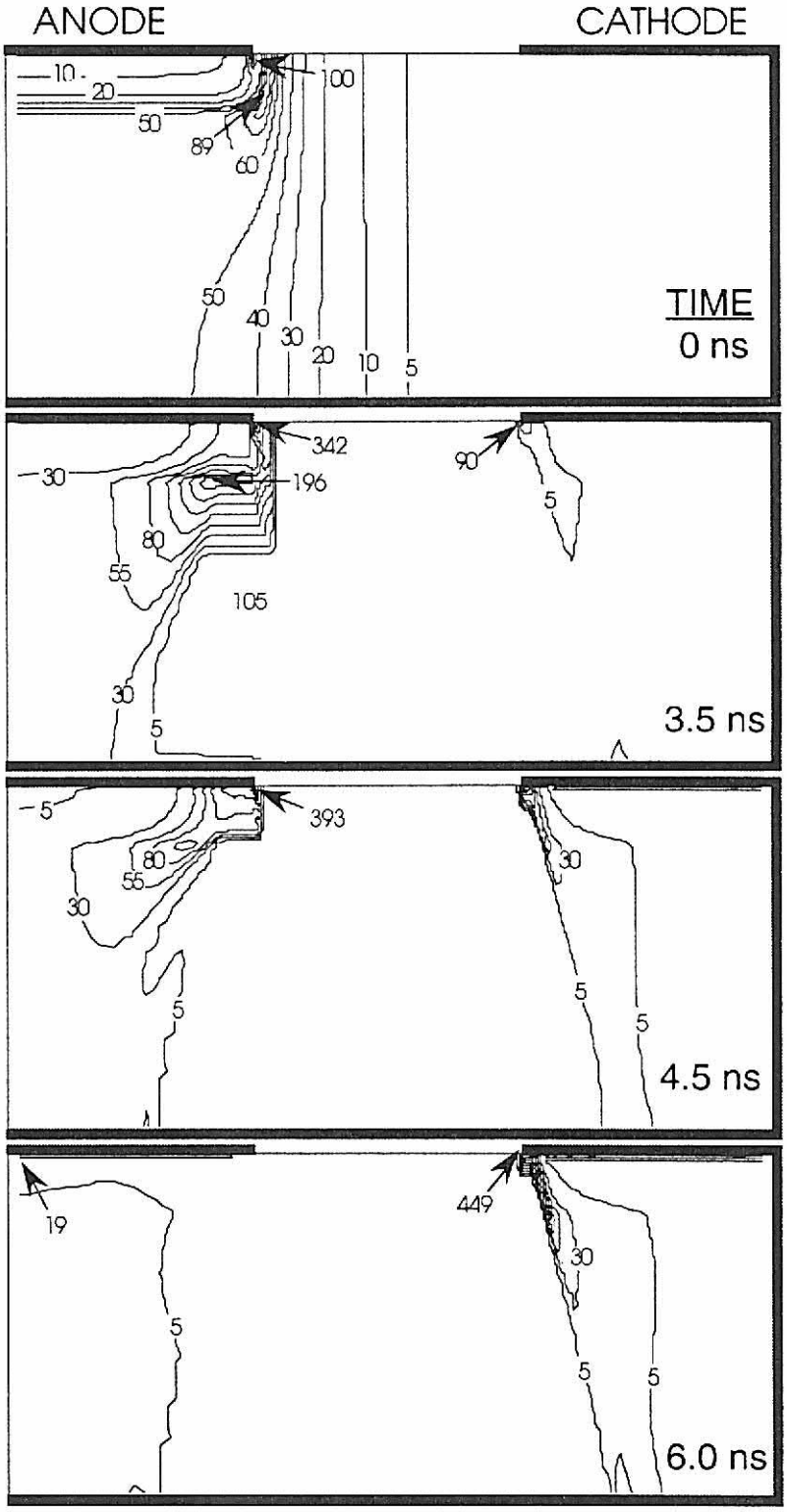

Figure V-29. The electric field (kV/cm) for the grounded graded contact case with focused light 1.0 mm away and shallow contacts. The compression of the electric field to the anode due to the grounding of the base and side of the switch dominates the character of the electric field development. In the grounded case it takes longer for the electric field to collapse completely to the cathode than it does in the ungrounded case (Figure V-27).

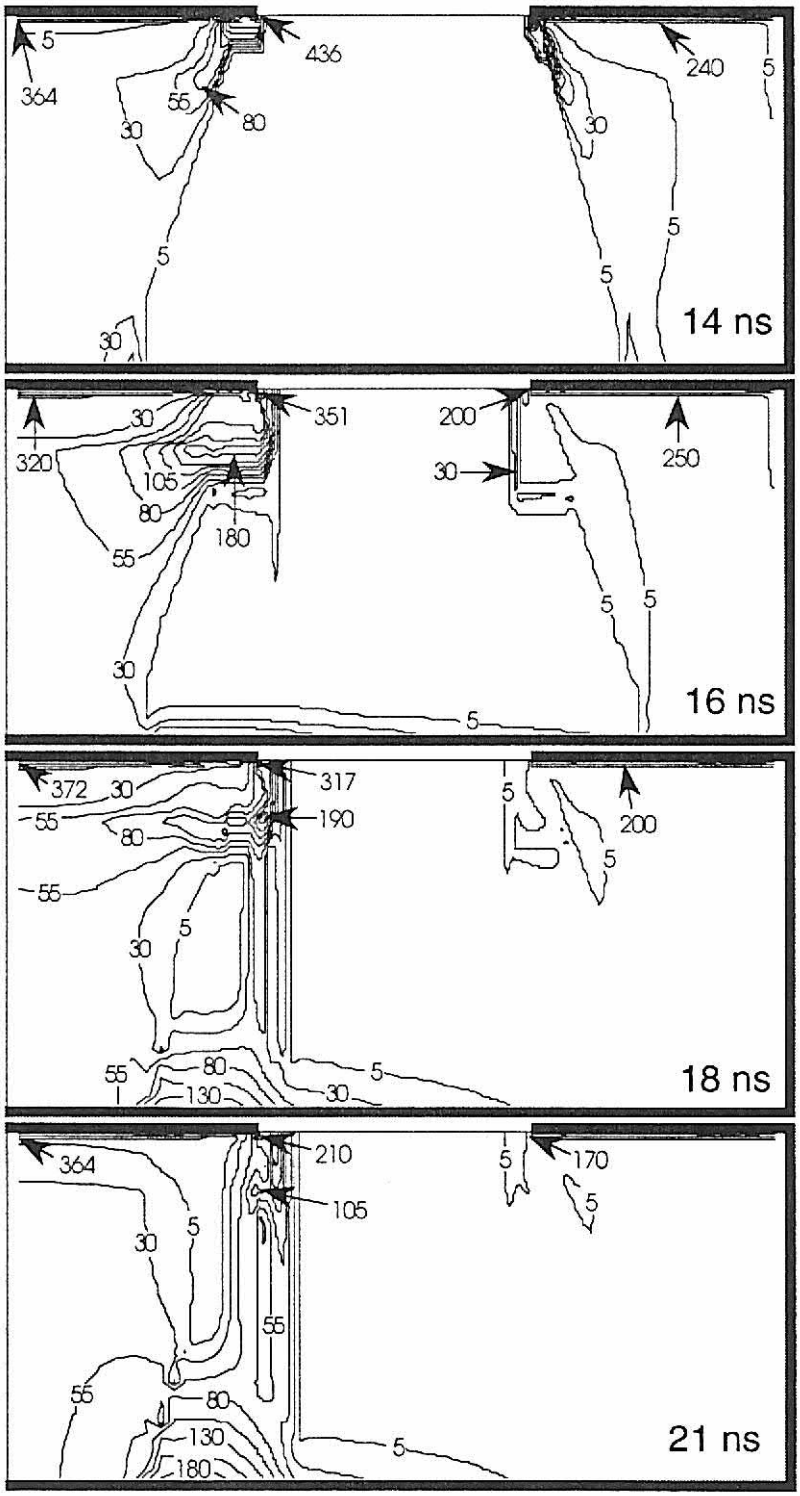

Figure V-29 (cont.) The electric field (kV/cm) for the grounded graded contact case with focused light 1.0 mm away and shallow contacts. In the opening phase of the switch cycle, the electric field forms at the anode instead of the cathode. The stationary electric field enhancement at the anode inhibits carrier collection, which results in a lower opening level of the switch. The stationary enhancement is also sweeping away carriers at the base of the switch, which causes additional enhancement at the base of the device as time progresses.

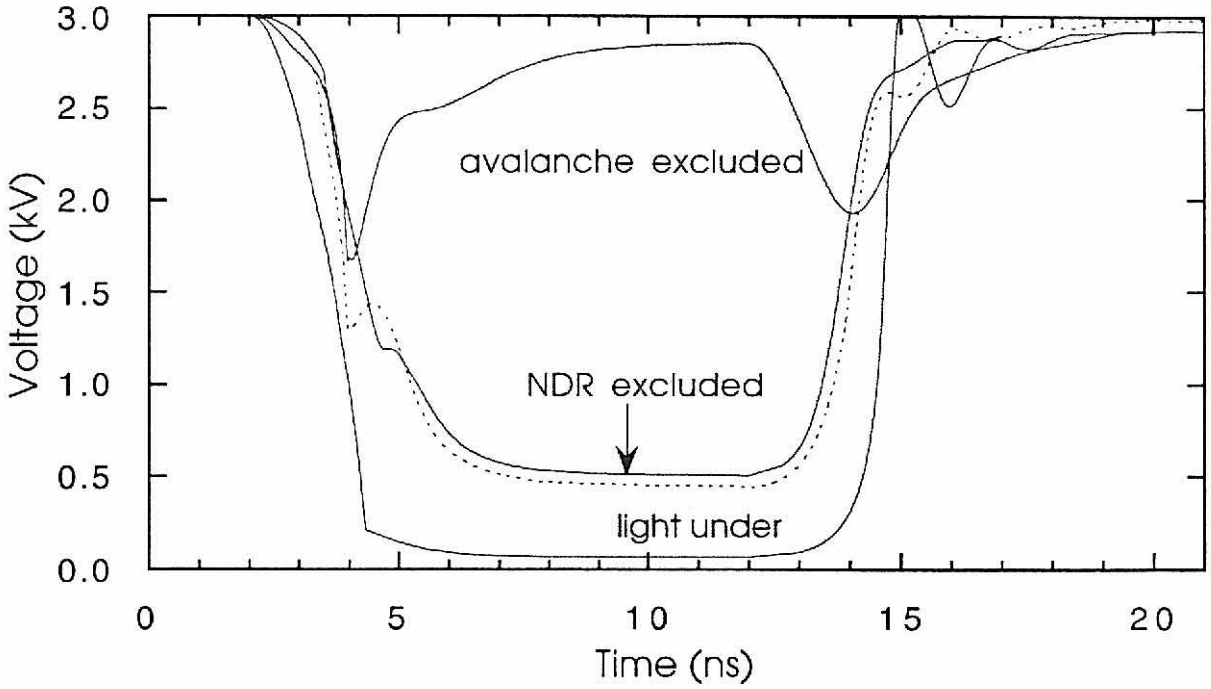

Figure V-30. The voltage characteristics for the ungrounded graded shallow contact case with light applied from the bottom, with no avalanche, and with no negative differential resistance. The dotted line is the 5 mm case from Figure V-25 and is included for comparison. Applying light from the bottom of the switch allows light to reach under the contacts which increases the closure of the switch. If negative differential resistance is taken out of the model, the ringing observed in the opening phase is reduced, which suggests that part of the ringing is due to Gunn instabilities. If the avalanche term is taken from the model, the switch does not close, although the conductivity is being affected by the application of the laser pulses.

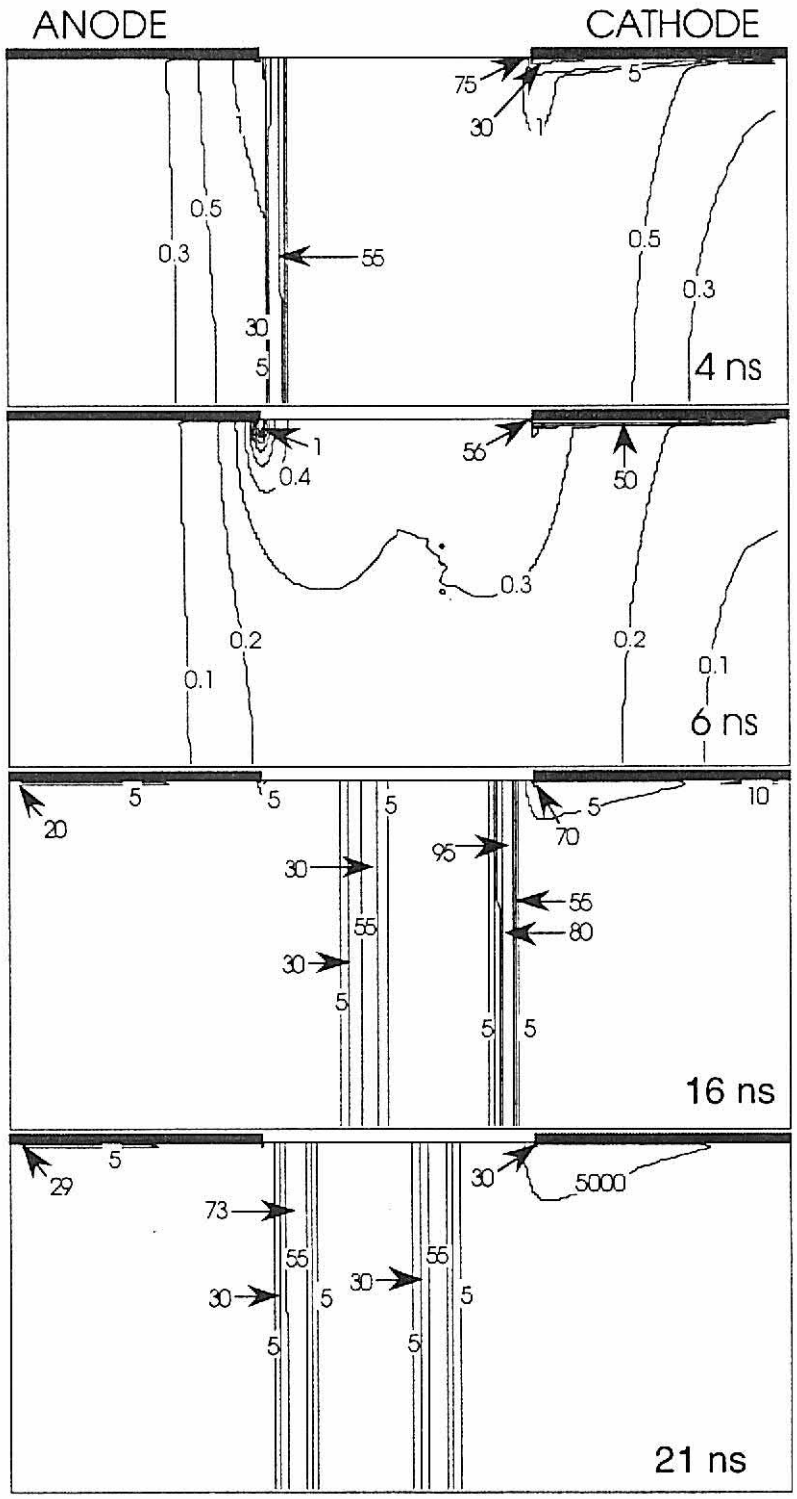

Figure V-31. The electric field for the ungrounded graded shallow contact case with light applied from the bottom. Applying light under the contacts exhibits similar electric field characteristics as using a Gaussian profile when applying the light. The previous Gaussian case can be interpreted as switch illumination under the contacts.

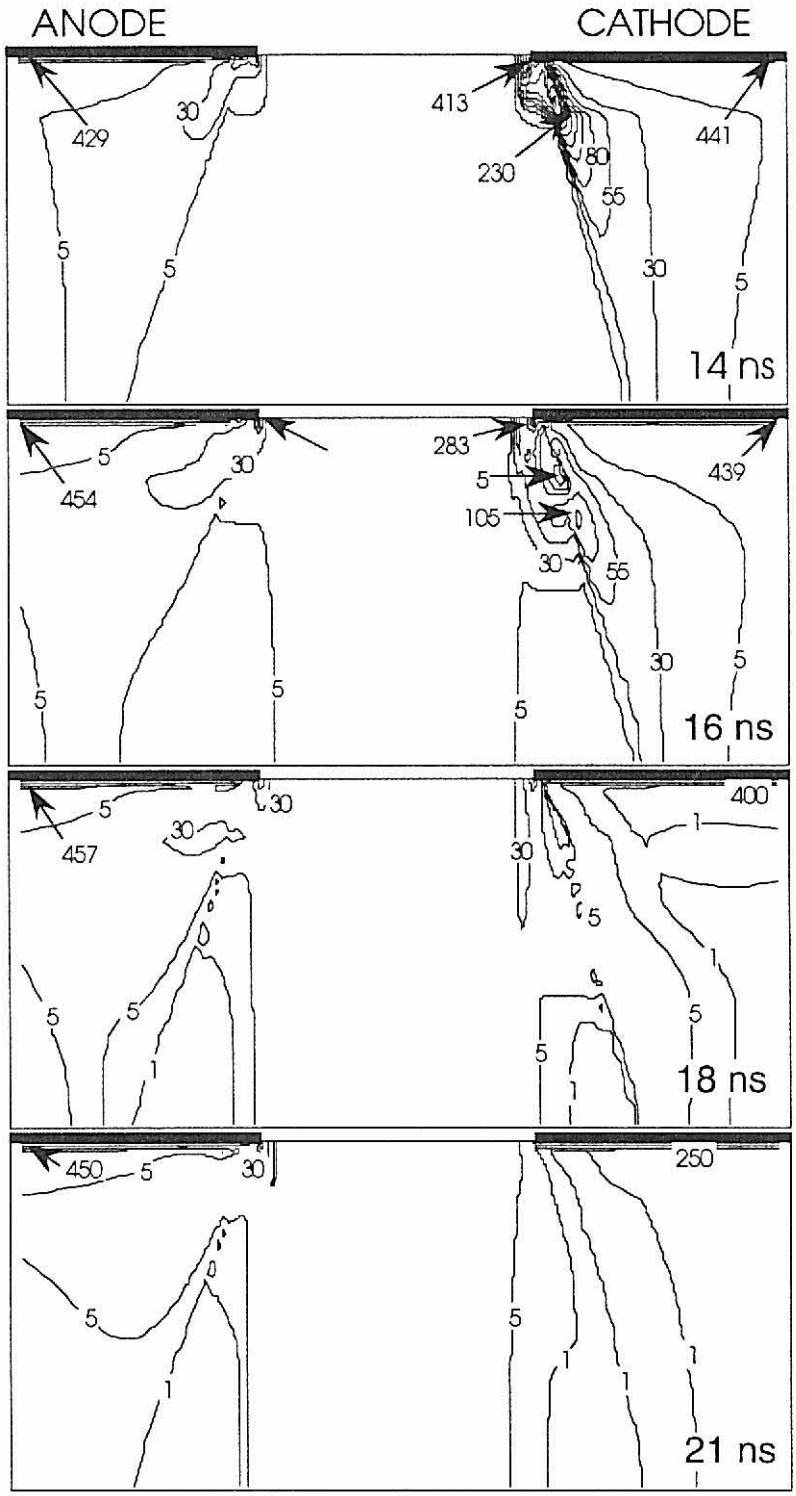

Figure V-32. The electric field for the ungrounded graded shallow contact case with no negative differential resistance. The electric field enhancement fronts are absent. One can conclude that negative differential resistance is essential in the formation of these mobile electric field enhancement regions.

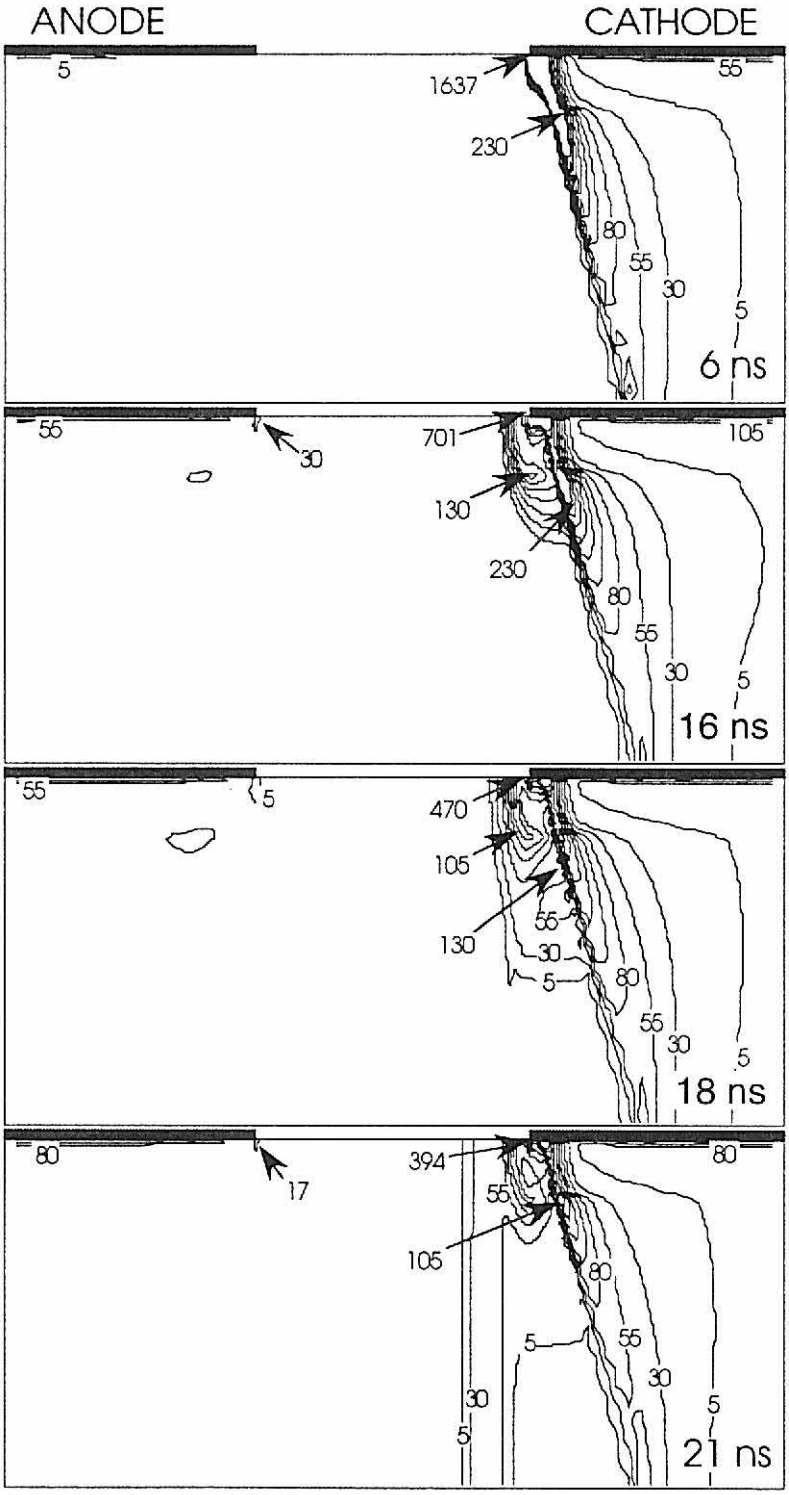

Figure V-33. The electric field for the ungrounded graded shallow contact case with no avalanche. With the absence of avalanche in the model, the peak electric field levels have dramatically increased in the device.

VI. COPLANAR GaAs SWITCHES AND SPOT ILLUMINATION

A. Introduction

A more typical photoconductive semiconductor switch material is semi-insulating GaAs. Most GaAs, when grown, has residual amounts of shallow acceptors such as carbon and zinc which are trapped by the native donor EL2, which decreases the free carrier concentration of the semiconductor. The absence of free carriers in the material raises its resistance to the point that it is referred to as semi-insulating GaAs. The model does not take into account these deep trap levels. Therefore, the term intrinsic GaAs is employed to emphasize the absence of these deep levels. The closing phase of the switching cycle is instigated by laser light with an energy near the GaAs band gap energy or, if semi-insulating GaAs is chosen, subband gap energy could be used to trigger the switch as well as band gap energy. The absorption length of band gap light in GaAs material is extremely small at 2 μm.[81] Therefore, carriers are generated only at the switch surface. At longer, subband gap wavelengths, the conduction level of the closing phase is primarily from carriers generated through transitions involving impurity levels within the band gap. The absorption depth at these wavelengths can be long enough to generate carriers throughout the bulk. The below-band gap 1.054-μm wavelength light (Nd:Glass laser) works well with the GaAs switch. With an absorption depth greater than 1-mm[81] at 1.054-μm, carriers are generated throughout the switch. With a Nd:Glass laser, a 10 mJ, 540 ns square pulse is sufficient to lower a 5 mm cube PCSS resistance to ≈ 1 Ω, which is well below the typical 50 Ω load resistance.[84] The time of the opening phase of the switching cycle is not controlled by a laser pulse of a specific hν as in the BOSS material, but by the electron-hole pair lifetime of the material. When operated in the nonlinear mode with optical trigger gain, the closing phase of the switching cycle can be controlled by a laser spot instead of by uniform illumination. Chapter VI investigates switching intrinsic GaAs material with a spot of light with electric fields high enough for gain mechanisms to be important, that is, operated in the nonlinear mode.

B. Uniform vs. Spot Switching

The coplanar switch geometry for the intrinsic GaAs photoconductive semiconductor switch is modeled in the top view. For our purposes, intrinsic GaAs is a material having no trapping levels and low EL2 levels. The simulation geometry and mesh for a top view of the coplanar switch are shown in

Figure VI-1. This figure is a top view of a coplanar switch with contacts 1.0 mm apart, 3.0 mm wide, and a switch depth of 0.4 - 0.5 mm. The computational mesh ends at the contact/semiconductor interface; thus, the carriers under the contacts are not resolved. The anode at the left and the cathode at the right are both current injecting. The 64 x 64 mesh is concentrated at the contacts. Any boundary not set to a voltage has the electric field component normal to its surface set to zero. In our simulations the PCSS is intrinsic GaAs with only the thermal concentration of free carriers initially present. The on laser pulse has the GaAs band gap energy, with a typical level of $\Phi = 10^{22} - 10^{23}$ cm^{-2}-s^{-1} ($\approx$ 2 to 23 kW/cm^2), and a Gaussian temporal shape with $\Delta t = 2$ ns. It is applied at 6 ns and has a FWHM of 2 ns. It should be emphasized that optical carrier generation is being achieved by valence-to-conduction band transitions and not through intermediate trapping levels in the band gap as in some semi-insulating GaAs switches. The laser pulses are either spatially uniform or are Gaussian spots of light near the anode or cathode as shown in Figures VI-1(c) and VI-1(d). The switch is in parallel with a 50.3 pF capacitor, and in series with a 20 nH inductor and a 50 Ω load resistor.

Uniform illumination increases carrier concentration uniformly between the contacts, which allows a fast reduction in the resistivity of the switch. However, a spot of light generates carriers only near one contact, thereby requiring some carrier movement before the switch can activate. The nonuniform generation of carriers also generates a space charge electric field which hinders the movement of carriers. The voltage across the switch using the coplanar geometry for intrinsic GaAs is shown in Figure VI-2 for uniform and spot illumination. The uniform illumination produces complete switching from 3 kV to $\approx$50 V. However, for both cases using spot illumination, the switch fails to completely switch. When a spot is applied near the cathode, the voltage is reduced by only 15%. When a spot is applied near the anode, the voltage is reduced by only 3%.

Failure to completely close the switch with a laser spot even when operating in the nonlinear mode (high electric fields with avalanche included) indicates the absence of an important process in the model. A mechanism is necessary for carriers to traverse the switch at speeds greater than the saturation velocity to enable the light spots to activate the switch. One such process that the model used to generate the results in Figure VI-2 lacks is transport and reabsorption of band-to-band recombination radiation, which will be shown to be important for optical trigger gain.

C. Band-to-Band Recombination Radiation

After the production of large carrier densities from the laser pulse ($\approx 10^{17}$ cm^{-3}), recombination immediately begins. In direct band gap semiconductors, band-to-band recombination produces a photon having the band gap energy. This photon can be reabsorbed, which creates an EHP. With the large densities typical of PCSS operation, this may be a significant process. The source for the recombination radiation is $n_e n_p k_r \approx (10^{17}\ \text{cm}^{-3})^2 \bullet 10^{-10}\text{cm}^3/\text{s} \bullet 10^{-9}\text{s/ns} = 10^{15}$ photons/ns-cm^3.

Implementing band-to-band recombination radiation using a full radiation transport calculation would have unacceptably increased computer time. Instead, the radiation transport is implemented using a diffusion equation. It should be noted that Holstein[85] has shown that simulating the absorption and emission of light quanta cannot be formulated exactly in terms of a diffusion equation. The purpose of this work, however, is to investigate the importance of the effect and minimize computer effort. Thus a fair approximation of light transport is sufficient. Holstein also recognized that although using a diffusion equation for radiation transport is not exact, it can show fair agreement in certain situations over limited parameter space. Of course, for a more thorough investigation (which these results will show is warranted), a more detailed radiation transport calculation is necessary.

The recombination radiation is represented as a photon density n_ϕ, which diffuses throughout the switch to a steady-state distribution every time step ($\approx 5.0 \times 10^{-13}$ s). The photon transport diffusion equation used in the model has a diffusive term, a source term, and an absorption term as shown in Eq. (III.6) and rewritten here.

$$\frac{d}{dt}[n_\phi] = D_\phi \nabla^2 n_\phi + n_e n_p k_r - \frac{n_\phi}{\tau_\phi} = 0 \qquad \text{(VI.1)}$$

The absorption term n_ϕ/τ_ϕ is also added into the continuity equations for electrons Eq. (III.1), and holes Eq. (III.2) as source terms.

The values for the radiation transport "diffusion coefficient" D_ϕ and "recombination time" τ_ϕ are determined by equating the absorption length of the light to the computational radiation transport "diffusion length" as shown in Eqs. (VI.2) and (VI.3).

$$\tau_\phi \approx \left[\alpha \frac{c}{\sqrt{\varepsilon_r}}\right]^{-1} \approx 10^{-14}\ s \qquad \text{(VI.2)}$$

$$D_\phi = \frac{1}{\alpha^2 \tau_\phi} \approx 4 \times 10^6\ cm^2/s \qquad \text{(VI.3)}$$

The absorption coefficient, α, is 5000 cm^{-1}.

D. Effect of Transport of Recombination Radiation

The switching currents are shown in Figure VI-3 for spot activation near the cathode with and without radiation transport. Without radiation transport, the device switches to ≈ 30% of the circuit current limit of 60A. With radiation transport the device switches to 95% of the circuit current limit 1 ns after the application of the triggering laser pulse. Therefore, including radiation transport allows the spot of light to close the switch. If nonlinear effects are excluded (no avalanche), the closing of the switch takes more time to develop. If radiation transport is included and avalanche is neglected, the device switches but on a longer time scale. Avalanche appears essential for the fast rise times of the switch when spot illumination is used. The switching delay between the peak of the laser pulse and actual activation of the switch is also an effect seen in experimental devices.

A time evolution of the electric field when radiation transport is included is shown in Figure VI-4. The electric field with radiation transport excluded is shown in Figure VI-5. When the spot of light is applied near the cathode, thereby introducing excess carriers, the electric field begins to compress near the anode. At 4 ns the electric fields for both cases are similar. When radiation transport is included, the electric field begins to collapse at the anode as switching proceeds (6.5 ns). Eventually the electric field completely collapses, which enables a path for carrier collection with a consequent decrease in switch resistance. If carriers due to reabsorption of recombination radiation are not present, the electrons traveling at the saturation velocity are not fast enough to completely collapse the electric field enhancement near the anode. During their slow transit, their density begins to decrease due to recombination losses.

The log of the electron density is shown in Figure VI-6 for light activation near the cathode when radiation transport is considered. The log of the electron density is shown in Figure VI-7 when radiation transport is neglected. The electron density is nearly an order of magnitude larger (10^{16} cm^{-3})

at 7 ns near the anode with radiation transport compared to the case in which radiation transport is neglected. The density near the laser spot center is increasing and expanding as the effective lifetime of the carriers increases. Instead of EHPs recombining to reduce n_e, the EHPs recombine, emitting photons which are reabsorbed elsewhere creating other EHPs. The electron density near the contacts continues to increase in the closed phase of the switch, reflecting the high level of injection into the contacts that is occurring to support the closed switch current. Radiation transport allows electrons to spread more quickly, which reduces the electric field near the anode. Without radiation transport, electrons are slowed by ambipolar electric field enhancement at the density front.

E. Varying The Absorption Coefficient

The spreading of carriers at speeds greater than the characteristic saturation velocity allows switch triggering with a spot of light. If the carriers "diffusion length" were increased, the switch should close at an even faster rate. In Figure VI-8 the absorption coefficient is varied when a switch is triggered with a spot of light near the cathode to show the effect of the spreading of recombination flux on the current. Decreasing the absorption coefficient (increasing the "diffusion length") allows carriers to spread further and, consequently, allows the device to switch faster. The smaller absorption coefficients α (larger "diffusion lengths") are seen to switch faster. If the absorption coefficient becomes too small (50 cm^{-1}), however, the "diffusion length" becomes larger than the characteristic device size. Therefore, instead of carriers being generated in the device from reabsorbed radiation, the radiation is emitted into the ambient and potential carriers are lost from the device. As a result, the switch fails to close completely before recovering. These cases occur when the trigger flux $\Phi = 10^{22}$ $cm^{-2}s^{-1}$ ($\approx$ 2 kW/cm^2) is an order of magnitude less than that shown in Figure VI-3. Consequently, the 5000 cm^{-1} case closes to a lower current level than that shown in Figure VI-3. Figure VI-9 shows the electron density at 7 ns for α = 5000 cm^{-1}, 500 cm^{-1}, and 50 cm^{-1}. At large α, the location of the laser spot is evident and the electron densities at spot center are very large. As α is decreased to exceed the device dimensions, there is little evidence of the location of the laser spot and carriers created from reabsorption of radiation. Since the diffusion length exceeds the device dimensions, the radiation has been lost from the device before being reabsorbed.

F. Laser Activation at Anode and Cathode

An investigation was made into the sensitivity of switching on the location of the laser spot. The voltage across the switch is shown in Figure VI-10 for the spot located near the cathode or anode. The switch is more sensitive to laser activation near the cathode, which agrees with observations by Zutavern et al.[56] At 7 ns, the switch activated near the cathode has completely closed, whereas the switch activated near the anode is still in commutation.

The electric field is shown in Figure VI-11 for laser activation near the anode. The electric field near the cathode does not collapse on the time scale required for rapid switching. Some reduction occurs, but a compete collapse does not. As shown in Figure VI-4 for a light spot near the cathode, electric field collapse near the contacts is required for complete switching. The distribution of the electron density also changes with activation near the anode as shown in Figure VI-12. Even with the electron densities approaching 10^{17} cm^{-3} near the anode, the device has yet to completely close. The reabsorbed recombination radiation is not sufficient to completely collapse the electric field. Activation near the cathode generates extra carriers near the anode through gain processes. Activation near the anode appears to rely primarily on transport of electrons created by photoionization with a small contribution from avalanche. Also, the electron density tails extending to either end of the device that are seen in the cathode activation case are absent in the anode activation case.

G. Summary

The two-dimensional time dependent computer model has been used to examine the important processes involved in trigger gain for an intrinsic GaAs lateral switch operated in the nonlinear mode and activated with a laser spot. Results from the model show that band-to-band recombination radiation transport plays an important role in carrier transport when the switch is closed with a nonuniform laser pulse. Reabsorption of radiation is a mechanism that allows carriers to move throughout the device at speeds greater than their saturation velocities. Reabsorption of the radiation ultimately reduces the electric field at the contacts, which allows for the closing of the switch. The model also predicts that the switch is sensitive to the location of the activating laser pulse. Less laser fluence is required to close the switch near the cathode than near the anode.

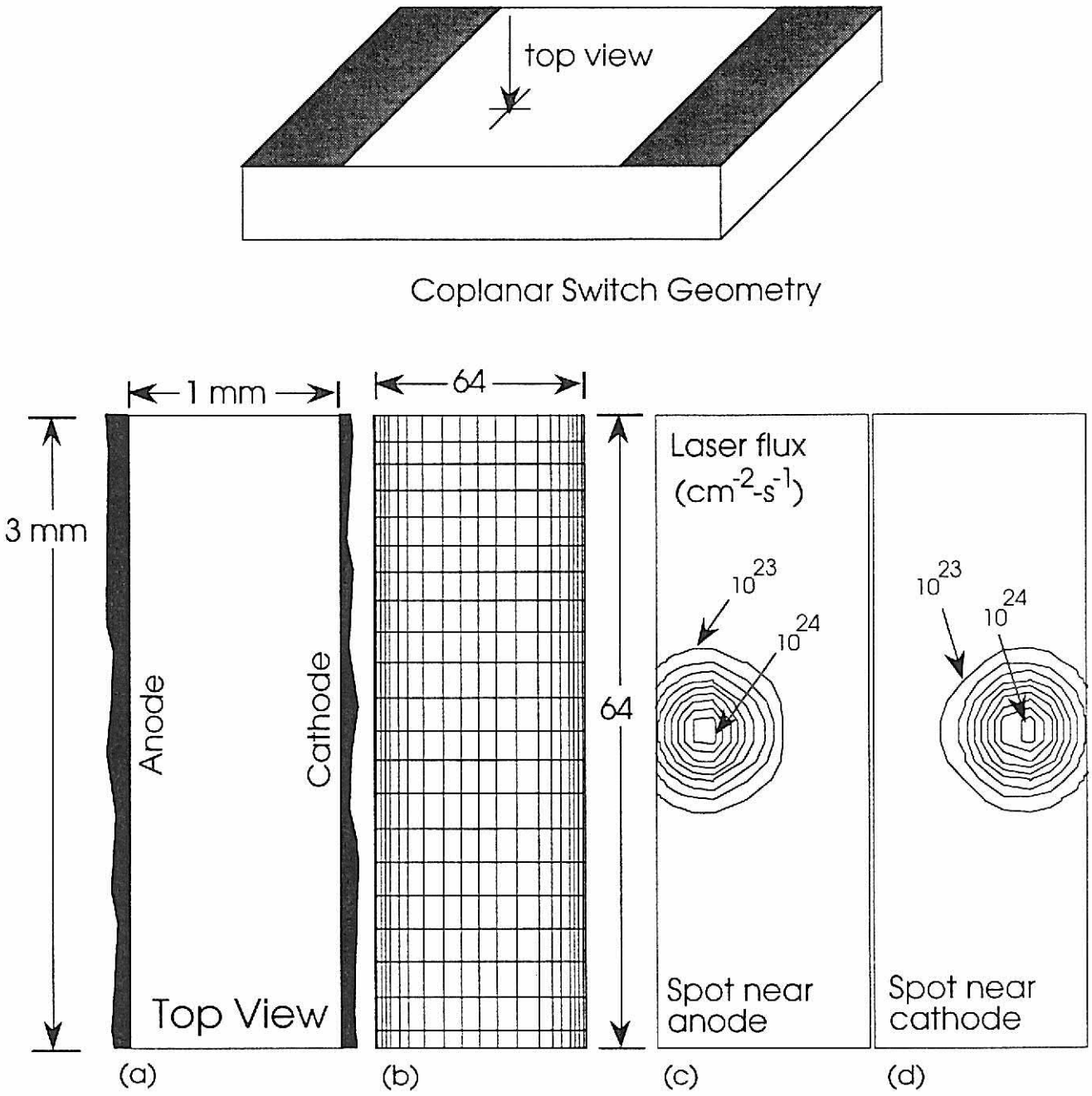

Figure VI-1. Coplanar geometry: top view. (a) A coplanar geometry has both contacts on the same plane. In the top view the typical dimensions are 3 x 1 x 0.4 - 0.5 mm. (b) The mesh used for finite differencing is a nonrectilinear mesh concentrated at both contacts. The photon flux Φ (cm^{-2}-s^{-1}) distribution is shown for (c) light spot activation near the cathode and (d) light spot activation near the anode.

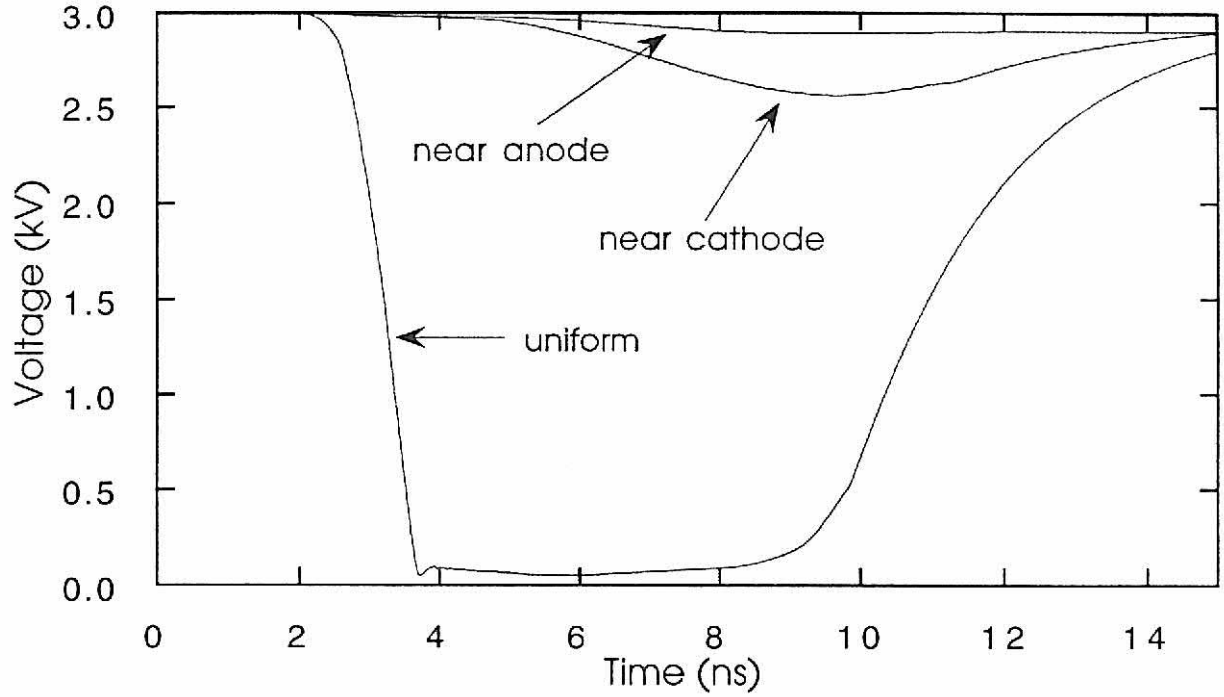

Figure VI-2. Voltage vs. time for a coplanar intrinsic GaAs switch activated with uniform light between the contacts, with a spot of light near the cathode and a spot near the anode. The uniform application of light is more effective in switching the device. Applying a spot of light near the anode or the cathode as in Figure VI-1(c-d) fails to switch the device. Since real switches can be triggered with light spots, an important effect is not being considered in these cases, namely, band-to-band recombination radiation transport.

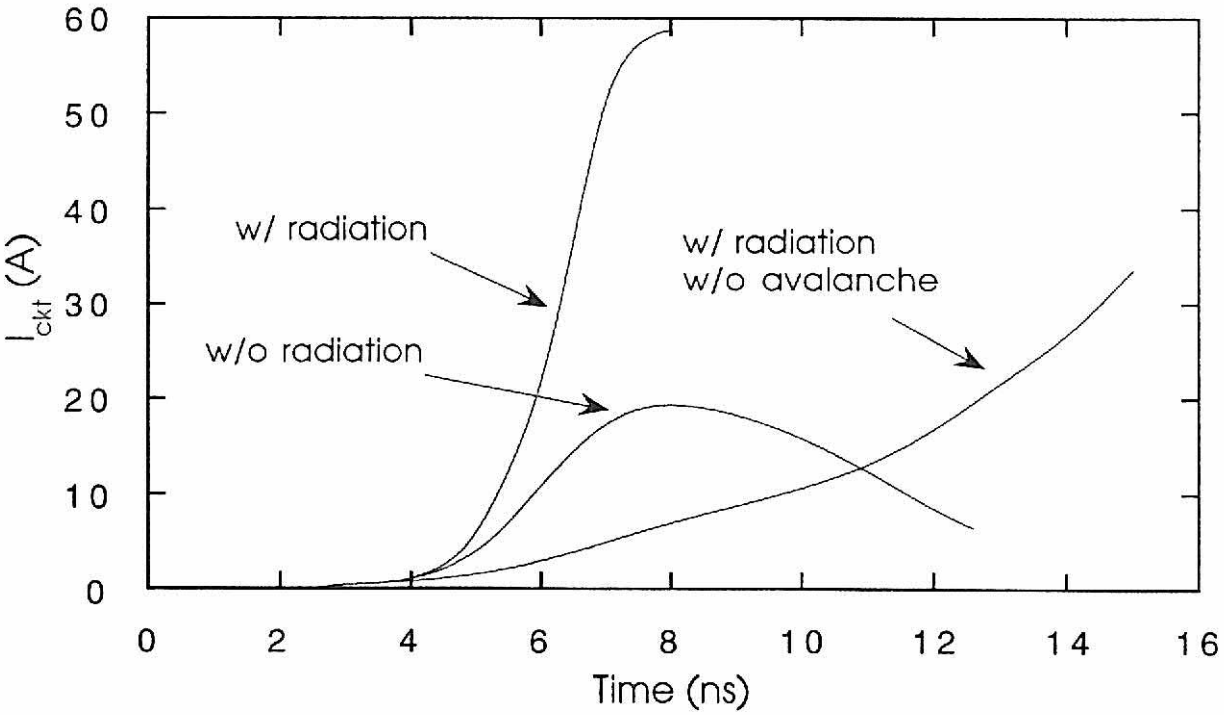

Figure VI-3. Current vs. time for a coplanar intrinsic GaAs switch activated near the cathode ($\Phi = 10^{23}$ $cm^{-2}s^{-1}$) with and without radiation transport, and with avalanche neglected. With radiation transport, it is possible to simulate the triggering of the devices with a spot of light. Thus radiation transport is an important process which provides a mechanism for the activation of the switch by a spot of light.

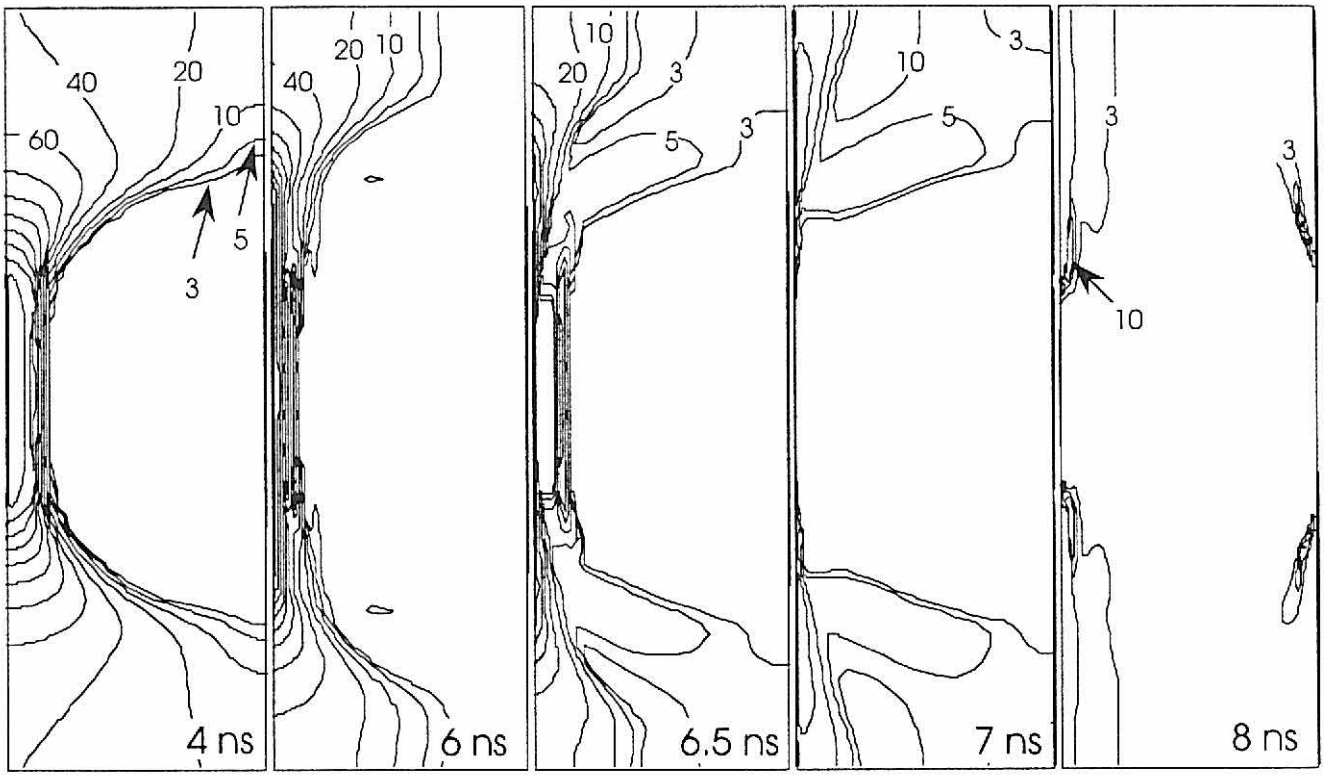

Figure VI-4. Time evolution of the electric field (kV/cm) for light activation near the cathode with radiation transport. The electric field completely collapses at switch closure, which allows a path for the conduction current.

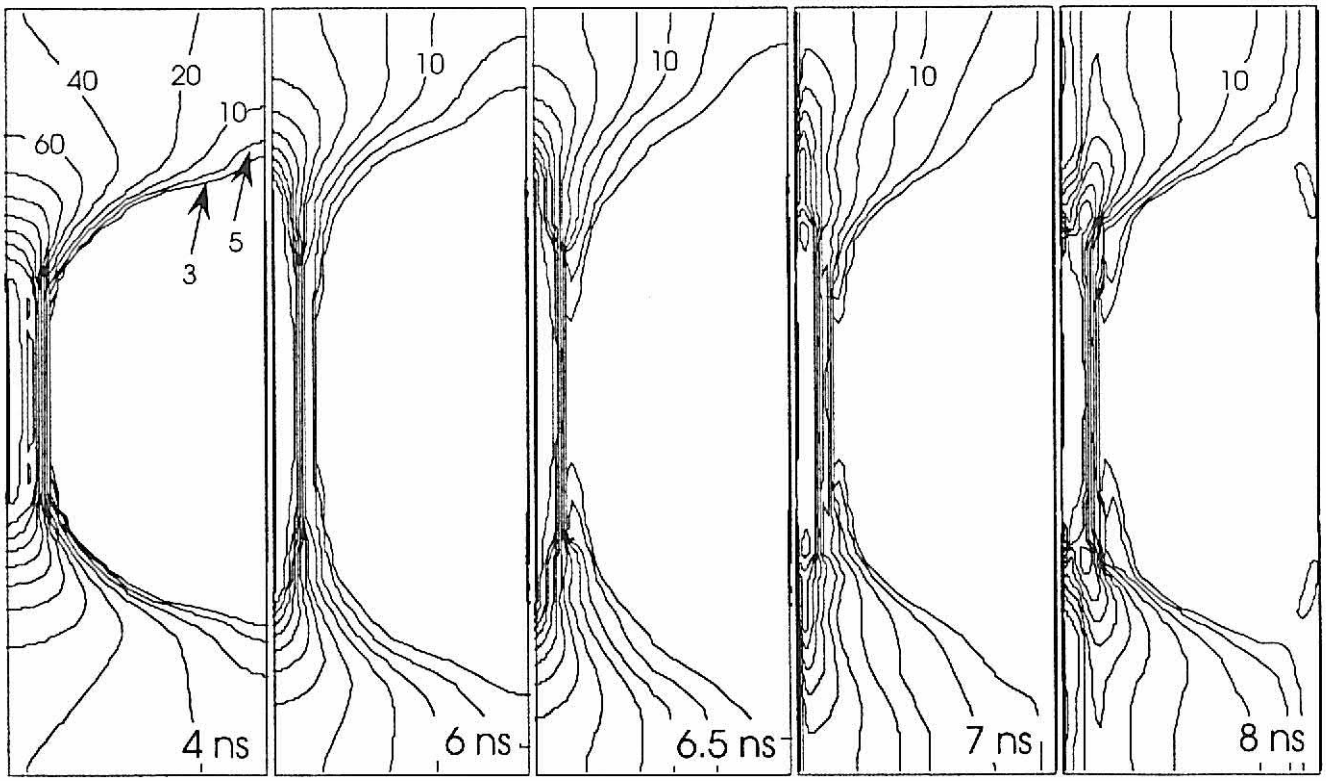

Figure VI-5. Time evolution of the electric field (kV/cm) for light activation near the cathode. Radiation transport is not considered. The electric field has not completely collapsed, which indicates the failure of the device to be triggered.

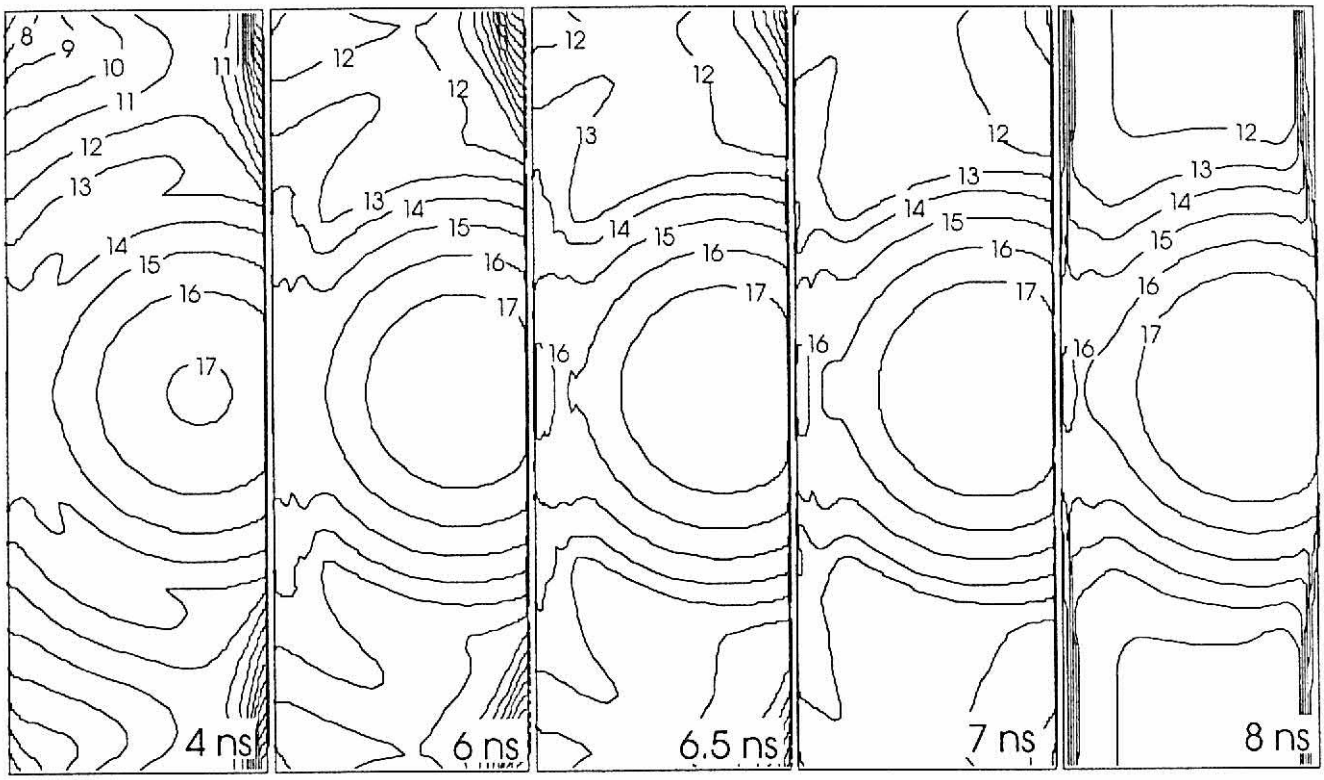

Figure VI-6. Time evolution of log of the electron density (Log(cm-3)) for light activation near the cathode with radiation transport. Radiation transport enables the carriers to spread throughout the device at speeds greater than the saturation velocity, which allows the switch to be triggered in sub-nanosecond times.

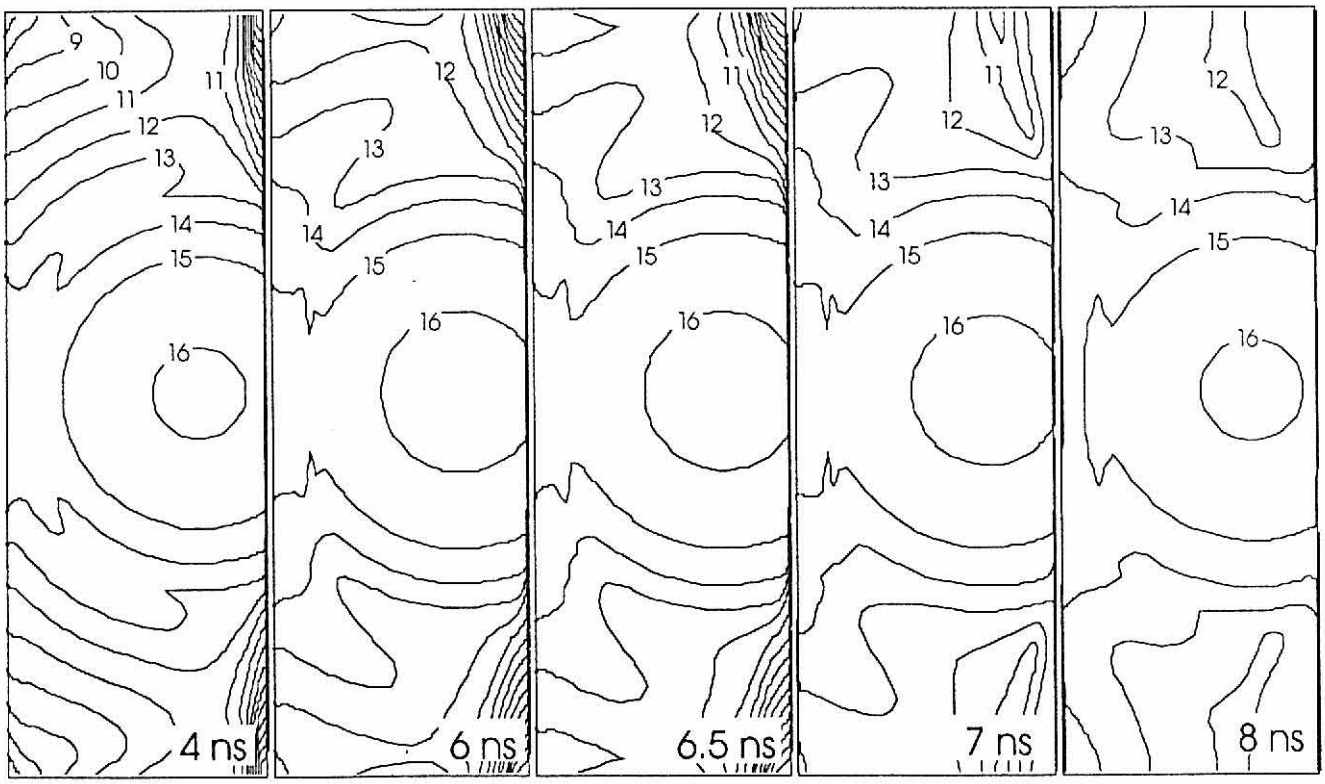

Figure VI-7. Time evolution of log of the electron density (Log(cm^{-3})) for light activation near the cathode without radiation transport. Without a mechanism to spread carriers quickly and to increase the effective lifetime in the device, the switch cannot close.

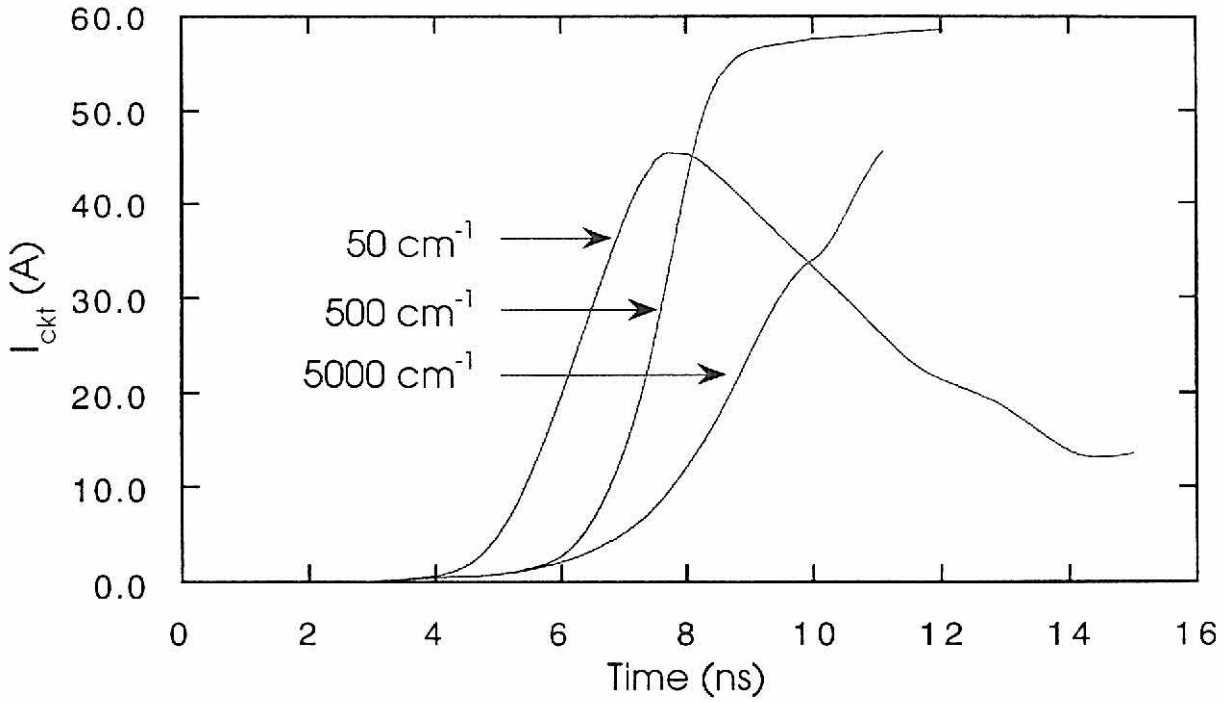

Figure VI-8. The voltage vs. time for a coplanar intrinsic GaAs switch activated with a spot of light ($\Phi = 10^{22}$ cm^{-2}-s^{-1}) near the cathode and with the absorption coefficients varied. As the absorption coefficient is decreased, the recombination travels farther before being reabsorbed. The faster spreading of the radiation leads to shorter closure times.

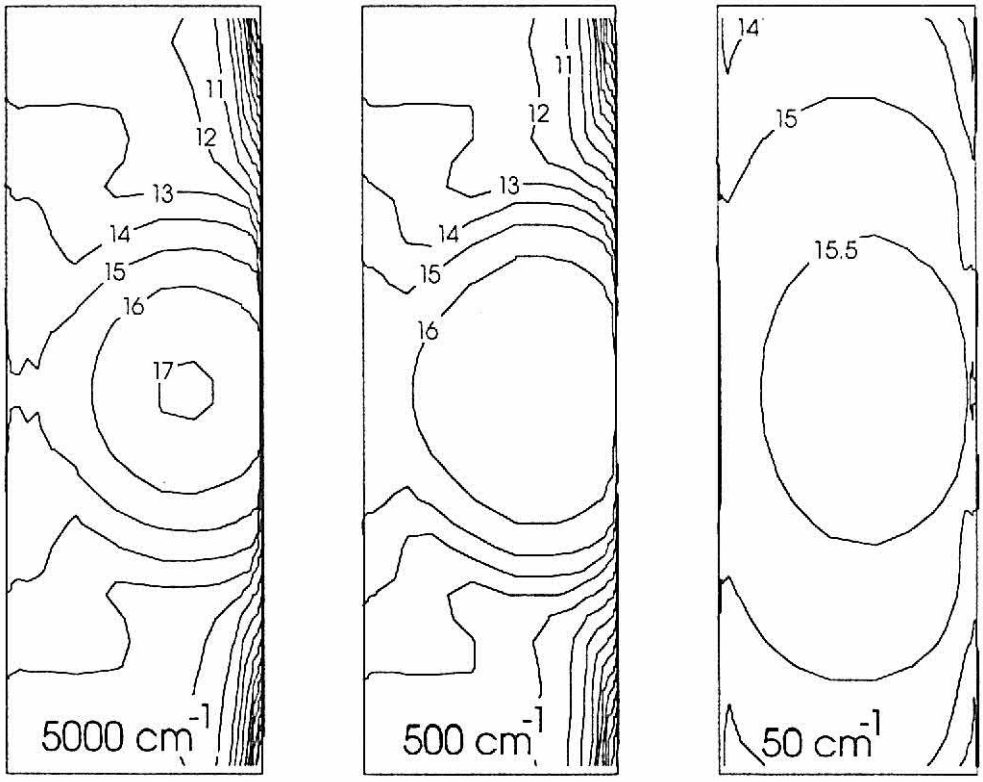

Figure VI-9. The log of the electron density (Log(cm^{-3})) at 7 ns for the α = 5000 cm^{-1}, 500 cm^{-1}, and 50 cm^{-1} cases of Figure VI-8. The smaller the absorption coefficient (the larger the diffusion length), the farther the carriers spread from the light spot. If the absorption coefficient is small enough, the radiation is emitted from the switch before being reabsorbed.

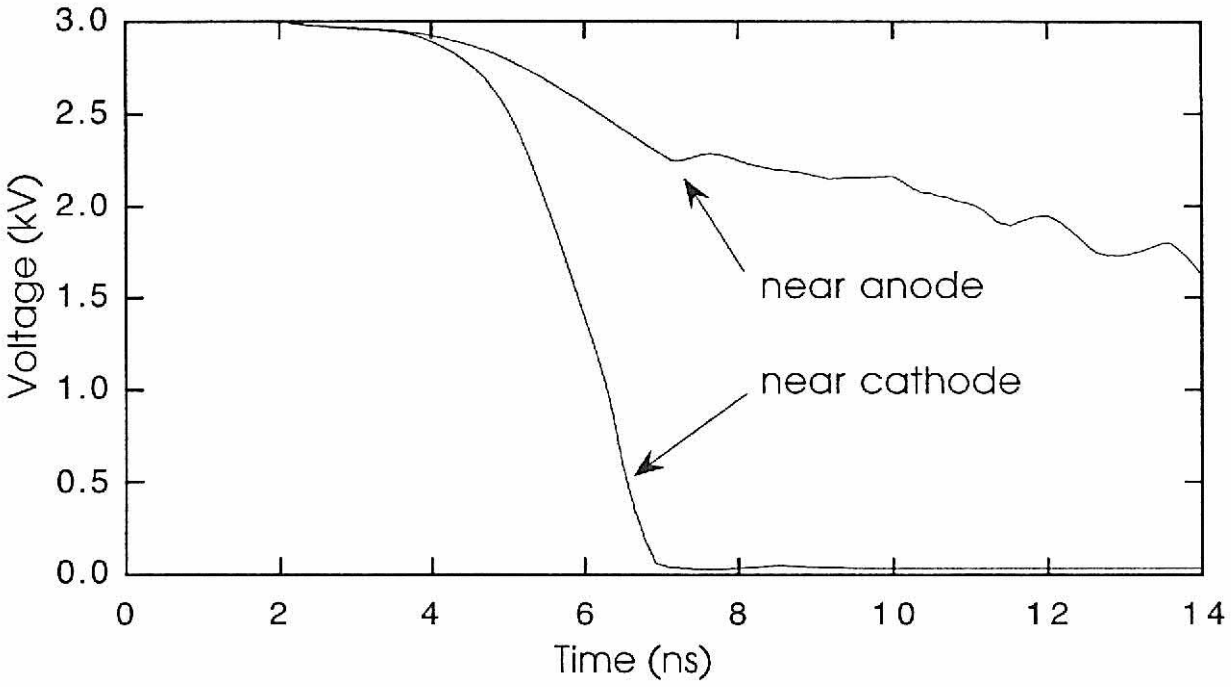

Figure VI-10. Voltage vs. time for a coplanar intrinsic GaAs switch activated with a spot of light near the cathode and a spot of light near the anode. Activating the switch with a spot of light near the cathode is more effective than activation near the anode.

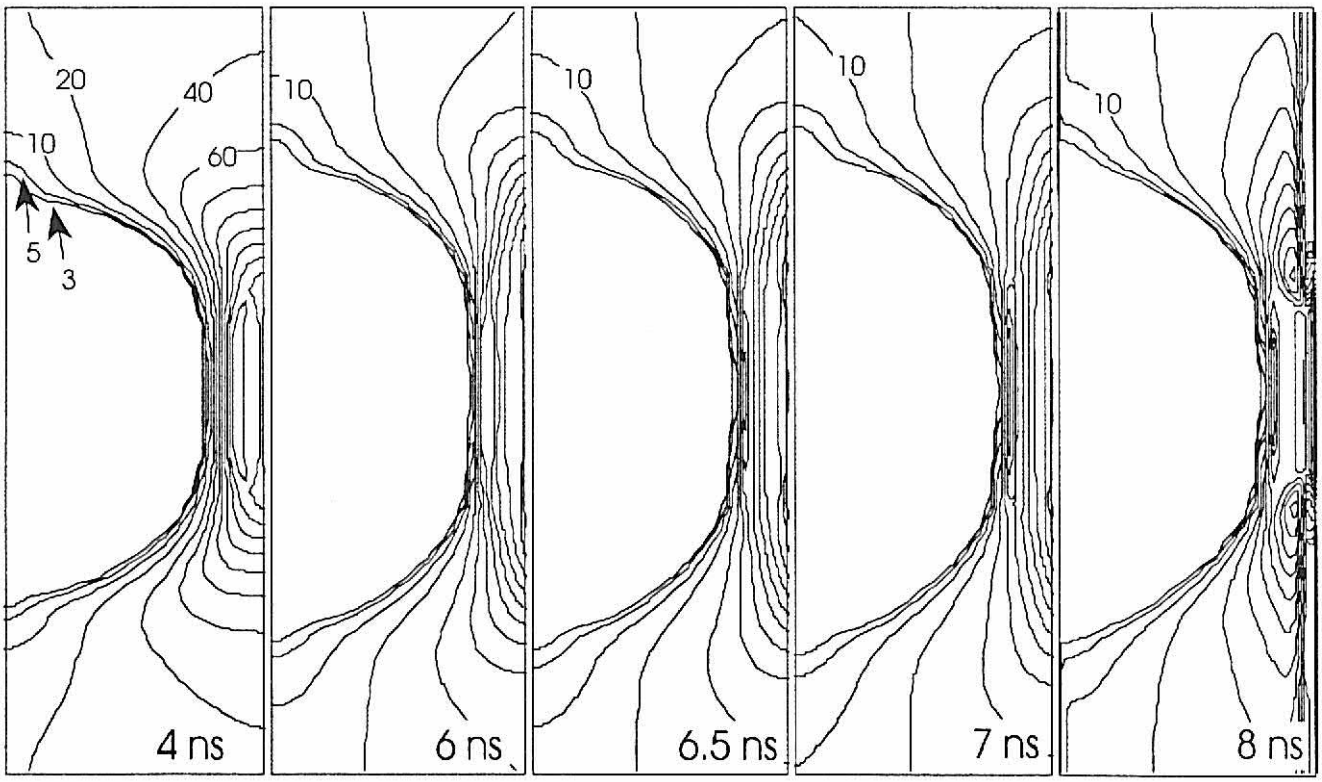

Figure VI-11. Time evolution of the electric field (kV/cm) for light activation near the anode. The electric field has not collapsed to the contacts, which indicates a failure to close the switch completely.

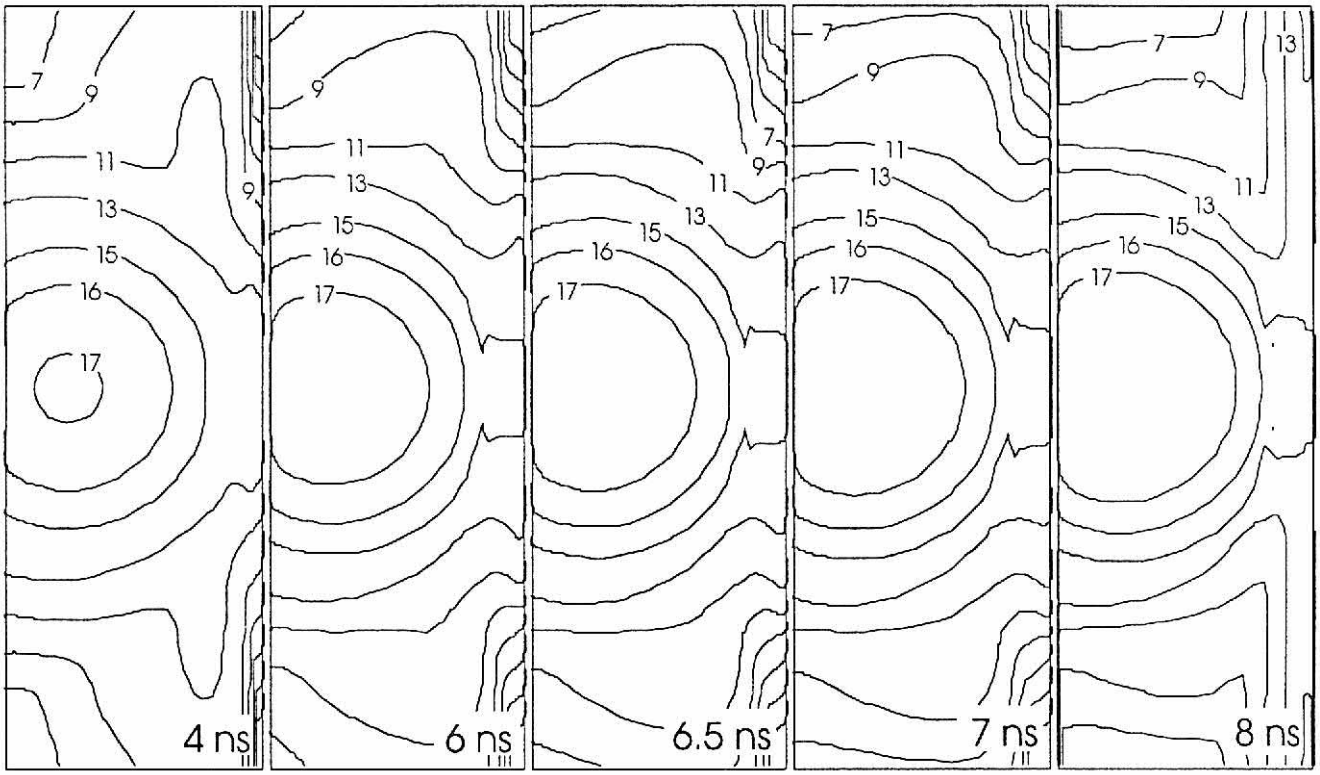

Figure VI-12. Time evolution of log of the electron density (Log(cm-3)) for light activation near the anode. The high n_e near the anode is not sufficient to close the switch completely. Also, there are no electron tails near the anode as there are in the cathode triggered case.

VII. CONCLUSION

Electric field nonuniformities were found to be dependent on the switch geometry and laser pulse distribution. The effect of negative differential resistance, contact geometries and carrier nonuniformities are sufficient to enhance the electric field to the levels necessary for intrinsic impact ionization to be important. The electric field nonuniformities are mobile in the switch during the switching cycle and inhibit the opening of the switch if they form near the anode.

This treatise is certainly not inclusive and leaves many questions unanswered; therefore, further inquiry into PCSS operation is warranted. All the cases shown were for one switching cycle. If multiple pulses were simulated, a more effective determination of temperature's role in the operation of these devices could be explored. Band bending affects such as increased electric field, temperature and large carrier densities could be taken into account since band bending effects the radiation absorption coefficients, the thermal level of carriers and the trapping cross section of deep impurities. A three-dimensional code may be necessary to model filament formation. The large current densities and electric field levels stress the numerical algorithms. To resolve the large enhancement electric fields and the abrupt boundaries of 10^{17} cm^{-3} to 10^{6} cm^{-3} carrier densities, an adaptive mesh may prove useful. Since lock-on occurs at lower electric fields than does intrinsic impact ionization, the role of trap impact ionization on switch performance requires further investigation.

REFERENCES

1 G. Schaefer, M. Kristiansen, and A. Guenther, eds. *Gas Discharge Closing Switches* (Plenum Press, New York, 1990), pp. 119-188.

2 C. H. Lee, "Picosecond optoelectronic devices based on optically injected electron-hole plasma," in *Picosecond Optoelectronic Devices*, edited by C. H. Lee (Academic Press, New York, 1984).

3 C. H. Lee, ed., *Picosecond Optoelectronic Devices* (Academic Press, New York, 1984).

4 R. L. Druce, M. D. Pocha, K. L. Griffin, J. M. Stein, and B. J. O'Bannon, "Wideband microwave generation with GaAs photoconductive switches," *Proceedings of the 8th IEEE International Pulsed Power Conference*, 1991.

5 U. Katschinski and J. G. H. Salge, "Optically triggered semiconductor switch for a low-impedance Blumlein generator," Optically Activated Switching II SPIE **1632**, 39 (1992).

6 G. Mourou, W. H. Knox, and S. Williamson, in *Picosecond Optoelectronic Devices*, edited by C. H. Lee (Academic Press, New York, 1984), pp. 219-248.

7 E. E. Funk, E. A. Chauchard, M. J. Rhee, and Chi H. Lee, "80-kW inductive pulsed power system with a photoconductive semiconductor switch," IEEE Photonics Tech. Lett. **3**, 576 (1991).

8 D. H. Auston, "Picosecond optoelectronic switching and gating in silicon," Appl. Phys. Lett. **26**, 101-103 (1975).

9 C. H. Lee, "Picosecond optoelectronic switching in GaAs," Appl. Phys. Lett. **30**, 84 (1977).

10 G. Mourou and W. Knox, "High-power switching with picosecond precision," Appl. Phys. Lett. **35**, 492-495 (1979).

11 W. C. Nunnally and R. B.Hammond, "80-MW photoconductor power switches," Appl. Phys. Lett. **44**, 980-982 (1984).

12 F. J. Zutavern, G. M. Loubriel, B.B. Mckenzie, M. W. O'Malley, R.A. Hamil, L.P. Schanwald, and H. P. Hjalmarson, "Photoconductive Semiconductor Switch (PCSS) Recovery," *Proceedings of the 7th IEEE International Pulsed Power Conference*, Monterey, CA, 1989, p. 412.

13 D. H. Auston, "Picosecond photoconductivity: high-speed measurements of devices and materials," Semiconductors and Semimetals **28**, 85-134 (1990).

14 K. H. Schoenbach, V. K. Lakdawala, R. Germer, and S. T. Ko, "An optically controlled closing and opening semiconductor switch," J. Appl. Phys. **63**, 2460 (1988).

15 W. R. Donaldson, "Optical probing of field dependent effects in GaAs photoconductive switches," *Proceedings of the 8th International Pulsed Power Conference*, San Diego, CA, 1991, p. 45.

16 W. R. Donaldson, L. E. Kingsly, M. Weiner, A. Kim, and R. Zeto, "Electro-optic imaging of the internal fields in a GaAs Photoconductive Switch," J. Appl. Phys. **68**, 6453-6457 (1990).

17 K. H. Schoenbach, J. S. Kenney, A. Koenig, and B. J. Ocampo, "Electric field measurements in photoconductive GaAs switches," *Proceedings of the 8th International Pulsed Power Conference*, San Diego, CA, 1991, p. 105.

[18] K. H. Schoenbach, J. S. Kenney, and R. J. Allen, "Optical measurements of the electric field and temperature distributions in photoconductive GaAs switches," Optically Activated Switching II SPIE **1632**, 54 (1992).

[19] J. S. Kenney, K. H. Schoenbach, and F. E. Peterkin, "Temporal development of electric field structures in photoconductive GaAs switches for linear and lock-on mode," *Proceedings of the 9th IEEE International Pulsed Power Conference*, Albuquerque, NM, 1993.

[20] L. E. Kingsley and W. R. Donaldson, "Electrooptic imaging of surface electric fields in high power photoconductive switches," IEEE Trans. Electron Devices **37**, 2449-2458 (1990).

[21] F. J. Zutavern, G. M. Loubriel, M. W. O'Malley, L.P. Schanwald, W.D. Helgeson, D. L. McLaughlin, and B. B. Mckenzie, "Photoconductive semiconductor switch experiments for pulsed power applications," IEEE Trans. Electron Devices **37** (12), 2472-2477 (1990).

[22] F. J. Zutavern, G. M. Loubriel, M. W. O'Malley, W. D. Helgeson, and D. L. McLaughlin, "High gain photoconductive semiconductor switching," *Proceedings of the 8th IEEE International Pulsed Power Conference*, San Diego, CA, 1991, p. 23.

[23] R. Aaron Falk, J. C. Adams, and G. Bohnhoff-Hlavacek, "Optical probe techniques for avalanching photoconductors," *Proceedings of the 8th International Pulsed Power Conference*, San Diego, CA, 1991, p. 29-36.

[24] J. C. Adams, R. A. Falk, C. D. Capps, and S. G. Ferrier, "Dark current characterization of photoconductive switches," Optically Activated Switching II SPIE **1632**, 110-119 (1992).

[25] W. C. Nunnally, "Linear photoconductive power switches," in *High-power optically activated solid-state switches*, edited by A. Rosen and F. J. Zutavern (Artech House, Boston, 1994), Chap. 2, pp. 29-42.

[26] C. H. Lee, "Optical control of semiconductor closing and opening switches," IEEE Trans. Electron Devices **37**, 2438 (1990).

[27] S. Feng, P.-T. Ho, and J. Goldhar, "Photoconductive switching in diamond under high bias field," IEEE Trans. Electron Devices **37**, 2511 (1990).

[28] W. Jiang, K. Zinsmeyer, M. Less, K. H. Schoenbach, and M. Kristiansen, "Electron-beam controlled switching using quartz and polycrystalline ZnS," IEEE Trans. Electron Devices **41** (4), 582-586 (1994).

[29] Krishna Shenai, R. S. Scott, and B. J. Baliga, "Optimum semiconductors for high-power electronics," IEEE Trans. Electron Devices **36** (9), 1811-1823 (1989).

[30] R. K. F. Germer, K. H. Schoenbach, and S. G. E. Pronko, "A bulk optically controlled semiconductor switch," J. Appl. Phys. **64**, 913 (1988).

[31] R. K. F. Germer and K. H. Schoenbach, "Stimulated switch-off and repetitive switching of a bistable optically controlled semiconductor switch," J. Phys. D, Appl. Phys. **22**, 398 (1989).

[32] F. J. Leonberger and P. F. Moulton, "High-speed InP optoelectronic switch," Appl. Phys. Lett. **35**, 712 (1979).

[33] P. Ho, F. Peng, and J. Goldhar, "Photoconductive switching using polycrystalline ZnSe," IEEE Trans. Electron Devices, **37**, 2517-2519 (1990).

[34] R. H. Bube, *Photoelectric Properties of Semiconductors* (Cambridge Press, 1992).

[35] M. D. Pocha, R. L. Druce, M. J. Wilson, and W. W. Hofer, "Avalanche photoconductive switching," *Proceedings of the 7th IEEE International Pulsed Power Conference*, 1989, pp. 866-868.

[36] W. C. Nunnally, "High power microwave generation using optically activated semiconductor switches," IEEE Trans. Electron Devices **37**, 2439-2448 (1990).

[37] E. J. Johnson, J. A. Kalfalas, and R. W. Davies, "The role of deep-level centers and compensation in producing semi-insulating GaAs," J. Appl. Phys. **54**, 204-207 (1983).

[38] M. D. Pocha and R. L. Druce, "35-kV GaAs Subnanosecond Photoconductive Switches," IEEE Trans. Electron Devices **37** (12), 2486-2492 (1990).

[39] F. J. Zutavern, G. M. Loubriel, M. W. O'Malley, L.P. Schanwald, and D. L. McLaughlin, "Recovery of high-field GaAs photoconductive semiconductor switches," IEEE Trans. Electron Devices **38** (4), 696-700 (1991).

[40] F. J. Zutavern and G. M. Loubriel, "High-voltage lateral switches from silicon or gallium arsenide," in *High-Power Optically Activated Solid-State Switches*, edited by A. Rosen and F. J. Zutavern (Artech House, Boston, 1994), Chap. 11, pp. 245-296.

[41] C. G. B. Garrett and W. H. Brattain, "Some experiments on, and a theory of, surface breakdown," J. Appl. Phys. **27**, 299-306 (1956).

[42] M. D. Pocha and W. W. Hofer, "High-speed switching in photoconductors," in *High-power optically activated solid-state switches*, edited by A. Rosen and F. J. Zutavern (Artech House, Boston, 1994), Chap. 3, pp. 43-60.

[43] A. Kim, M. Wade, M. Weiner, R. Youmans, and R. Zeto, "Bulk GaAs photonic devices with two opposite gridded electrodes," *Proceedings of the 7th IEEE International Pulsed Power Conference*, Monterey, CA, 1989, p. 430.

[44] J. C. Adams, C. D. Capps, R. A. Falk, and S. G. Ferrier, "Below band-gap electroabsorption in bulk semi-insulating GaAs," Appl. Phys. Lett. **63**, 633-635 (1993).

[45] M. Caulton *et al.*, "p-i-n diodes for low frequency high power switching applications," IEEE Trans. Microwave Theory & Tech. **30** (6) (1982).

[46] A. Rosen, P. Stabile, D. Bechtle, W. Janton, A. Gombar, J. McShea, A. Rosenberg, P. Herczfeld, and A. Bahasadri, "Optically achieved p-i-n diode switch utilizing a two dimensional laser array at 808 nm as an optical source," IEEE Trans. Electron Devices **36**, 367 (1989).

[47] A. Rosen, P. Stabile, A. M. Gombar, W. M. Janton, A. Bahasadri, and P. Herczfeld, "100 kW DC-biased all semiconductor switch using Si p-i-n diodes and AlGaAs 2D laser arrays," IEEE Photonics Tech. Lett. **1**, 132 (1989).

[48] F. Cibulka, L. Crane, and J. Marks, "Field evaluation of industry's first self-protected, light-triggered thyristor," IEEE Trans. Power Delivery **5** (1), 110-115 (1990).

[49] P. M. Campbell, W. Garwacki, A. R. Sears, P. Menditto, and B. J. Baliga, "Trapezoidal-groove Schottky-gate vertical channel GaAs FET (GaAs static induction transistor)," IEEE Electron Device Lett. **6** (6), 304-306 (1985).

[50] Mutsuhiro Mori and Tsutomu Yatsuo, "High voltage GaAs power static induction transistor," *Proceedings of the 19th Conference on Solid State Devices and Materials*, Toyko, Japan, 1987, pp. 279-282.

[51] P. Hadizad, J. H. Hur, H. Zhao, J. Osinski, P. D. Dapkus, M. A. Gundersen, and H. R. Fetterman, "GaAs optoelectronic static induction transistor for high frequency pulsed power switching," *Proceedings of the 8th IEEE International Pulsed Power Conference*, San Deigo, CA, 1991, pp. 200-203.

[52] P. Hadizad, J. H. Hur, H. Zhao, and M. A. Gundersen, "A comparative study of Si- GaAs-based devices for repetitive, high-energy, pulsed switching applications," J. Appl. Phys. **71** (7) (1992).

[53] Jun-Ichi Nishizawa, Takeshi terasaki, and Jiro Shibata, "Field-effect transistor versus analog transistor (Static Induction Transistor)," IEEE Trans. Electron Devices **22** (4), 185-197 (1975).

[54] D. C. Stoudt, R. P. Brinkmann, R. A. Roush, M. S. Mazzola, F. J. Zutavern, and G. M. Loubriel, "Effects of 1-MeV neutron irradiation on the operation of a Bistable Optically Controlled Semiconductor Switch (BOSS)," IEEE Trans. Electron Devices **41** (6), 913-919 (1994).

[55] F. J. Zutavern, G. M. Loubriel, and M. W. O'Malley, "Recent developments in opening photoconductive semiconductor switches," *Proceedings of the 6th IEEE International Pulsed Power Conference*, 1987, pp. 577-580.

[56] F. J. Zutavern, G. M. Loubriel, D. L. McLaughlin, W. D. Helgeson, and M. W. O'Malley, "Electrical and optical properties of high gain GaAs Switches," Optically Activated Switching II SPIE **1632**, 152-159 (1992).

[57] F. J. Zutavern, G. M. Loubriel, M. W. O'Malley, W. D. Helgeson, D. L. McLaughlin, and G. J. Denison "Characteristics of current filamentation in high gain photoconductive semiconductor switching," *Proceedings of the 20th IEEE Power Modulator Symposium*, Myrtle Beach, SC, 1992, pp. 305-311.

[58] G. M. Loubriel, W. D. Helgeson, D. L. McLaughlin, M. W. O'Malley, F. J. Zutavern, A. Rosen, and P. J. Stabile, "Triggering GaAs lock-on switches with laser diode arrays," IEEE Trans. Electron Devices **38** (4), 692-695 (1991).

[59] S. N. Vainshtein, Yu. V. Zhilyaev, and M. E. Levinshtein, "Comparative study of turn-on of gallium arsenide and silicon thyristors," Sov. Phys. - Tech. Phys. **31** (7), 788-790 (1986).

[60] Yu. M. Zadiranov, V. I. Korol'kov, V. G. Nikitin, S. I. Ponomarev, and A. V. Rozhkov, "Pulse thyristors based on GaAs-AlGaAs heterostructures," Sov. Tech. Phys. Lett. **9** (6), 280-281 (1983).

[61] G. M. Loubriel, F. J. Zutavern, H. P. Hjalmarson, and M. W. O'Malley, "Closing photoconductive semiconductor switches," *Proceedings of the 7th IEEE International Pulsed Power Conference*, Monterey, CA, 1989, pp. 365-367.

[62] G. M. Loubriel, F. J. Zutavern, W. D. Helgeson, D. L. McLaughlin, and M. W. O'Malley, "Physics and applications of the lock-on effect," *Proceedings of the 8th IEEE International Pulsed Power Conference*, San Diego, CA, 1991, pp. 33-36.

[63] R. P. Brinkman and K. H. Schoenbach, "Electron beam controlled switching with wide bandgap semiconductors," *Proceedings of the 8th IEEE International Pulsed Power Conference*, San Deigo, CA, 1991, pp. 94-101.

[64] P. S. Cho, J. Goldhar, and C. H. Lee, "Electrical pulse compression using photoconductive zinc selenide opening switches," IEEE Photonics Tech. Lett. **6** (5), 642-644 (1994).

[65] K. H. Schoenbach, J. S. Kenney, F. E. Peterkin, and R. J. Allen, "Temporal development of electric field structures in photoconductive GaAs switches," Appl. Phys. Lett. **63** (15), 2100 (1993).

[66] G. M. Loubriel, F. J. Zutavern, H. P. Hjalmarson, R. R. Gallegos, W. D. Helgeson, and M. W. O'Malley, "Measurement of the velocity of current filaments in optically triggered, high gain GaAs switches," Appl. Phys. Lett. **64** (24), 3323-3325 (1994).

[67] W. R. Donaldson and L. E. Kingsly "Optical probing of field dependent effects in GaAs photoconductive switches," Optically Activated Switching SPIE **1378**, 226 (1990).

[68] Session 6, Optically Activated Switching II SPIE **1632** (1992), and Session 4, Optically Activated Switching III SPIE **1873** (1993).

[69] L. Mu and W. R. Donaldson, "Simulating Photoconductive Switches in a Microwave Transmission Line," *Proceedings of the 9th IEEE International Pulsed Power Conference*, Albuquerque, NM, 1993, pp. 629-37.

[70] H. Zhao, P. Hadizad, Jung H. Hur, and M. A. Gundersen, "Avalanche injection model for the lock-on effect in III-V power photoconductive switches," J. Appl. Phys. **73**, 1807 (1993).

[71] W. T. White III, C. G. Dease, M. D. Pocha, and G. H. Khanaka, "Modeling GaAs high-voltage, subnanosecond photoconductive switches in one spatial dimension," IEEE Trans. Electron Devices **37** (12), 2532-2541 (1990).

[72] L. Partain, D. Day, and R. Powell, "Metastable impact ionization of traps model for lock-on in GaAs photoconductive switches," J. Appl. Phys. **74**, 335 (1993).

[73] C. D. Capps, R. A. Falk, and J. C. Adams, "Time-dependent model of an optically triggered GaAs switch," J. Appl. Phys. **74** (11), 6645-6654 (1993).

[74] R. P. Brinkman, K. H. Schoenbach, D. C. Stoudt, V. K. Lakdawala, G. A. Gerdin, and M. K. Kennedy, "The lock-on effect in electron-beam-controlled gallium arsenide switches," IEEE Trans. Electron Devices **38**, 701 (1991)

[75] R. P. Brinkman, K. H. Schoenbach, D. C. Stoudt, and R. A. Roush, "Sudden breakdown of bulk semiconductor switches," Optically Activated Switching III SPIE **1873**, 192 (1993).

[76] R. P. Brinkmann, "Modeling of electron-beam controlled semiconductor switches," J. Appl. Phys., **68**, 318-323 (1990).

77 L. E. Kingsley and W. R. Donaldson, "Numerical analysis of electric field profiles in high-voltage GaAs photoconductive switches and comparison with experiment," IEEE Trans. Electron Devices **40** (12), 2344-2351 (1993).

78 S. T. Ko, V. K. Lakdawala, K. H. Schoenbach, and M. S. Mazola, "Optimization studies of materials for optically controlled semiconductor switches," *Proceedings of the 7th IEEE International Pulsed Power Conference*, Monterey, CA, 1989, p. 861.

79 R. P. Brinkman, K. H. Schoenbach, M. S. Mazzola, R. A. Roush, and D. C. Stoudt, "Analysis of time-dependent current transport in an optically controlled, Cu-compensted GaAs switch," Optically Activated Switching II SPIE **1632**, 262 (1992).

80 P. L. G. Ventzek, R. J. Hoekstra, and M. J. Kushner, "Two-dimensional modeling of high plasma density inductively coupled sources for material processing" J. Vac. Sci. Tech. B. **12** (1), 461-477 (1994).

81 S. M. Sze, *Physics of Semiconductor Devices*, 2nd ed., (John Wiley & Sons, New York, 1981), Chap. 1.

82 A. G. Milnes, *Deep Impurities in Semiconductors* (John Wiley and Sons, New York, 1973).

83 V. K. Lakdawala, K. H. Schoenbach, R. A. Roush, G. R. Barevadia, and M. S. Mazola, "Photoquenching and characterization studies in a bulk optically controlled GaAs semiconductor switch," Optically Activated Switching SPIE **1378**, 259 (1990).

84 E. E. Funk, C. C. Kung, E. A. Chauchard, M. J. Rhee, and C. H. Lee, " Photoconductive switch controlled inductive pulsed power system," in *High-power optically activated solid-state switches*, edited by A. Rosen and F. J. Zutavern (Artech House, Boston, 1994), Chap. 4, p. 61.

85 T. Holstein, "Imprisonment of resonance radiation in gases," Phys. Rev., **72** (12), pp. 1212-1233 (1947).

VITA

Phillip Stout was born in Illinois. His collegiate studies were pursued at the University of Illinois at Urbana-Champaign where he obtained a B.S. (1989), M.S. (1991), and Ph.D. (1995) all in Electrical and Computer Engineering. His graduate studies were accomplished under the direction of Professor Mark J. Kushner. The master's thesis was an exploration of the surface kinetics of SiO_2 deposition using $TEOS/O_2$ chemistry.

Phillip Stout is a member of the Institute of Electrical and Electronic Engineers, the American Vacuum Society, and the American Physical Society.